Controller Design and Optimization for Rotor System Supported by Active Magnetic Bearings

Von der Fakultät für Ingenieurwissenschaften, Abteilung Maschinenbau und Verfahrenstechnik
der
Universität Duisburg-Essen
zur Erlangung des akademischen Grades
eines
Doktors der Ingenieurwissenschaften
Dr.-Ing.
genehmigte Dissertation

von

Chunsheng Wei
aus
Jilin, China

Gutachter: Univ.-Prof. Dr.-Ing. Dirk Söffker
Univ.-Prof. Dr.-Ing. Richard Markert
Tag der mündlichen Prüfung: 11. Februar 2015

Acknowledgement

This thesis is the result of the research work I carried out at the Chair of Dynamics and Control (SRS) at the University of Duisburg-Essen during 2009-2012. I would like to express my sincere gratitude to those people who supported me during this important period in my life.

First of all, I would like to thank my supervisor Univ.-Prof. Dr.-Ing. Dirk Söffker for offering the opportunity to be his student, for the scientific freedom, and for the invaluable scientific guidance towards completing this work.

Secondly, I would like to thank Prof. Dr.-Ing. Richard Markert, my second supervisor, for his interest in my work and his valuable comments.

I would like to thank all my colleagues in the Chair of SRS, specially Dr.-Ing. Lou'i Al-Shrouf, Dr.-Ing. Kai-Uwe Dettmann, Dr.-Ing. Mohammad Ali Karbaschian, Dr.-Ing. Marcel Langer, Prof. Dr.-Ing. Yan Liu, Dr.-Ing. Matthias Marx, Dr.-Ing. Xi Nowak and Dr.-Ing. Fan Zhang, for fruitful scientific and non-scientific conversations. I also would like to thank Yvonne Vengels for her assistance in my daily life at SRS.

I gratefully acknowledge the support provided by Siemens AG, Duisburg. Thanks to all colleagues from the department of development mechanics in Siemens Duisburg. Special thanks to Dr.-Ing. Rainer Gausmann for his many valuable comments and help in the experimemtal test.

Very special thanks to my parents, sisters and brother for their love, encouragement, and support through my life.

Most importantly, I would like to thank my wife, Leran, for her great love and support, specially during the period of writing this thesis.

Duisburg, December 2015 Chunsheng Wei

Abstract

Active Magnetic Bearings (AMBs) have been receiving increased attention in industry because of the advantages (contact-free, oil-free, etc.,) that they display in comparison with conventional bearings. They are used extensively in rotor system applications, especially in conditions where conventional bearing systems fail. Most AMBs are controlled by Proportional-Integral-Derivative (PID)-controllers. Controller design for AMB systems by means of hand tuning is time-consuming and requires expert knowledge. In order to avoid this situation and reduce the effort to tune the controller, multi-objective optimization with genetic algorithm is introduced to design and optimize the AMB controllers. In the optimization, criteria both in time and frequency domain are considered. A hierarchical fitness function evaluation procedure is used to accelerate the optimization process and to increase the probability of convergence. This evaluation procedure guides the optimizer to locate the small feasible region resulting mainly from the requirement for stability of control system. Another strategy to reduce the number of optimization parameters is developed, which is based on a sensitivity analysis of the controller parameters. This strategy reduces directly the complexity of the optimization problem and accelerates the optimization process. Controller designs for two AMB systems are considered in this thesis. Based on the introduced and presented hierarchical evaluation strategy, the controller design for the first AMB system is obtained without specific requirements related to initial solutions. The optimal controller design is applied to a test rig with a flexible rotor supported by AMBs. The results show that the introduced optimization procedure realizes the desired results of the controlled system's behavior. The maximal speed of 15000 rpm is reached. The second AMB system is designed for a turbo-compressor. The introduced parameter reduction strategy is applied for the controller design of this AMB system. The controller design is optimized in the search space around an initial solution. Optimization results show the efficiency of the introduced strategy.

Zusammenfassung

Aufgrund vieler Vorteile (wie z. B. Kontaktfreiheit, Ölfreiheit) gegenüber konventionellen Lagern etablieren sich aktive Magnetlager zunehmend in der Industrie. Aktive Magnetlager werden zum großen Teil in Rotorsystemen verwendet, wo konventionelle Öllager für die Anwendung versagen. PID-Regler werden häufig für Magnetlager verwendet. Die Auslegung des Reglers wird durch manuelle Einstellung (trial and error) bestimmt und ist sehr zeitaufwendig. Zudem bedarf es spezieller Fachkenntnisse zur Einstellung. Um diese Situation zu vermeiden und den Aufwand für die Reglerauslegung zu reduzieren, wird die Mehrzieloptimierung mit Genetischen Algorithmen in der vorliegenden Arbeit zur Optimierung des Reglerentwurfs eingesetzt. In der Optimierung werden die Zielfunktionen sowohl im Zeit- wie auch im Frequenzbereich definiert. Um den Optimierungsprozess zu beschleunigen und die Wahrscheinlichkeit der Konvergenz der Optimierung zu erhöhen, wird eine hierarchische Struktur zur Bewertung der Zielfunktionen eingeführt. Dies hilft dem Optimierer bei der Lokalisierung des kleinen zulässigen Bereichs, der im Wesentlichen aus der Anforderung an die Stabilität des Magnetlagersystems resultiert. Desweitern wird eine Strategie zur Reduzierung der Optimierungsparameter entwickelt, die auf der Sensitivitätsanalyse der Reglerparameter basiert. Diese Strategie reduziert die Komplexität des Optimierungsproblems und führt zu einer Beschleunigung des Optimierungsprozesses. In der vorliegenden Arbeit wird der Reglerentwurf von zwei Magnetlagersystemen berücksichtigt. Mit Hilfe der eingeführten Strategie zur Bewertung der Zielfunktionen, werden die Reglerparameter von dem ersten Magnetlagersystem bestimmt bzw. optimiert, ohne dass irgendeine Information über die Anfangslösung erforderlich ist. Der optimale Reglerentwurf wird dann in einem Versuchstand implementiert, in dem eine elastische Welle durch zwei Magnetlager gelagert ist. Die Versuchsergebnisse zeigen, dass das gewünschte dynamische Verhalten des geregelten Magnetlagersystems durch die Optimierung erzielt wird. Die maximal zulässige Drehzahl (15000 rpm) des Versuchsstandes wird mit dem optimalen Regler ohne Probleme erreicht. Als zweites Beispiel wird der Reglerentwurf eines magnetgelagerten Rotorsystems eines Turboverdichters betrachtet. In der Reglerauslegung wird die vorgeschlagene Optimierungsstrategie mit Hilfe

von Parameterreduktion verwendet. Die optimale Lösung wird lokal in der Nähe einer Anfangslösung gesucht. Die Optimierungsergebnisse zeigen die Effizienz der Optimierungsstrategie.

Contents

List of Symbols

ACO	Ant Colony Optimization
AD	Analog-to-Digital
AMB	Active Magnetic Bearing
DA	Digital-to-Analog
DC	Direct Current
DE	Driven-End
DSP	Digital-Signal-Processing
DoE	Design of Experiment
DoF	Degree of Freedom
FEM	Finite Element Method
FFGA	Fonseca and Flemming's multi-objective Genetic Algorithm
FPGA	Field Programmable Gate Array
GNA	Gauss-Newton Algorithm
HLGA	Weighting-based genetic algorithm
HSC	High-Speed-Cutting
IAE	Integrated Absolute Error
IPM	Interior Point Method
ISE	Integrated Squared Error
ISO	The International Organization for Standardization
ITAE	Integrated Time Absolute Error
LMA	Levenberg-Marquardt Algorithm
LP	Linear-Periodic
LQ	Linear Quadratic
LQR	Linear Quadratic Regulator
LTI	Linear-Time-Invariant
MIMO	Multi-Input and Multi-Ouput
MOEA	Multi-Objective Evolutionary Algorithm
MOEA/D	Decomposition-based evolutionary algorithm

MOGA . . . . . Multi-Objective Genetic Algorithm
$\mathcal{NP}$ . . . . . Non-deterministic Polynomial-time
NDE . . . . . Non-Driven-End
NPGA . . . . . Niched Pareto Genetic Algorithm
NSGA . . . . . Nondominated Sorting Genetic Algorithm
PID . . . . . Proportional-Integral-Derivative
PIDD . . . . . Proportional-Integral-Derivative-Derivative
PT2 . . . . . Proportional transfer element of second order
QNM . . . . . Quasi-Newton Method
SBX . . . . . Simulated Binary Crossover
SISO . . . . . Single-Input and Single-Ouput
SPEA . . . . . Strength Pareto Evolutionary Algorithm
SPX . . . . . Simplex Crossover
TSP . . . . . Travel Salesman Problem
VEGA . . . . . Vector Evaluated Genetic Algorithm
WCA . . . . . Weighted Clustering Algorithm
$\mathbf{A}$ . . . . . System matrix in state-space description
$\mathbf{B}$ . . . . . Input matrix in state-space description
$\mathbf{C}$ . . . . . Output matrix in state-space description
$\mathbf{C}$r . . . . . Output position matrix of a rotor system
$\mathbf{D}$ . . . . . Feedforward matrix in state-space description
$\mathbf{D}$r . . . . . Damping matrix of a rotor system
$\mathbf{F}$ . . . . . Input position matrix of a rotor system
$\mathbf{G}$r . . . . . Gyroscopic matrix of a rotor system
$\mathbf{K}$ . . . . . Feeback gain matrix for LQ-controller design
$\mathbf{K}$r . . . . . Stiffness matrix of a rotor system
$\mathbf{K}_{\mathrm{i}}$ . . . . . Current stiffness matrix
$\mathbf{K}_{\mathrm{s}}$ . . . . . Negative stiffness matrix
$\mathbf{M}$r . . . . . Mass matrix of a rotor system
$\mathbf{Q}$ . . . . . Weighting matrix for LQ-controller design
$\mathbf{R}$ . . . . . Weighting matrix for LQ-controller design
$\mathbf{R}_{\mathrm{corr}}$ . . . . . Correlation matrix
$\mathbf{R}_{\mathrm{red}}$ . . . . . Modal reduction matrix
$\mathbf{S}$ . . . . . Sensitivity function matrix
$\mathbf{S}_{\mathrm{NH}}$ . . . . . Static reduction matrix
$\mathbf{T}$ . . . . . Complementary sensitivity function matrix
$\mathbf{T}_{\mathrm{red}}$ . . . . . Transformation matrix

$\mathbf{X}$	Search space
$\mathbf{X}_\mathrm{f}$	Feasible region
$\mathbf{Y}$	Objective space
$\mathbf{f}_\mathrm{E}$	External force vector of a rotor system
$\mathbf{g}$	Constraint function vector
$\mathbf{q}$	Displacement vector of a rotor system
$\mathbf{q}_\mathrm{H}$	Master DoFs
$\mathbf{q}_\mathrm{N}$	Slave DoFs
$\mathbf{q}_\mathrm{u}$	Unbalance force vector of a rotor system
$\mathbf{u}$	Input vector in state-space description
$\mathbf{v}_i$	The i-th eigenvector
$\mathbf{w}$	Force vector of a rotor system
$\mathbf{x}$	(1) State vector in state-space description or (2) Decision parameter vector in optimization
$\mathbf{x}_0$	Initial solution for controller design of AMB system II
$\mathbf{y}$	(1) Output vector in state-space description or (2) Fitness vector in optimization
α_d	Mass-proportional coefficient of damping
β_d	Stiffness-proportional coefficient of damping
$\Im(\cdot)$	Imaginary part of a complex number
λ_i	The i-th eigenvalue
μ	(1) Magnetic permeability or (2) Mean value
μ_0	Vacuum permeability
Ω	Rotational speed
ω	Angular frequency
Φ	Magnetic flux
$\Re(\cdot)$	Real part of a complex number
$\sigma(i)$	Standard deviation of the i-th parameter
$\sigma(S)$	Singular value of sensitivity function
$\sigma(\mathbf{S})$	Singular value of sensitivity function matrix
ζ_i	Damping ratio of the i-th eigenvalue
A_os	Percentage overshoot
B	Magnetic flux densitiy
$E[\cdot]$	Expected value
$f_x^{+/-}$	Force in positive or negative direction in x-direction
$f_y^{+/-}$	Force in positive or negative direction in y-direction

$f_{\mathrm{m/M}}$	Magnetic force
F_i	(1) The i-th filter of a PID-controller or (2) The i-th fitness function
G_0	Open loop transfer function
H	Magnetic field strength
i_0	Bias current
i_{c}	Control current
i_{max}	Saturation current or maximal coil current
$i_{x/y}$	Coil current in x- or y-direction
k_{i}	Current stiffness of magnetic bearing
K_{P}	Proportional term of a PID-controller
k_{s}	Negative (position) stiffness of magnetic bearing
L	Coil inductance
N	System dimension
p_{c}	Crossover probability
p_{m}	Mutation probability
R	Coil resistance
S	Sensitivity function
s	Laplace variable
s_0	Nominal air gap between rotor and magnet
T_{d}	Time constant of the low-pass filter for the derivative term of a PID-controller
T_{n}	Time constant of the integral term of a PID-controller
t_{r}	Rise time
t_{s}	Settling time
T_{v}	Time constant of the derivative term of a PID-controller
u	Coil voltage
u_0	Bias voltage
U_{air}	Magnetic field energy stored in the air gap
$\mathrm{cov}(x_i, x_j)$	Covariance between two parameters

Chapter 1

Introduction

Active Magnetic Bearings (AMBs) hold rotors in suspension without any mechanical contact by means of actively controlled magnetic forces. The main advantages of AMB system can be summarized as follows [Lar90, Lan97]:

- contact-free, no mechanical wear and friction,
- oil-free, no lubricant necessary,
- low energy consumption,
- high rotational speed possible,
- active vibration control and unbalance force compensation,
- long service life and long maintenance intervals
- suitable for vacuum and clean environments,
- online monitoring without any additional sensing device, and
- using as identification system.

The drawbacks of AMBs include high cost, large size, low load capacity, requiring backup bearings, and requiring expert knowledge to operate them (e.g. for controller tuning).

AMBs have been receiving increased attention in industry because of the advantages mentioned above that they display in comparison with conventional bearings. They are used extensively in rotor system applications, especially in conditions where conventional bearing systems fail. Various applications that utilize AMBs have been found in turbo-compressors, machine tool spindles, energy storage flywheel systems, blood pumps, etc.

1.1 Motivation and Goal of the Thesis

1.1.1 Motivation

The inherent negative stiffness of an AMB system causes instability in the open loop of the system; therefore, a feedback control loop is required to stabilize the AMB system. The controller design therefore becomes a central task in AMB system design. Different control methods have been applied successfully in the control of magnetic bearing systems. An optimal method (LQ-controller) [JP09, SB08] is used to obtain the optimal (high-performance) solution regarding control energy and control error. A drawback of this method is that the robustness properties are not taken into account explicitly, and all states are required for feedback (therefore, an observer becomes necessary). Robust control methods (H_∞-controller [WS11], μ-synthesis [MLA12, Pes13]) have been developed to compensate for some of the drawbacks of the LQ method, focusing on both performance and robustness of the controlled system. However, these methods result in a high order controller that can cause implementation problems because of hardware limitations. Additionally, structured and unstructured uncertainties have to be properly formulated as weighting matrices, which requires prior knowledge about the AMB system. Classical Proportional-Integral-Derivative (PID)-control methods are used widely in AMB systems [PRv+06].

Most industrial AMB systems are controlled by PID-controllers because of their simple structure and transparent design [PRv+06]. Nowadays, rotor systems are more complex (because of higher energy density, higher speed, more complex rotor structure, etc.). A classical PID-controller with only three parameters (K_P, T_n, and T_v) can hardly achieve various requirements, therefore a more complex controller structure is necessary, e.g., PID-controller with notch, lead-lag, and low-pass filters. Consequently, this extended PID-controller structure can also be described as a complex transfer function of higher order. This complicates the controller design. Experience is required to tune the controller parameters, thus the design procedure has to be realized iteratively and is therefore time-consuming.

By using optimization approaches for controller design, additional complex criteria in the time and frequency domains can be considered. The designer is able to use this advantage to integrate system-, sensor-, actuator-, and requirement-specific criteria. The key to dealing with such a complex design, with a large number of design parameters as well as criteria to be fulfilled, is the utilization of a heuristic multi-objective optimization algorithm, such as the Multi-Objective Genetic Algorithm (MOGA). An advantage is that the MOGA allows one to solve a multi-objective optimization problem with little

knowledge or information about the objective system to be optimized. The MOGA has been applied successfully to diverse engineering optimization problems as well as controller design tasks and the optimization of AMB systems. In [SCFG97] a PID-controller design has been applied to a Rolls-Royce turbo-machine supported by AMBs. The structure and controller parameters were optimized by using the MOGA. The nondominated sorting genetic algorithm (NSGA-II, a variant of the MOGA) has been applied to tune parameters of a classic PID-controller for a magnetic levitation system [PY06].

Genetic and other heuristic algorithms (such as simulated annealing, ant colony optimization, and particle swarm optimization) do not guarantee either a global or local optimal solution. Therefore, the main task that remains is how to apply these heuristic algorithms to find a good solution.

When using the MOGA, different criteria of the optimization problem are formulated as objectives (integrated in the so-called fitness functions). Some of these criteria can be considered to be constraints. The optimization problem can be solved quite efficiently with well-defined fitness functions as well as their evaluation process, but it may also fail because of non-convergence.

Another challenge arising from the control problem is the requirement for closed-loop stability. Often the feasible region (in which the closed loop of the controlled system is stable) is small with respect to the search space of the controller parameters. This can lead to a non-convergence in optimization. As a consequence, the optimization may fail after a predefined number of attempts (or generations as termination criterion).

The number of controller parameters to be designed and optimized also appears as a challenge. More design parameters allow more Degrees of Freedom (DoFs) for system design and optimization, but also increase the optimization complexity. Not all design parameters have a strong influence on the optimization results. Such parameters may therefore be neglected in the optimization process.

1.1.2 Goal of the Thesis

Controller design for AMB systems by means of hand tuning is time-consuming and requires expert knowledge. The first goal of the thesis is, therefore, trying to reduce the effort to tune the controller parameters by using multi-objective optimization algorithms. Controller design criteria for AMB systems shall be provided, which shall cover objectives and/or constraints in time and frequency domains.

The second goal of the thesis is to develop optimization strategies to overcome the diffi-

culties in using MOEAs/MOGAs for controller design of AMB systems. This intends to accelerate the optimization process and prevent optimization algorithms from premature and failure to solve the optimization tasks.

Finally, for validation purpose experimental tests have to be performed. Controller design obtained from optimization algorithms shall be validated by comparing simulation results with experimental results.

1.2 Structure of this Thesis

This thesis is organized as follows:

In Chapter 2, a review of magnetic bearing technique is provided with focus on controller design, self-sensing, backup bearing, and application.

In Chapter 3, the physical model of AMB actuator is developed. Modeling of fexible rotors and model reduction techniques are then introduced. The plant including rotor system, AMB actuators, and sensors is then provided in state-space representation for control design purpose. In the end, the two AMB systems considered in this contribution are introduced.

In Chapter 4, two control configuration are introduced: decentralized and centralized control configuration. A general structure of PID-controller is described. It includes a PID-part connecting with different filters, e.g. low-pass and notch filters. The controller design for the two AMB systems are then introduced. Controller design criteria both in time and frequency domain are then presented.

In Chapter 5, optimization with focus on multi-objective optimization is introduced. Various heuristic optimization algorithms are reviewed. The difficulties in using multi-objective optimization algorithms especially for controller design are discussed in detail. The detailed optimization strategy to overcome these difficulties is then presented, which is the core of this contribution. The optimization results for the controller design of the two AMB systems are discussed.

In Chapter 6, experimental results for the first AMB system concerning the performance of the selected controller candidates are presented and compared with the simulation results for validation.

Finally, a summary is given in Chapter 7.

Chapter 2

Review of Magnetic Bearing Technique

According to the last three conferences of International Symposium on Magnetic Bearings (ISMBs), activities in the area of magnetic bearing techniques focus on the following aspects:

- controller design,
- self-sensing,
- backup bearing, and
- application.

In the following, a brief overview of magnetic beaing technique with the focus on the above aspects is given.

2.1 Controller Design

The inherent negative stiffness of AMB systems causes instability. A feedback control loop becomes necessary to stabilize the rotor system and to achieve high performance. Different control methods are successfully applied to control of magnetic bearing systems.

The classical PID-control methods are widely used in AMB systems due to their structure and transparent design. In many applications, they can fulfill the operating requirements [BGH+94] and there is not necessary to replace PID-controllers with other complex control algorithms. In [Ble84], a method to design optimal decentralized PD controllers

for AMB systems by solving Riccati equation is given. Analogously, Lang [Lan97] uses the design approach of Linear Quadratic Regulator (LQR) to calculate the optimal parameters of a PID-controller. In [WKA90], a design procedure of a digital Proportional-Integral-Derivative-Derivative (PIDD) controller is reported. A simple design approach for a cascade PI/PD controller is given in [PRv+06]. The proposed cascade PI/PD controller shows superior results compared with conventional PID control.

Optimal control calcuates the feedback law $\mathbf{u} = -\mathbf{K}\mathbf{x}$ by minimizing a quadratic cost function

$$J = \int_0^\infty (\mathbf{x}^T\mathbf{Q}\mathbf{x} + \mathbf{u}^T\mathbf{R}\mathbf{u})dt,$$

with the state vector $\mathbf{x}$ of a plant, the input vector $\mathbf{u}$, feedback gain matrix $\mathbf{K}$, and weighting matrices $\mathbf{Q}$ and $\mathbf{R}$. The minimization problem is solved by solving the Riccati equation. By minimizing the cost function, this method obtains the optimal (high performance) solution concerning control energy and control error. The tradeoff between control energy and control error is adjusted by selection of the weighting matrices $\mathbf{R}$ and $\mathbf{Q}$. A drawback of this method is that the robustness properties are not explicitly taken into account and that all states are needed to be used for feedback (therefore, an observer becomes necessary). Optimal control has been discussed and applied to magnetic bearing system in the early 1980s. Linear Quadratic (LQ)-controller applied to AMB system is repored in [Ant84]. Specially, output feedback control design by mininizing the same quadratic cost function is discussed. In [Ulb79], a LQ-controller with observer is designed and realized in a test rig supported by two AMBs. It shows that the LQ-controller with observer achieves a clearly better dynamic behavior of the system than the one with a differentiator because of sensor noise. In [Sal87], different methods are introduced to determine optimal output feedback controller. This controller is defined based on a simplified system model and guarantees robustness related to spillover effect due to neglecting high-order dynamics of the real system. The suggested methods are used to design controller for two AMB systems. The performance is validated with experimental tests. Genetic algorithm is applied in [JP09] to optimize LQ-controllers. The simulation and experimental results with LQ-controllers show a better performance compared with the ones with PID and cascade PI/PD controllers. Analogously, superior results obtained by LQ-controller are illustrated in [SB08] with the help of step response and impulse response compared with a PID-controller.

Robust control methods are developed to cover up some drawbacks of LQ methods, focusing on both performance and robustness of the controlled system. Those methods try to minimize the H_∞ norm of weighted transfer function matrix. The aspects relating to performance and robustness can be directly introduced in the minimization with the help of the weighting matrices. However those methods result in high order controller which can

cause implementation problems due to hardware limitations. Weighting functions have to be carefully tuned. In [Sch03] μ-synthesis controller is designed and implemented on a flywheel system supported by two AMBs. Experimental results show that the specified performances, e.g. robustness to gyroscopic effect, are achieved with the μ-synthesis controller. In [Lös02] an automated μ-synthesis controller design procedure for AMB-systems is suggested. The suggested approach is applied to design controllers for a test rig with three rotor configurations. Satisfactory experimental results are obtained. The design time is significantly reduced, the final controllers for each rotor configuration are obtained within two hours, additionally, neither an initial rotor model nor a startup controller is required for controller design. In [MLA12] a test rig designed to investigate rotordynamic instability due to aerodynamic loads (i.e. seal forces) is supported by two AMBs, which are controlled by μ-synthesis controller. Two additional AMBs are used to excite the rotor with simulated aerodynamic loads. Compared with traditional PID-control, the μ-synthesis controller shows an improved stability and performance. The test rig operates successfully up to a speed of 3200 rpm. In [Pes13] a μ-synthesis controller is designed for controlling an industry machining spindle supported by AMBs. In this work, especially the chatter effect is considered in the controller design by introducing a cutting force model in the synthesis process. The chatter avoiding controller is compared with a dynamic stiffness μ-synthesis controller, which is designed to maximize the tool's dynamic stiffness. Simulation results show the chatter avoiding controller is better in terms of improving the critical chatter limit than the dynamic stiffness controller. The measured frequency response at tool location shows that a larger critical cutting stiffness is achieved with the chatter avoiding controller in comparison to the dynamic stiffness controller. The initial levitation behavior is measured. It shows the control current reaches its limited value during the liftoff process, i.e. ± 4 A. This indicates that an instable behavior might occur during a real machining process because a very high and suddenly changing cutting force is expected in a real machining process. The proposed chatter avoiding μ-synthesis is of order 74. Althougth the controller is reduced to an order of 44 for implementation, the controller order might be a problem for industry application.

It should be noted that, beside the methods mentioned above, other control methods have also been applied to control AMB systems, such as fuzzy control [HL00, DZJG10], sliding mode control [CW10, RDD96], etc.

2.2 Self-Sensing AMBs

Self-sensing or sensorless AMBs is refered to the technique that the position signal of a rotor in magnetic bearing systems is estimated by using the available signals in the electromagnets, e.g., coil currents and voltages. In such systems, the traditional position sensing devices, which is associated with high cost, is entirely eliminated. The main advantages can be summarized as follows [Noh96, BCK+09]:

- reducing the cost,
- enabling a more compact design by eliminating sensors and the related cables,
- increasing reliability, i.e. the failure of the magnetic bearing system caused by sensor defect is removed, and
- removing the difficulties in stabilizing the AMB system due to sensor/actuator non-collocation.

There are two mainstream methods to estimate position signal in self-sensing AMBs [Noh96]:

- Observer technique is used to reconstruct the displacement and velocity signals by using the only measured current signal [VB93]. A LQ-controller can be then used to control AMB system.
- The air gap between rotor and electromagnets is considered as a system parameter. The relation between the voltage, current, and air gap signals can be considered as a modulation process. Switching amplifier generates a high frequency bi-state voltage signal. The air gap displacement signal (a low frequency signal) modulates the voltage signal and the resulting signal is the current signal, which is a switching waveform. In [OMN92], demodulation technique is used to estimate the displacement signal. In a similar manner, Noh and Maslen [Noh96] use a forward path filter in an estimator to estimate the displacement signal. In [Skr04] impedance is used to calculate the rotor position. The magnitude of the impedance $|Z|$ of a magnet with coil current i and voltage u is determined by

$$|Z| = \frac{|u|}{|i|} = |R + j\omega L| = \sqrt{R^2 + \omega^2 L^2},$$

with the coil resistance R and the inductance L. Hereby only the high-frequency part of the measured coil current and voltage signal, which has a frequency of the

switching frequency ω of the amplifier, is used. The air gap s_g can be then calculated as

$$s_g = 2k_M\omega|Z|\frac{1}{\sqrt{1-R^2|Z|}},$$

where the parameter k_M denotes the magnetic bearing constant. The nonlinearities including magnetic saturation effect and magnetic cross-coupling effect are considered in [Skr04]. Both effects degrade the quality of position identification.

A main drawback of self-sensing AMBs is their poor robustness. The word "robustness" defines the ability of a controller to tolerate uncertainties from the system to be controlled. In [TS02, BCK+09] it is shown that achievable robustness is limited due to the presence of a pair of zero and pole on the right half s-plane. In their analysis the self-sensing AMB system is considered as a Linear-Time-Invariant (LTI) model. Robustness can be however improved by using a Linear-Periodic (LP) model [MMI06].

2.3 Backup Bearing

Backup bearings (also called retainer bearings, auxiliary bearings, or touchdown bearings in the literature) prevent the destruction of the AMB system and even the machine in case of an emergency, e.g., overloading, power or components failure. In this emergency situation, a complex interaction between the high speed rotor and the backup bearings arises, which consists of nonlinear Hertzian contact, friction, and chaotic motion. As a worst case, backward whirl can appear which results in an unstable vibration of the rotor system and can lead to the destruction of the system [Xie09]. There are three types of backup bearings [Kär07]: bushing type backup bearings, rolling element bearings, and the combination of the bushing and rolling element types of bearings. Ball bearings are the most frequently used as backup bearings [Fum97]. The inner race of the rolling element bearings can be rapidly accelerated to the rotor speed, therefore, to prevent the whirl motion of the rotor [Fum97].

Because of the complexity of the interaction between the backup bearings and the rotor, research up to now mostly focuses on building a reliable model of the backup bearing and validating the model by comparing with experimental results. In [Fum97], a contact model is presented, which is derived based on Hertz theory and focuses on the initial impact behavior after the drop-down of a rotor. To verify the contact model, experiments are performed. Different types of bearings including ball bearings are measured. Based on the measurements, the parameters of the contact model is determined. Detailed simulation

models for ball bearings are given in [Kär07]. The models include damping and stiffness properties, oil film, inertia of rolling elements, and friction. The models are verified by comparing with measurements. In the measurement, it is observed that misalignment of the backup bearings has a great influence on the stability of rotor motion, specifically in case of a vertical misalignment. In [Xie09] a detailed model of backup bearings including a tolerance ring installed between stator and ball bearing is introduced. This tolerance ring provides a soft mounting stiffness to avoid a hard landing of the rotor after drop-down and to recenter the backup bearing after the interaction between the rotor and the bearing. In the simulation model, the discontinuous stiffness due to bearing clearance effects, the nonlinear Hertzian contact and Coulomb friction forces are taken into acount. Important parameters of the model are estimated by analysing experimental results. In the experiments, three types of motion of the rotor after drop-down are observed: spring motion, oscillatory motion, and backward whirl motion.

Active backup bearings are also reported in the literature. In [GU08] an active backup bearing is reported. The backup bearing is controlled to minimize the contact force. Experimental results show that the contact forces in case with control are reduced up to 85% compared with the one without control. A design of an active backup bearing system is reported in [KSBC08]. In the backup bearing systems, piezoelectric actuators are used to adjust the backup bearing parameters and to make the backup bearing to execute synchronous forward whirl orbit. Simulation results show that contact-free motion can be recovered by inducing a forward synchronous whirl motion of the backup bearing. It is assumed that the magnetic bearing system is functional but shortly overloaded and it leads to a rotor/bearing contact.

2.4 Application

Various applications that utilize AMBs have been reported in the literature. Spindles with high rotational speed and high precision position control can be obtained when using magnetic bearings. For tool machine spindles, this reduces the cutting time and improves the surface quality of workpieces. High-Speed-Cutting (HSC) spindles are typically used for aluminum and plastic materials. The HSC-spindle prototype discussed in [Sie89] reaches a cutting rate of up to 6000 m/min with a maximum speed of 40000 rpm and a power of 35 kW. In the subsea environment, maintenance cannot be carried out frequently and robustness must be guaranteed for long-term operation. AMBs are the best choice to fulfill these requirements. A subsea motorcompressor equipped with AMBs (three radial bearings and one axial bearing) is presented in [MVL+10]. The motor compressor (power of

12.5 MW and speed of 11000 rpm) has a 2270 kg rotor that is 3.8 m long. In some applications, the compressor requires a wide operating speed range. It is difficult to achieve high performance in terms of damping over the entire operating range by using conventional bearings, but this can be achieved by using AMBs with carefully-tuned controllers. A centrifugal compressor supported by AMBs and driven by a 23 MW motor has been reported on in [NSS99]. It operates from 600 to 6300 rpm. Flywheel is used as an energy storage device, e.g., for satellites. The stored energy in a flywheel is proportional to the square of the rotational speed, Ω^2. To achieve high energy density, the flywheel must rotate with a very high speed. In combination with the high circumferential speed, this leads to high energy losses because of air friction. Therefore, ideally, the flywheel should operate in a vacuum. Magnetic bearings have found a natural application in vacuum environments because they are oil-free and are capable of achieving a high rotational speed. The design of a flywheel system supported by AMBs is discussed in [Ahr96]. The useful energy stored in the flywheel system reaches up to 1 kWh with 250 kW of power. An AMB-supported flywheel system [NRK$^+$08] has also been used in an electric vehicle to replace conventional battery power systems. Other applications include blood pumps [Pet06, CCD$^+$08], turbomolecular pumps [Pet06], and system identification [WS97].

Chapter 3

Modeling of AMB System

In this chapter, the work principle of AMB systems is introduced, then the modeling of AMB systems is briefly summarized. In the end, the two AMB systems considered in this contribution are introduced.

3.1 Introduction of AMB System

An AMB system contains the rotor system to be controlled, sensors, Analog-to-Digital (AD)-converters, controllers, Digital-to-Analog (DA)-converters, amplifiers, and actuators. A schematic diagram of an AMB system is illustrated in Figure 3.1. The operation principle can be easily explained with the help of the schematic diagram: The sensor measures the position of the rotor. The analog sensor siginal is transformed into digital signal with the help of an AD-converter and then sent to the controller, which is implemented in a Digital-Signal-Processing (DSP) unit. The controller compares the measured signal with a predefined reference signal and adjusts the current of the magnet coil through the amplifier, consequently, the magnet generates a proper magnetic force depending on the coil-current to hold the rotor in the position as the defined reference signal. In the proceeding section, the modeling of the elements of AMB system is given.

3.2 Active Magnetic Bearing

Active Magnetic Bearing (AMB) supports a load without physical contact by using magnetic levitation, for example, they can levitate a rotating shaft and permit relative motion without friction or wear. They are in service in such industrial applications as electric

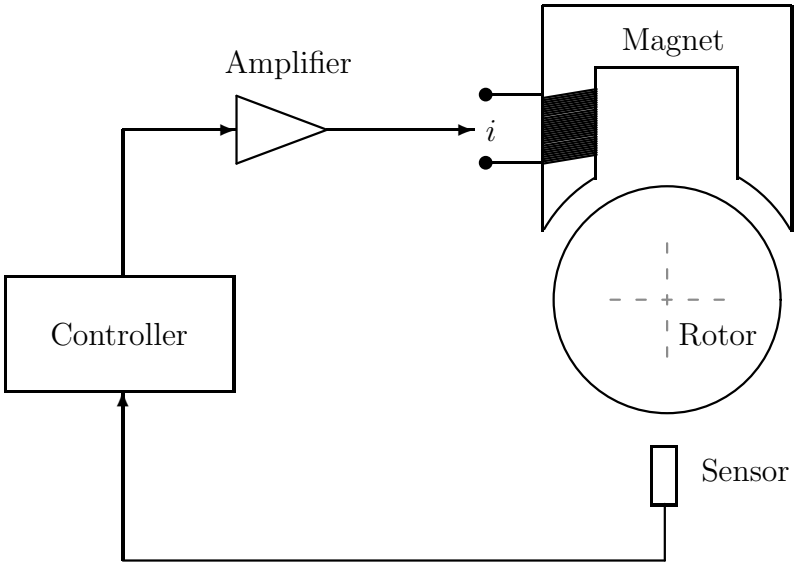

Figure 3.1: *Schematic diagram of an AMB system*

power generation, petroleum refining, machine tool operation, and natural gas pipeline compressors.

In the following section, modeling of the magnetic bearing will be addressed.

3.2.1 Physical Basics of Electromagnets

The magnetic field is usually described by the magnetic flux density B, measured in Tesla, and the magnetic field strength H in $[A/m]$. The relation between them is

$$B = \mu H, \tag{3.1}$$

$$\mu = \mu_0 \, \mu_\mathrm{r}, \quad \text{and} \tag{3.2}$$

$$\mu_0 = 4\pi \times 10^{-7} \frac{Vs}{Am}. \tag{3.3}$$

The parameter μ is called permeability, and the parameter μ_r (usually $\mu_\mathrm{r} \geq 1$) is known as relative permeability depending on the medium which the magnetic field acts upon. In vacuum, the permeability $\mu = \mu_0$ (i.e. $\mu_\mathrm{r} = 1$) is constant as described in Eq. 3.3. As the case of magnetic bearing, ferromagnetic material is usually used, where $\mu_r \gg 1$.

The relation between the magnetic flux density and the magnetic field strength for a ferromagnetic material can be visualized in a magnetic hysteresis loop (see Figure 3.2). For small values of H, the magnetisation curve (also called $B-H$ curve) can be treated as linear, and hysteresis effects are neglected, i.e. $\mu_{\mathrm{r}}(H) = const.$ Increasing the magnetic field strength, the magnetic flux density B will follow the $B-H$ curve up to point 1 where further increasing in magnetic field strength will result in no further change in flux density. This condition is called magnetic saturation, and the corresponding current $i_{\max}$ is called saturation current. It leads to the limitation of load capacity of magnetic bearings. Reduing the magnetic field strength to zero, the magnetic flux density will go along the $B-H$ curve from point 1 to 2 and it will stay at point 2 due to the remaining magnetism, although the magnetic field strength is zero. To bring the flux density to zero (from point 2 to 3), it has to apply a negative magnetic field. Continuing to increase the strength of the negative magnetic field, the flux density will become negative and reach the saturation point 4. The flux density B will go from point 4 to 1 by reducing the negative field strength and applying a positive magnetic field. This magnetising process forms a magnetic hysteresis loop as shown in Figure 3.2.

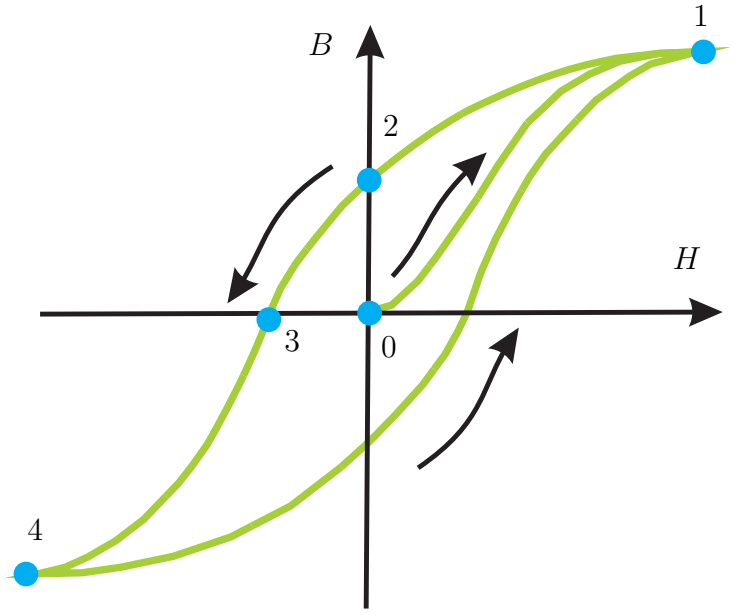

Figure 3.2: *Qualitative illustration of a magnetic hysteresis loop*

The magnetic field can be generated by a current, or a permanent magnet. For instance, a rotation-symmetrical magnetic field H is generated around a straight conductor with a constant current, i. The contour integral around the conductor gives

$$\oint H ds = i. \tag{3.4}$$

The magnetic field is independent on the medium around the conductor. For a coil with n turns (n: number of turns), the integral contour surrounds all n-turns of the coil. The integral gives

$$\oint Hds = ni. \tag{3.5}$$

Magnetic forces developed in magnetic field can be calculated by using *Principle of Virtual Work for Applied Forces*

$$\delta W - \delta U = 0, \tag{3.6}$$

with

$$\delta W = \sum_i f_i \, \delta r_i + \sum_j M_j \, \delta \varphi_j,$$

where δW and δU denote the virtual work and the potential energy, respectively. Parameters f_i and M_j denote the external force and moment associated with the virtual displacement δr_i and $\delta \varphi_j$, respectively.

3.2.2 Magnetic Forces

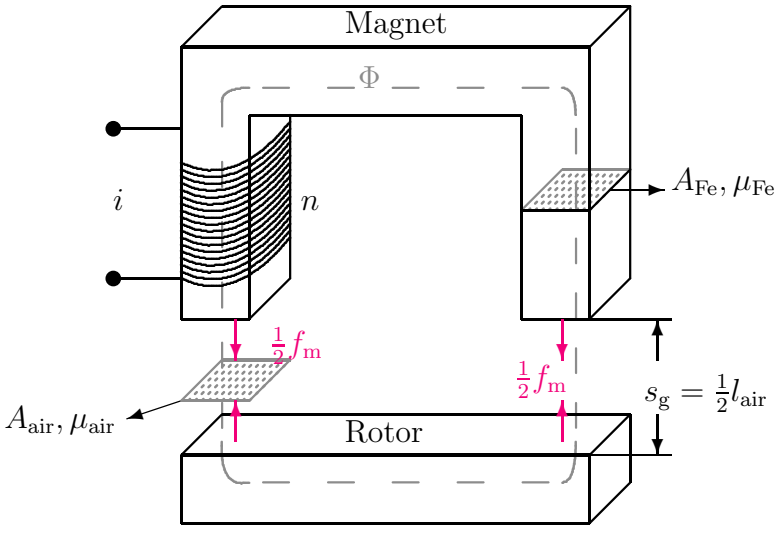

Figure 3.3: *Magnetic actuator*

In order to derive the magnetic forces of a magnetic bearing, one can use the simplified magnetic bearing configuration as shown in Figure 3.3. It consists of a single two-pole magnetic bearing element. It is assumed that the flux density B along the path of the

magnetic flux Φ is constant (i.e. $B_{\mathrm{Fe}} = B_{\mathrm{air}} = const.$). The integral along the path of the magnetic flux Φ yields

$$H_{\mathrm{Fe}}\, l_{\mathrm{Fe}} + H_{\mathrm{air}}\, l_{\mathrm{air}} = ni, \tag{3.7}$$

where i denotes the coil current and n denotes the number of turns of the coil.

The magnetic field strength in iron is neglected (i.e. $H_{\mathrm{Fe}} = 0$) because of $\mu_{\mathrm{r}} \gg 1$ for ferromagnetic material. It leads to

$$H_{\mathrm{air}} = \frac{ni}{l_{\mathrm{air}}}. \tag{3.8}$$

With Eq. 3.3 and $\mu_{\mathrm{r}} \approx 1$ for air, it can be obtained

$$B_{\mathrm{air}} = \mu_0 H_{\mathrm{air}} = \mu_0 \frac{ni}{l_{\mathrm{air}}}. \tag{3.9}$$

With Eqs. 3.8 and 3.9, the magnetic field energy (potential energy) stored in the air gap is given by

$$U_{\mathrm{air}} = -\frac{1}{2}\int_{V_{\mathrm{air}}} B_{\mathrm{air}}\, H_{\mathrm{air}}\, dV_{\mathrm{air}} = -\frac{1}{2} B_{\mathrm{air}}\, H_{\mathrm{air}}\, V_{\mathrm{air}} = -\frac{\mu_0 A_{\mathrm{air}} n^2}{4}\, \frac{i^2}{s_{\mathrm{g}}}, \tag{3.10}$$

with $s_{\mathrm{g}} = \frac{1}{2} l_{\mathrm{air}}$.

Using the *Principle of Virtual Work for Applied Forces* , i.e. Eq. 3.6, the magnetic force can be expressed as

$$f_{\mathrm{m}} = \frac{\partial U_{\mathrm{air}}}{\partial s_{\mathrm{g}}} = \frac{\mu_0 A_{\mathrm{air}} n^2}{4} \left(\frac{i}{s_{\mathrm{g}}}\right)^2. \tag{3.11}$$

In case of a radial bearing magnet, the force of both magnetic poles act onto the rotor

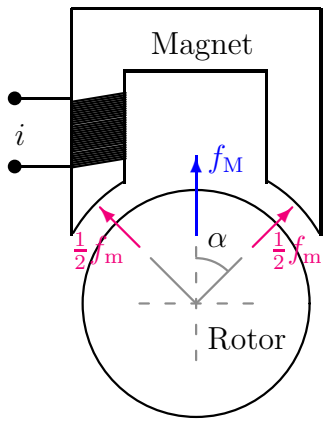

Figure 3.4: *Radial bearing geometry*

with an angle α (see Figure 3.4), the sum of both forces gives

$$f_{\mathrm{M}} = f_{\mathrm{m}} \cos\alpha = \frac{\mu_0 A_{\mathrm{air}} n^2}{4} \cos\alpha \left(\frac{i}{s_{\mathrm{g}}}\right)^2 = k \cos\alpha \left(\frac{i}{s_{\mathrm{g}}}\right)^2, \tag{3.12}$$

with

$$k = \frac{\mu_0 A_{\mathrm{air}} n^2}{4}. \tag{3.13}$$

Magnetic force (Eq. 3.12) is obviously nonlinearly related to coil current and air gap. It can be linearized around a nominal working point with the nominal air gap s_0 and the so-called bias current i_0. With the definitions

$$i_x = i - i_0,$$

and

$$x \cos\alpha = s_0 - s_{\mathrm{g}},$$

it can then be rewritten as

$$f_{\mathrm{M}} = k \cos\alpha \left(\frac{i_0 + i_x}{s_0 - x\cos\alpha}\right)^2. \tag{3.14}$$

With Taylor-expansion, it gives

$$\begin{aligned} f_{\mathrm{M,lin}}(i_x, x) =& f_{\mathrm{M}}|_{i_{x_0}, x_0} + \frac{\partial f_{\mathrm{M}}}{\partial i_x}|_{i_{x_0}, x_0}(i_x - i_{x0}) \\ &+ \frac{\partial f_{\mathrm{M}}}{\partial x}|_{i_{x_0}, x_0}(x - x_0) + O(i_x^2, x^2). \end{aligned} \tag{3.15}$$

It is admissible to neglect the higher order terms $O(i_x^2, x^2)$ since only small deflections around the working point (i_{x_0}, x_0) are allowed. Let $i_{x_0} = 0,\ x_0 = 0$ and neglecting the higher order terms, it yields

$$f_{\mathrm{M,lin}}(i_x, x) = k \cos\alpha \left(\frac{i_0}{s_0}\right)^2 + 2k \cos\alpha \frac{i_0}{s_0^2} i_x + 2k \frac{i_0^2}{s_0^3} \cos^2\alpha\ x. \tag{3.16}$$

From Eq. 3.16, it is known that the magnetic force is linearly related to the displacement x and the current i_x with respect to the working point. Both coefficients relating to displacement and current can be adjusted by modifying bias current i_0 and nominal air gap s_0. For a certain magnetic bearing system, air gap s_0 is normally fixed, hence, bias current i_0 can be used to modify the magnetic bearing coefficients.

A single electromagnet as shown in Figure 3.4 has a disadvantage, namely, it can only produce a pull-force. Fortunately, for magnetic bearing this disadvantage can be eliminated

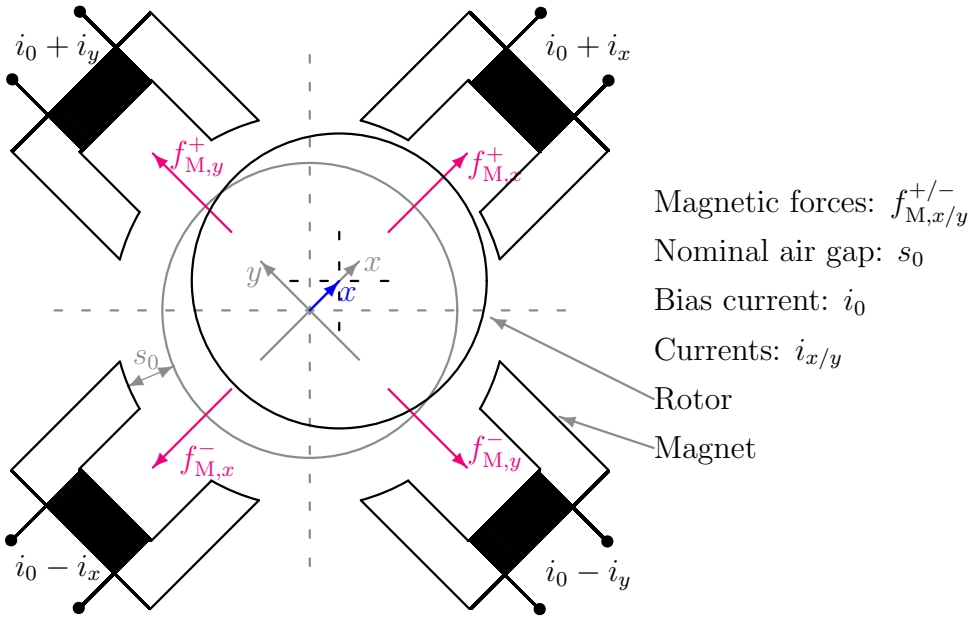

Figure 3.5: *A typical arrangement of magnets in a radial magnetic bearing with differential drive configuration [WS10, WS11, WS12a]*

by a pair of oppositely arranged magnets which are used in combination to provide forces in two opposite directions.

A typical arrangement of magnets in a radial magnetic bearing is illustated in Figure 3.5. The bearing consists of two pairs of magnets. Each pair of magnets are responsible for genenating a magnetic force in x- or y-directon (either in positive or negative direction). Additionally, a bias current i_0 is added to each magnet-pair. This configuration is known as differential drive configuration. This configuration partially linearizes the force-current relation of the magnetic bearing as it will be shown in below.

From Eq. 3.14, the magnetic force (exerted on the rotor) in x-direction then can be written as

$$f_x = f^+_{\mathrm{M},x} - f^-_{\mathrm{M},x} = k\cos\alpha\left(\left(\frac{i_0 + i_x}{s_0 - x\cos\alpha}\right)^2 - \left(\frac{i_0 - i_x}{s_0 + x\cos\alpha}\right)^2\right). \tag{3.17}$$

Again, the magnetic force can be linearized and it gives

$$f_x = k_\mathrm{i} i_x + k_\mathrm{s} x, \tag{3.18}$$

with

$$k_\mathrm{i} = \frac{\partial f}{\partial i_x}|_{i_{x_0}, x_0 = 0} = 4k\frac{i_0}{s_0^2}\cos\alpha, \tag{3.19}$$

and

$$k_{\mathrm{s}} = \frac{\partial f}{\partial x}|_{i_{x_0},x_0=0} = 4k\frac{i_0^2}{s_0^3}\cos^2\alpha. \tag{3.20}$$

The above derived magnetic force (Eqs. 3.17—3.20) is valid only under the assumption that the rotor is centered between the pair of magnets. As mentioned above, the nominal gap s_0 is fixed by the geometry of the rotor-bearing system. The magnetic bearing coefficients k_{i} and k_{s} are normally adjusted by modifying bias current i_0. In principle, the bearing coefficients of each axis can be adjusted, individually. However, in almost all practical applications, the both axes (x and y) of a radial magnetic bearing are designed to have identical coefficients, i.e. $k_{\mathrm{s},x} = k_{\mathrm{s},y} = k_{\mathrm{s}}$ and $k_{\mathrm{i},x} = k_{\mathrm{i},y} = k_{\mathrm{i}}$.

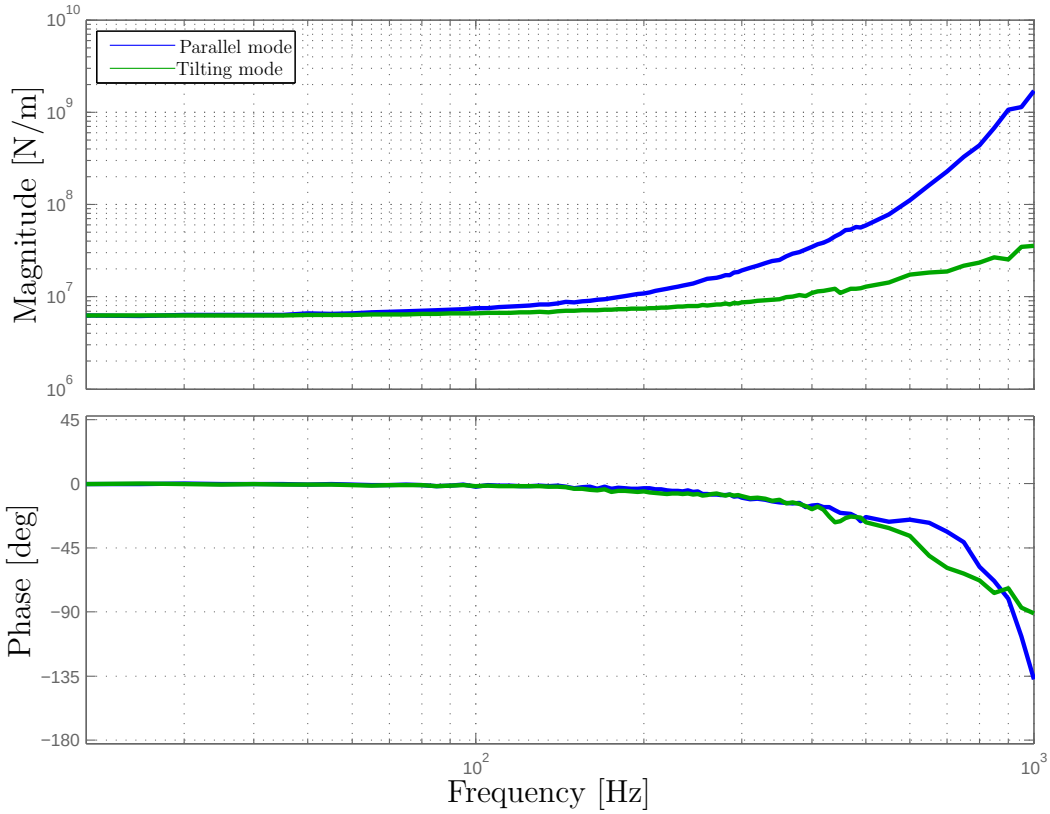

Figure 3.6: *Transfer functions of bearing coefficient k_s for the first AMB system with bias current $i_0 = 7A$*

Although, k_{s} and k_{i} are considered as constants, they can be modeled as frequency-dependent coefficients in the form of tranfer functions, in which nonlinear effects like eddy current losses, hysteresis, windage losses, etc., can be partially considered. For instance, in Figure 3.6 the transfer functions of k_{s} of both parallel and tilting modes for the first

AMB system (see Section 3.5.1) are shown. At low frequencies, k_s remains approximately constant, however, starting from the frequency of 100 Hz, the magnitude of k_s for both parallel and tilting modes goes up while the phase decreases.

3.2.3 State-Space Model

State-space model is used for controller design purpose. A state-space model is a mathematical representation of a dynamical system in form of

$$\begin{aligned} \dot{\mathbf{x}} &= \mathbf{A}\mathbf{x} + \mathbf{B}\mathbf{u}, \\ \mathbf{y} &= \mathbf{C}\mathbf{x} + \mathbf{D}\mathbf{u}, \end{aligned} \tag{3.21}$$

with:

A:	System matrix,	**B**:	Input matrix,
C:	Output matrix,	**D**:	Feedforward matrix,
x:	System state vector,	**y**:	Output vector, and
u:	Input vector.		

In the following a state-space model [BCK+09] for AMB systems is introduced. It should be noted that a system can be modeled with different state-space models, which all represent the same system.

Referring to Figure 3.3, the magnet circuit is governed by

$$u = Ri + n\frac{\partial \Phi}{\partial t}, \tag{3.22}$$

with

$$\Phi = BA_{\text{air}}.$$

It can be rewritten as

$$nA_{\text{air}}\frac{\partial B}{\partial t} = u - iR. \tag{3.23}$$

With Eq. 3.9 and $s_0 = \frac{1}{2}l_{\text{air}}$, for the pair of electromagnets in x-direction as shown in Figure 3.5, one obtains

$$nA_{\text{air}}\frac{\partial B_x^+}{\partial t} = u_x^+ - i_x^+ R = u_x^+ - \frac{2(s_0 - x\cos\alpha)R}{\mu_0 n^2 A_{\text{air}}} nAB_x^+, \tag{3.24a}$$

$$nA_{\text{air}}\frac{\partial B_x^-}{\partial t} = u_x^- - i_x^- R = u_x^- - \frac{2(s_0 + x\cos\alpha)R}{\mu_0 n^2 A_{\text{air}}} nAB_x^-. \tag{3.24b}$$

Subtracting Eq. 3.24b from Eq. 3.24a yields

$$\frac{\partial(B_x^+ - B_x^-)}{\partial t} = -\frac{2s_0 R}{\mu_0 n^2 A_{\text{air}}}(B_x^+ - B_x^-) + \frac{2x\cos\alpha R}{\mu_0 n^2 A_{\text{air}}}(B_x^+ + B_x^-) + \frac{u_x^+ - u_x^-}{nA_{\text{air}}}. \tag{3.25}$$

With Eq. 3.9 and $s_0 = \frac{1}{2}l_{\text{air}}$, the nominal inductance can be rewitten as

$$L = n\frac{\partial\Phi}{\partial i} = nA_{\text{air}}\frac{\partial B}{\partial i} = \frac{\mu_0 n^2 A_{\text{air}}}{2s_0}. \tag{3.26}$$

Multipling Eq. 3.25 by $\frac{s_0}{\mu_0 n}$ and inserting Eq. 3.26 gives

$$\begin{aligned}\frac{\partial}{\partial t}\underbrace{\left(\frac{s_0}{\mu_0 n}(B_x^+ - B_x^-)\right)}_{x_m} = &-\underbrace{\frac{2s_0}{\mu_0 n^2 A_{\text{air}}}}_{\frac{1}{L}} R\,\underbrace{\frac{s_0}{\mu_0 n}(B_x^+ - B_x^-)}_{x_m} \\ &+\underbrace{\frac{2s_0}{\mu_0 n^2 A_{\text{air}}}}_{\frac{1}{L}}\frac{R\cos\alpha}{s_0}\,x\,\underbrace{\frac{s_0}{\mu_0 n}(B_x^+ + B_x^-)}_{x_n} \\ &+\underbrace{\frac{2s_0}{\mu_0 n^2 A_{\text{air}}}}_{\frac{1}{L}}\underbrace{\frac{1}{2}(u_x^+ - u_x^-)}_{u_x}.\end{aligned}$$

It follows

$$\frac{\partial}{\partial t}x_m = -\frac{R}{L}x_m + \frac{R\cos\alpha}{Ls_0}x\;x_n + \frac{1}{L}u_x, \tag{3.27}$$

with the defined variables

$$\begin{array}{llllll} x_m &=& \frac{s_0}{\mu_0 n}(B_x^+ - B_x^-), & x_n &=& \frac{s_0}{\mu_0 n}(B_x^+ + B_x^-), \\ u_x &=& \frac{1}{2}(u_x^+ - u_x^-), & u_0 &=& \frac{1}{2}(u_x^+ + u_x^-), \\ i_x &=& \frac{1}{2}(i_x^+ - i_x^-), \quad \text{and} & i_0 &=& \frac{1}{2}(i_x^+ + i_x^-). \end{array}$$

It should be noted that the parameter i_0 is bias current as defined previously and the parameter u_0 is the bias voltage of the magnetic bearing.

Recalling Eq. 3.9, it can be simply obtained

$$i_x = x_m - \frac{\cos\alpha}{s_0}x\;x_n, \tag{3.28a}$$

$$i_0 = x_n - \frac{\cos\alpha}{s_0}x\;x_m. \tag{3.28b}$$

Recalling Eq. 3.11, the net magnetic force for the pair of magnets can be written as

$$f_x = \frac{A_{\text{air}} \cos\alpha}{\mu_0 n}(B_x^{+2} - B_x^{-2}) = \frac{\mu_0 n^2 A_{\text{air}} \cos\alpha}{s_0^2} x_n \, x_m. \tag{3.29}$$

Linearizing the Eqs. 3.27, 3.28, and 3.29 around the working point ($x_m = 0$, $x_n = X_n$) gives

$$\frac{\partial}{\partial t} x_m = -\frac{R}{L} x_m + \frac{R \cos\alpha X_n}{L s_0} x + \frac{1}{L} u_x, \tag{3.30a}$$

$$i_x = x_m - \frac{\cos\alpha}{s_0} X_n \, x, \tag{3.30b}$$

$$i_0 = x_n, \quad \text{and} \tag{3.30c}$$

$$f_x = \frac{\mu_0 n^2 A_{\text{air}} \cos\alpha}{s_0^2} x_n \, x_m. \tag{3.30d}$$

Substituting the parameters k_{i} and k_{s} as defined in Eqs. 3.19 and 3.20, it gives

$$\frac{\partial}{\partial t} x_m = -\frac{R}{L} x_m + \frac{R k_{\text{s}}}{L k_{\text{i}}} x + \frac{1}{L} u_x, \tag{3.31a}$$

$$i_x = x_m - \frac{k_{\text{s}}}{k_{\text{i}}} x, \tag{3.31b}$$

$$i_0 = x_n, \quad \text{and} \tag{3.31c}$$

$$f_x = k_{\text{i}} \, x_m. \tag{3.31d}$$

For the underlying current control configuration [Hir03], the actual current difference i_x is fed back to a current controller, which usually is a P-controller as shown in Figure 3.7.

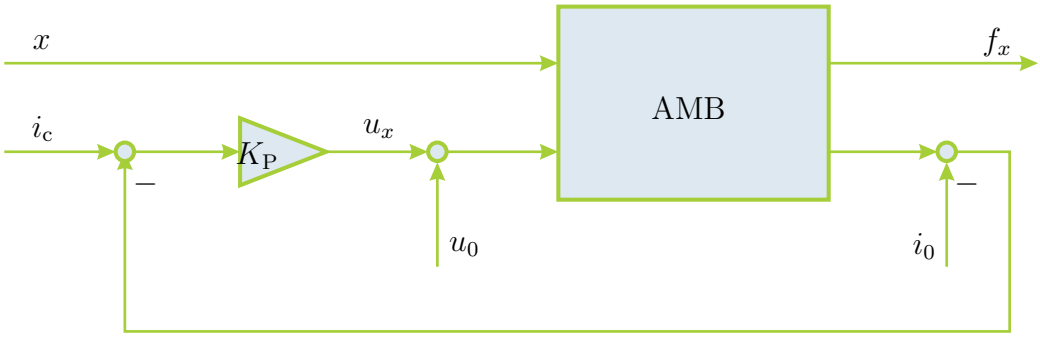

Figure 3.7: *Underlying current control configuration*

Connecting the actuator model (Eq. 3.31) with a P-controller K_P, it can be obtained

$$\begin{aligned} u_x &= K_\mathrm{P}(i_\mathrm{c} - i_x) \\ &= K_\mathrm{P}(i_\mathrm{c} - x_m + \frac{k_\mathrm{s}}{k_\mathrm{i}} x). \end{aligned} \tag{3.32}$$

Inserting Eq. 3.32 in Eq. 3.31 and selecting the control current i_c and displacement of the rotor x as inputs, as well as the magnetic force f_x as output, yields

$$\frac{\partial}{\partial t} x_m = -\frac{1}{L}(R - K_\mathrm{P}) x_m + \frac{k_\mathrm{s}}{L k_\mathrm{i}}(R + K_\mathrm{P}) x + \frac{K_\mathrm{P}}{L} i_\mathrm{c}, \tag{3.33a}$$

$$f_x = k_\mathrm{i}\, x_m. \tag{3.33b}$$

Assuming that the actuator in y-direction possesses the identical properties as in x-direction, the complete state-space model for an actuator of the magnetic bearing can be then expressed as

$$\begin{aligned} \underbrace{\begin{bmatrix} \frac{\partial}{\partial t} x_m \\ \frac{\partial}{\partial t} y_m \end{bmatrix}}_{\dot{\mathbf{x}}_\mathrm{m}} &= \underbrace{\begin{bmatrix} -\frac{1}{L}(R - K_\mathrm{P}) & 0 \\ 0 & -\frac{1}{L}(R - K_\mathrm{P}) \end{bmatrix}}_{\mathbf{A}_\mathrm{m}} \underbrace{\begin{bmatrix} x_m \\ y_m \end{bmatrix}}_{\mathbf{x}_\mathrm{m}} \\ &\quad + \underbrace{\begin{bmatrix} \frac{k_\mathrm{s}}{L k_\mathrm{i}}(R + K_\mathrm{P}) & 0 & \frac{K_\mathrm{P}}{L} & 0 \\ 0 & \frac{k_\mathrm{s}}{L k_\mathrm{i}}(R + K_\mathrm{P}) & 0 & \frac{K_\mathrm{P}}{L} \end{bmatrix}}_{\mathbf{B}_\mathrm{m}} \underbrace{\begin{bmatrix} x \\ y \\ i_{cx} \\ i_{cy} \end{bmatrix}}_{\mathbf{u}_\mathrm{m}}, \end{aligned} \tag{3.34a}$$

$$\underbrace{\begin{bmatrix} f_x \\ f_y \end{bmatrix}}_{\mathbf{y}_\mathrm{m}} = \underbrace{\begin{bmatrix} k_\mathrm{i} & 0 \\ 0 & k_\mathrm{i} \end{bmatrix}}_{\mathbf{C}_\mathrm{m}} \underbrace{\begin{bmatrix} x_m \\ y_m \end{bmatrix}}_{\mathbf{x}_\mathrm{m}}. \tag{3.34b}$$

It can be seen from Eq. 3.34 that an actuator consists of four inputs (displacements and control current in x- and y-direction), two outputs (net magnetic forces in x- and y-direction) and two states. Usually two magnetic bearings are neccessary to support a rotor system in radial direction. In this case the actuator system (Eq. 3.34) can be easily extended as

$$\begin{aligned} \dot{\mathbf{x}}_\mathrm{M} &= \mathbf{A}_\mathrm{M}\mathbf{x}_\mathrm{M} + \mathbf{B}_\mathrm{M}\mathbf{u}_\mathrm{M} \\ \mathbf{y}_\mathrm{M} &= \mathbf{C}_\mathrm{M}\mathbf{x}_\mathrm{M} \end{aligned} \tag{3.35}$$

with eight inputs, four outputs, and four states.

3.3 Modeling of Rotor System

3.3.1 General Mathematical Form of Flexible Rotor

Rotor is modeled by using the *Finite Element Method* (FEM), in which the continuous rotor is discretized into finite number of (Timoshenko) beam elements. As a result, the dynamics of the rotor system can be represented by a set of ordinary differential equations (known as equations of motion) as follows:

$$\mathbf{M}_\mathrm{r}\ddot{\mathbf{q}} + (\mathbf{D}_\mathrm{r} + \Omega\mathbf{G}_\mathrm{r})\dot{\mathbf{q}} + \mathbf{K}_\mathrm{r}\mathbf{q} = \Omega^2\mathbf{q}_\mathrm{u} + \mathbf{f}_\mathrm{E} = \mathbf{F}\mathbf{w}, \tag{3.36a}$$

$$\mathbf{y}_\mathrm{r} = \mathbf{C}_\mathrm{r}\mathbf{q}. \tag{3.36b}$$

The parameters of the rotor system are defined as given in Table 3.1.

Table 3.1: *Parameters of a generalized rotor system*

Parameter	Description
$\mathbf{M}_\mathrm{r}$	Mass matrix (symmetrical, positive definite, $\mathbf{M}_\mathrm{r} \in \mathbb{R}^{n\times n}$)
$\mathbf{D}_\mathrm{r}$	Damping matrix (symmetrical, $\mathbf{D}_\mathrm{r} \in \mathbb{R}^{n\times n}$)
$\mathbf{G}_\mathrm{r}$	Gyroscopic matrix (skew-symmetrical, $\mathbf{G}_\mathrm{r} \in \mathbb{R}^{n\times n}$)
$\mathbf{K}_\mathrm{r}$	Stiffness matrix (symmetrical, positive semi-definite, $\mathbf{K}_\mathrm{r} \in \mathbb{R}^{n\times n}$)
$\mathbf{q}_\mathrm{u}$	Unbalance vector ($\mathbf{q}_\mathrm{u} \in \mathbb{R}^{n}$)
$\mathbf{q}$	Displacement vector ($\mathbf{q} \in \mathbb{R}^{n}$)
Ω	Rotational speed in $[rad/s]$
$\mathbf{f}_\mathrm{E}$	External force vector (e.g. bearing forces, $\mathbf{f}_\mathrm{E} \in \mathbb{R}^{n}$)
$\mathbf{F}$	Input position matrix ($\mathbf{F} \in \mathbb{R}^{n\times m}$)
$\mathbf{w}$	Force vector (e.g. bearing forces, unbalance forces, $\mathbf{w} \in \mathbb{R}^{m}$)
$\mathbf{C}_\mathrm{r}$	Output position matrix ($\mathbf{C}_\mathrm{r} \in \mathbb{R}^{r\times n}$)
$\mathbf{y}_\mathrm{r}$	Output vector (measurements, $\mathbf{y}_\mathrm{r} \in \mathbb{R}^{r\times n}$)

It should be noted that Eq. 3.36 is obtained under the assumption that the rotor speed is constant. Proportional damping is employed, i.e.

$$\mathbf{D}_\mathrm{r} = \alpha_\mathrm{d}\mathbf{M}_\mathrm{r} + \beta_\mathrm{d}\mathbf{K}_\mathrm{r},$$

where parameters α_d and β_d are constants. It is assumed $\alpha_\mathrm{d} = 0$, therefore the damping matrix can be expressed as

$$\mathbf{D}_\mathrm{r} = \beta_\mathrm{d}\mathbf{K}_\mathrm{r}. \tag{3.37}$$

In this thesis only the vibration in radial (x- and y-) direction is considered and the axial (z-direction) vibration is neglected. Thus each node possesses four Degrees of Freedom (DoFs), i.e. translation and rotation in x- and y-plane

$$\mathbf{q}_i = \begin{bmatrix} x_i \\ y_i \\ \alpha_i \\ \beta_i \end{bmatrix}.$$

The dynamics of a rotor system modeled with N_n nodes (i.e. N_n-1 elements) can be described by total of n (n: system dimension, $n = 4N_\mathrm{n}$) DoFs, i.e.

$$\mathbf{q} = \begin{bmatrix} \mathbf{q}_1 \\ \mathbf{q}_2 \\ \vdots \\ \mathbf{q}_i \\ \vdots \\ \mathbf{q}_{N_\mathrm{n}} \end{bmatrix}. \tag{3.38}$$

3.3.2 Model Reduction

Comparing with other complex structures (e.g. in automotive and aircraft industries) requiring several millions DoFs, rotor structure is simple. For a complex rotor structure (e.g. with frequent step changes of rotor diameter), it requires several hundreds up to several thousands DoFs to obtain more precise results, i.e. eigenfrequencies and modeshapes. Although the dimension of a rotor model is not so large and it requires normally less than one minute to calculate the eigenfrequencies and eigenforms, it can become time-consuming and even computationally unrealistic in case that a large number of repeated evaluations are needed, e.g., for optimization task.

Secondly, for rotordynamic analysis usually only the low-frequency eigenmodes are of interest. In fact, the high-frequency modes of a rotor system possess high degree of uncertainty by measurement (i.e. modal analysis) and they cannot be used as reference for validation purpose.

Because of the two main reasons mentioned above, in some cases model reduction for a rotor system becomes necessary.

Three types of model reduction techniques [GK89] to reduce the dimension of the system matrix can be used:

1. Static matrix reduction,
2. Modal matrix reduction, and
3. Mixed matrix reduction.

Normally, the modal matrix reduction is used because a high reduction ratio and a high degree of accuracy of selected eigenfrequencies can be achieved with little effort. A drawback of this technique is that the reduced system possesses only modal coordinates. They have to be transformed back to original physical coordinates in order to consider parameter change of the rotor system, e.g. changes on stiffness and damping of a fluid film bearing, which is speed-dependent [GK89]. This can be avoided by using the mixed matrix reduction technique, in which those DoFs (e.g. associated with bearing and sensor nodes) can be selected as master DoFs and remain explicitly in the reduced rotor system. In this work the mixed reduction method is therefore used for model reduction. The procedure of this method is described in the following.

The displacement vector $\mathbf{q}$ need be firstly rearranged as

$$\tilde{\mathbf{q}} = \begin{bmatrix} \mathbf{q}_\mathrm{H} \\ \mathbf{q}_\mathrm{N} \end{bmatrix}.$$

The master DoFs in vector $\mathbf{q}_\mathrm{H}$ shall include the DoFs of interest, such as bearing nodes, sensor nodes as well as other nodes which contribute greatly to the system behavior, e.g. nodes where large masses (e.g. impellers) are located and nodes which external forces exert on. The vector $\mathbf{q}_\mathrm{N}$ contains the rest of the DoFs to be omitted (slave DoFs).

Correspondingly, $\mathbf{M}_\mathrm{r}$, $\mathbf{D}_\mathrm{r}$, $\mathbf{G}_\mathrm{r}$ and $\mathbf{K}_\mathrm{r}$ have also to be rearranged with respect to the new displacment vector $\tilde{\mathbf{q}}$. Finally, Eq. 3.36 can be rewritten as

$$\tilde{\mathbf{M}}\ddot{\tilde{\mathbf{q}}} + (\tilde{\mathbf{D}} + \Omega\tilde{\mathbf{G}})\dot{\tilde{\mathbf{q}}} + \tilde{\mathbf{K}}\tilde{\mathbf{q}} = \tilde{\mathbf{F}}\mathbf{w}, \tag{3.39a}$$

$$\mathbf{y}_\mathrm{r} = \tilde{\mathbf{C}}\tilde{\mathbf{q}}, \tag{3.39b}$$

with

$$\tilde{\mathbf{M}} = \begin{pmatrix} \mathbf{M}_\mathrm{HH} & \mathbf{M}_\mathrm{HN} \\ \mathbf{M}_\mathrm{NH} & \mathbf{M}_\mathrm{NN} \end{pmatrix}, \quad \tilde{\mathbf{D}} = \begin{pmatrix} \mathbf{D}_\mathrm{HH} & \mathbf{D}_\mathrm{HN} \\ \mathbf{D}_\mathrm{NH} & \mathbf{D}_\mathrm{NN} \end{pmatrix},$$

$$\tilde{\mathbf{G}} = \begin{pmatrix} \mathbf{G}_\mathrm{HH} & \mathbf{G}_\mathrm{HN} \\ \mathbf{G}_\mathrm{NH} & \mathbf{G}_\mathrm{NN} \end{pmatrix}, \quad \tilde{\mathbf{K}} = \begin{pmatrix} \mathbf{K}_\mathrm{HH} & \mathbf{K}_\mathrm{HN} \\ \mathbf{K}_\mathrm{NH} & \mathbf{K}_\mathrm{NN} \end{pmatrix},$$

$$\tilde{\mathbf{F}} = \begin{bmatrix} \mathbf{F}_\mathrm{H} \\ \mathbf{F}_\mathrm{N} \end{bmatrix}, \qquad \tilde{\mathbf{C}} = \begin{bmatrix} \mathbf{C}_\mathrm{H} & \mathbf{C}_\mathrm{N} \end{bmatrix}.$$

In static case, the system is assumed to be at rest (i.e. $\ddot{\tilde{\mathbf{q}}} = \dot{\tilde{\mathbf{q}}} \stackrel{!}{=} \mathbf{0}$) and the forces on the slave DoFs are equal to zero (i.e. $\mathbf{F}_\mathrm{N} \stackrel{!}{=} \mathbf{0}$), then Eq. 3.39 can be expressed as

$$\begin{pmatrix} \mathbf{K}_\mathrm{HH} & \mathbf{K}_\mathrm{HN} \\ \mathbf{K}_\mathrm{NH} & \mathbf{K}_\mathrm{NN} \end{pmatrix} \begin{bmatrix} \mathbf{q}_\mathrm{H} \\ \mathbf{q}_\mathrm{N} \end{bmatrix} = \begin{bmatrix} \mathbf{F}_\mathrm{H} \\ \mathbf{0} \end{bmatrix}.$$

It follows

$$\mathbf{q}_\mathrm{N} = \underbrace{-\mathbf{K}_\mathrm{NN}{}^{-1}\,\mathbf{K}_\mathrm{NH}}_{\mathbf{S}_\mathrm{NH}}\,\mathbf{q}_\mathrm{H} = \mathbf{S}_\mathrm{NH}\,\mathbf{q}_\mathrm{H}. \tag{3.40}$$

Meanwhile, the influences from the slave DoFs, $\mathbf{q}_\mathrm{N}$, can be taken into account with the help of modal transformation.

The eigenvalues and eigenforms for the slave DoFs can be calculated by fixing the master DoFs, i.e.

$$\ddot{\mathbf{q}}_\mathrm{H} = \dot{\mathbf{q}}_\mathrm{H} = \mathbf{q}_\mathrm{H} \stackrel{!}{=} \mathbf{0}.$$

With Eq. 3.39a, it gives

$$\mathbf{M}_\mathrm{NN}\,\ddot{\mathbf{q}}_\mathrm{N} + \mathbf{K}_\mathrm{NN}\,\mathbf{q}_\mathrm{N} = \mathbf{0}. \tag{3.41}$$

With the ansatz

$$\mathbf{q}_\mathrm{N} = \mathbf{v}\mathrm{e}^{\lambda t},$$

it follows

$$(\mathbf{M}_\mathrm{NN}\lambda^2 + \mathbf{K}_\mathrm{NN})\mathbf{v} = \mathbf{0}, \tag{3.42}$$

with eigenvalue λ and the corresponding eigenvector $\mathbf{v}$. The eigenvalues can be then obtained by solving the equation

$$\det(\mathbf{M}_\mathrm{NN}\lambda^2 + \mathbf{K}_\mathrm{NN}) \stackrel{!}{=} 0.$$

The corresponding eigenvector for the i-th eigenvalue λ_i can be then calculated by solving

$$(\mathbf{M}_\mathrm{NN}\lambda_i^2 + \mathbf{K}_\mathrm{NN})\mathbf{v}_i = \mathbf{0}. \tag{3.43}$$

For modal reduction, only the first l lowest eigenfrequencies are considered. Then, it gives

$$\mathbf{q}_\mathrm{N} = \underbrace{\begin{bmatrix} \mathbf{v}_1 & \mathbf{v}_2 & \cdots & \mathbf{v}_\mathrm{L} \end{bmatrix}}_{\text{Modal transformation matrix: } \mathbf{R}_\mathrm{red}} \qquad \mathbf{q}_\mathrm{L} = \mathbf{R}_\mathrm{red}\,\mathbf{q}_\mathrm{L}, \tag{3.44}$$

where the matrix $\mathbf{R}_\mathrm{red}$ is the modal matrix including only the first l lowest eigenvectors. Vector $\mathbf{q}_\mathrm{L}$ is the modal coordinate of size l.

In combination with Eq. 3.40, it gives the resulting transformation matrix

$$\underbrace{\left[\begin{array}{c}\mathbf{q}_\mathrm{H}\\\hline\mathbf{q}_\mathrm{N}\end{array}\right]}_{\tilde{\mathbf{q}}} = \underbrace{\left(\begin{array}{c|c}\mathbf{I} & \mathbf{0}\\\hline\mathbf{S}_\mathrm{NH} & \mathbf{R}_\mathrm{red}\end{array}\right)}_{\text{Transformation matrix: } \mathbf{T}_\mathrm{red}} \underbrace{\left[\begin{array}{c}\mathbf{q}_\mathrm{H}\\\hline\mathbf{q}_\mathrm{L}\end{array}\right]}_{\mathbf{q}_\mathrm{red}}. \tag{3.45}$$

The equations of motion (Eq. 3.39) can then be reduced in the form,

$$\mathbf{M}_\mathrm{red}\,\ddot{\mathbf{q}}_\mathrm{red} + (\mathbf{D}_\mathrm{red} + \Omega\mathbf{G}_\mathrm{red})\,\dot{\mathbf{q}}_\mathrm{red} + \mathbf{K}_\mathrm{red}\,\mathbf{q}_\mathrm{red} = \mathbf{F}_\mathrm{red}\mathbf{w}, \tag{3.46a}$$

$$\mathbf{y}_\mathrm{r} = \mathbf{C}_\mathrm{red}\mathbf{q}_\mathrm{red}, \tag{3.46b}$$

with

$$\begin{aligned}
\mathbf{M}_\mathrm{red} &= \mathbf{T}_\mathrm{red}^T\,\tilde{\mathbf{M}}\,\mathbf{T}_\mathrm{red}, & \mathbf{D}_\mathrm{red} &= \mathbf{T}_\mathrm{red}^T\,\tilde{\mathbf{D}}\,\mathbf{T}_\mathrm{red}\\
\mathbf{G}_\mathrm{red} &= \mathbf{T}_\mathrm{red}^T\,\tilde{\mathbf{G}}\,\mathbf{T}_\mathrm{red}, & \mathbf{K}_\mathrm{red} &= \mathbf{T}_\mathrm{red}^T\,\tilde{\mathbf{K}}\,\mathbf{T}_\mathrm{red}\\
\mathbf{C}_\mathrm{red} &= \tilde{\mathbf{C}}\,\mathbf{T}_\mathrm{red}, & \mathbf{F}_\mathrm{red} &= \mathbf{T}_\mathrm{red}^T\,\tilde{\mathbf{F}}.
\end{aligned}$$

3.3.3 State-Space Model

With the state vector

$$\mathbf{x}_\mathrm{R} = \begin{bmatrix}\mathbf{q}\\\dot{\mathbf{q}}\end{bmatrix},$$

the state-space representation of the rotor system (Eqs. 3.36) can be written as

$$\begin{aligned}
\dot{\mathbf{x}}_\mathrm{R} &= \mathbf{A}_\mathrm{R}\mathbf{x}_\mathrm{R} + \mathbf{B}_\mathrm{R}\mathbf{u}_\mathrm{R},\\
\mathbf{y}_\mathrm{R} &= \mathbf{C}_\mathrm{R}\mathbf{x}_\mathrm{R},
\end{aligned} \tag{3.47}$$

where

$$\begin{aligned}
\mathbf{A}_\mathrm{R} &= \begin{bmatrix}\mathbf{0} & \mathbf{I}\\ -\mathbf{M}_\mathrm{r}^{-1}\mathbf{K}_\mathrm{r} & -\mathbf{M}_\mathrm{r}^{-1}(\mathbf{D}_\mathrm{r} + \Omega\mathbf{G}_\mathrm{r})\end{bmatrix}, & \mathbf{B}_\mathrm{R} &= \begin{bmatrix}\mathbf{0}\\ \mathbf{M}_\mathrm{r}^{-1}\mathbf{F}\end{bmatrix},\\
\mathbf{C}_\mathrm{R} &= \begin{bmatrix}\mathbf{C}_\mathrm{r} & \mathbf{0}\end{bmatrix}, & \mathbf{y}_\mathrm{R} &= \mathbf{y}_\mathrm{r}, \quad \text{and}\\
\mathbf{u}_\mathrm{R} &= \mathbf{w},
\end{aligned}$$

with the system matrix $\mathbf{A}_\mathrm{R}$ of size $2n \times 2n$, the input matrix $\mathbf{B}_\mathrm{R}$ of size $2n \times m$, and the output matrix $\mathbf{C}_\mathrm{R}$ of size $r \times 2n$.

For the reduced system (Eqs. 3.46), the system, input, and output matrices and the state vector will be then written as

$$\mathbf{A}_{\mathrm{R}} = \begin{bmatrix} \mathbf{0} & \mathbf{I} \\ -\mathbf{M}_{\mathrm{red}}^{-1}\mathbf{K}_{\mathrm{red}} & -\mathbf{M}_{\mathrm{red}}^{-1}(\mathbf{D}_{\mathrm{red}} + \Omega\mathbf{G}_{\mathrm{red}}) \end{bmatrix}, \quad \mathbf{B}_{\mathrm{R}} = \begin{bmatrix} \mathbf{0} \\ \mathbf{M}_{\mathrm{red}}^{-1}\mathbf{F}_{\mathrm{red}} \end{bmatrix},$$
$$\mathbf{C}_{\mathrm{R}} = \begin{bmatrix} \mathbf{C}_{\mathrm{red}} & \mathbf{0} \end{bmatrix}, \quad \mathbf{x}_{\mathrm{R}} = [\mathbf{q}_{\mathrm{red}}^T, \dot{\mathbf{q}}_{\mathrm{red}}^T]^T.$$

3.4 Plant

In the previous section, the modeling of the basic elements (including magnetic bearing and rotor) is introduced. An essential element has not yet mentioned, namely, the sensor. The dynamic behavior of sensors can be taken into account, which is generally considered as a low-pass filter. Normally a large bandwidth of the sensor is required, so that the cutoff frequency (corner frequency) of the sensor is located widely beyond the bandwidth of the other elements of the control system (including rotor system, magnetic bearing, and controller), therefore the sensor has no noticeable influence on the dynamic behavior of the control system in the low frequency region, and the sensor is therefore simplified as a constant gain. Meanwhile, the converters (including AD- and DA-conventers) in the DSP unit are commonly considered as constant gains.

Assembling all elements yields the plant model. This plant model will be used for system analysis, controller design, and controller optimization.

3.4.1 Complete Model

In case all elements are well modeled in state-space representation, combining the sensors, the rotor (Eqs. 3.47), and the magnetic bearing (Eqs. 3.35) models results to the complete plant model

$$\begin{aligned} \dot{\mathbf{x}}_{\mathrm{P}} &= \mathbf{A}_{\mathrm{P}}\mathbf{x}_{\mathrm{P}} + \mathbf{B}_{\mathrm{P}}\mathbf{u}_{\mathrm{P}}, \\ \mathbf{y}_{\mathrm{P}} &= \mathbf{C}_{\mathrm{P}}\mathbf{x}_{\mathrm{P}}, \end{aligned} \tag{3.48}$$

with the state vector

$$\mathbf{x}_{\mathrm{P}} = \left[\begin{array}{c} \mathbf{x}_{\mathrm{S}} \\ \hline \mathbf{x}_{\mathrm{R}} \\ \hline \mathbf{x}_{\mathrm{M}} \end{array}\right],$$

and the state vector of the sensors $\mathbf{x}_{\mathrm{S}}$.

The resulting plant possesses all states from the sensors, the rotor, and the magnetic bearings. The inputs of the plant are control currents, i.e.

$$\mathbf{u}_{\mathrm{P}} = \mathbf{i}_{\mathrm{c}},$$

and the outputs of the sensors are taken as the outputs of the plant.

3.4.2 Simple Model

For simplicity reasons, the magnetic bearing actuator is usually modeled as linear relation between magnetic force and control current as well as rotor displacement as given in Eq. 3.18, meanwhile the sensor is considered as constant gain, i.e. unity, the magnetic force model can be then directly integrated into the rotor system to gain the plant model.

Firstly, an additional stiffness matrix with the negative stiffness k_{s} of the magnetic bearing can be constructed as

$$\mathbf{K}_{\mathrm{s}} = \begin{pmatrix} 0 & 0 & \cdots & & & 0 \\ 0 & & & & & \\ & -k_{\mathrm{s}} & & & & \\ & & -k_{\mathrm{s}} & & & \\ & & & -k_{\mathrm{s}} & & \\ & & & & -k_{\mathrm{s}} & \\ & & & & & 0 \\ 0 & & \cdots & & 0 & 0 \end{pmatrix}^{n\times n}. \tag{3.49}$$

The location of the four parameters $-k_{\mathrm{s}}$ in the matrix $\mathbf{K}_s$ corresponds to the nodes of the two magnetic bearing actuators (in x- and y-direction), and all other elements of $\mathbf{K}_s$ are zeros. With the additional stiffness matrix, the new stiffness matrix of the rotor system can be expressed as

$$\mathbf{K}_{\mathrm{n}} = \mathbf{K}_{\mathrm{r}} + \mathbf{K}_{\mathrm{s}}. \tag{3.50}$$

Secondly, the force-current relation with coefficient k_{i} is modeled as an input position

matrix $\mathbf{K}_\mathrm{i}$

$$\mathbf{K}_\mathrm{i} = \begin{pmatrix} 0 & 0 & 0 & 0 \\ \vdots & \vdots & \vdots & \vdots \\ k_\mathrm{i} & 0 & & \\ 0 & k_\mathrm{i} & & \\ \vdots & \vdots & & \\ & & k_\mathrm{i} & 0 \\ & & 0 & k_\mathrm{i} \\ \vdots & \vdots & \vdots & \vdots \\ 0 & 0 & 0 & 0 \end{pmatrix}^{n\times 4} . \tag{3.51}$$

This matrix $\mathbf{K}_\mathrm{i}$ arranges control current $\mathbf{i}_\mathrm{c}$ to be located at the position corresponding to the nodes of the actuator for the rotor system (Eqs. 3.36), i.e.

$$\mathbf{f}_\mathrm{E} = \mathbf{K}_\mathrm{i}\mathbf{i}_\mathrm{c}.$$

Considering the unbalance forces

$$\Omega^2\mathbf{q}_\mathrm{u} = \mathbf{F}_\mathrm{o}\mathbf{w}_\mathrm{o},$$

with the input vector $\mathbf{w}_\mathrm{o}$ and the corresponding input position matrix $\mathbf{F}_\mathrm{o}$, the forces exerting on the rotor system can be written as

$$\mathbf{f} = \mathbf{f}_\mathrm{E} + \Omega^2\mathbf{q}_\mathrm{u} = \underbrace{[\mathbf{K}_i \mid \mathbf{F}_\mathrm{o}]}_{\text{Input position matrix: } \mathbf{F}} \begin{bmatrix} \mathbf{i}_\mathrm{c} \\ \mathbf{w}_\mathrm{o} \end{bmatrix}. \tag{3.52}$$

Inserting the input position matrix $\mathbf{F}$ into the state-space model, Eqs. 3.47, of the rotor system and replacing stiffness matrix $\mathbf{K}_\mathrm{r}$ by $\mathbf{K}_\mathrm{n}$, the plant model can be obtained.

In case the reduced rotor model is considered, the same procedure can be applied to obtain the plant model.

Once the plant model is expressed in state-space form, its transfer function form can be then defined by

$$\mathbf{Y}_\mathrm{P}(s) = \mathbf{G}_\mathrm{P}(s)\mathbf{u}_\mathrm{P}(s), \quad \text{with} \quad \mathbf{G}_\mathrm{P}(s) = \mathbf{C}_\mathrm{P}^T(s\mathbf{I} - \mathbf{A}_\mathrm{P})^{-1}\mathbf{B}_\mathrm{P} + \mathbf{D}_\mathrm{P}, \tag{3.53}$$

where the matrix $\mathbf{G}_\mathrm{P}$ denotes the tranfer function matrix of the plant. The inputs of the plant $\mathbf{u}_\mathrm{P}$ usually include the control current. Additionally, if unbalance forces and other external forces shall be considered, they can be correspondingly taken as inputs. The outputs of the plant $\mathbf{Y}_\mathrm{P}$ consist of the displacements measured by sensors.

3.5 The Two AMB Systems

In this work, two AMB systems are considered. The word "AMB system" denotes the resulting plant including rotor, sensors, and AMBs. In the following, the two systems will be introduced. It should be noted that the two AMB systems have been reported in author's previous publications [WS12a, WS12b, WGS13, WS15].

3.5.1 AMB System I

The AMB system contains a 12.4 kg rotor which is 0.46 m long. The discretized model of the rotor as illustrated in Figure 3.8 is modeled with 29 nodes and total of 116 DoFs (each node possesses four DoFs, i.e., translation and rotation in the x- and y-planes). The bearing and sensor nodes are also marked in Figure 3.8. The related state-space model therefore includes 232 states with bearing nodes as inputs and sensor nodes as outputs.

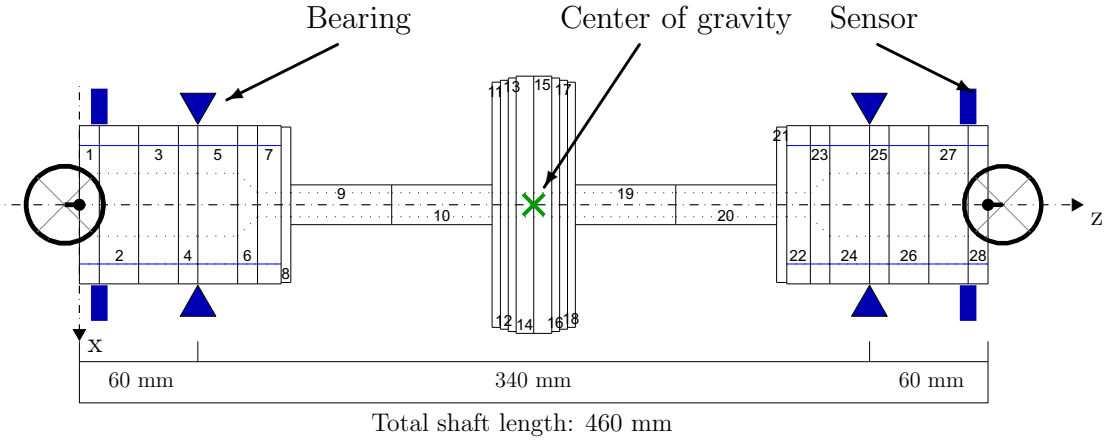

Figure 3.8: *Discretized rotor model from AMB system I [WS12a, WS15]*

The free-free bending eigenmodes of the rotor are shown in Figure 3.9. It is known that the eigenmodes and eigenfrequencies of a rotor system become speed-dependent if gyroscopic effect has to be considered; the eigenmodes of the system in Figure 3.9 are displayed for the rotor at rest, and consist of the first four bending modes.

The model of the magnetic bearing system is obtained by using the modeling procedure as described in Section 3.2.3. The sensors used in the AMB system are eddy current sensors. The sensors are taken as proportional transfer elements of second order (PT2) with an eigenfrequency out of the sampling region of the system.

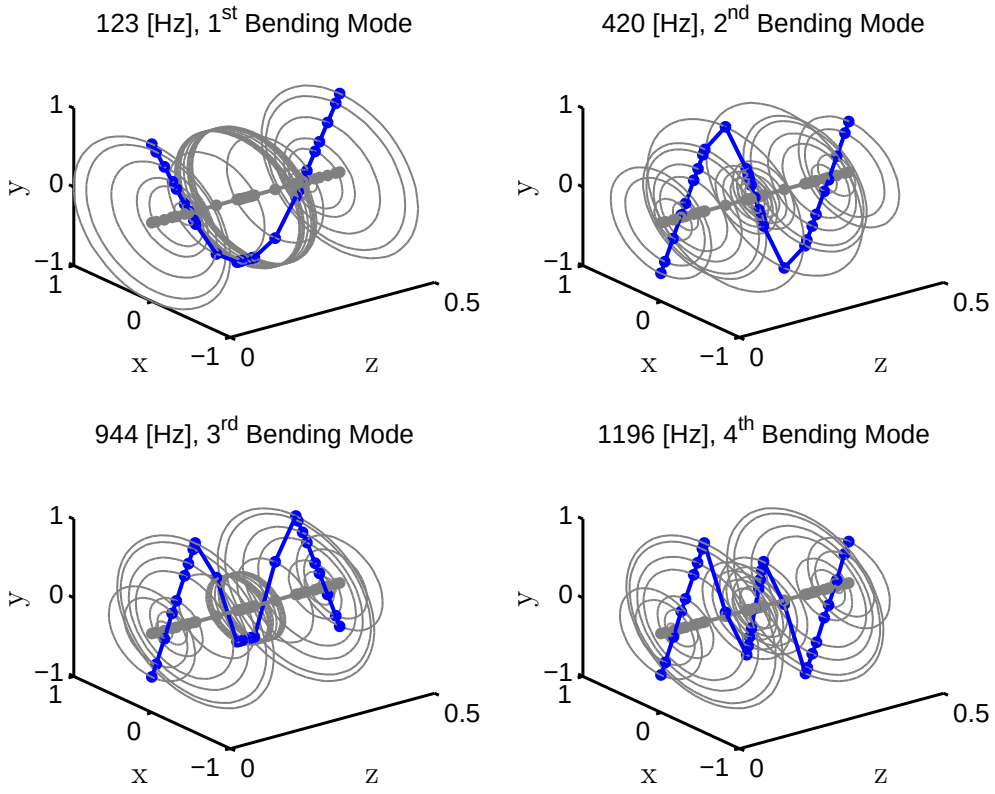

Figure 3.9: *Eigenmodes of the rotor system I [WS12a]*

Combining the sensor, the rotor, and the magnetic bearing models results to the complete plant model. The resulting plant possesses 244 states with four inputs and four outputs. The inputs of the plant are control currents and outputs of the sensors are considered as the outputs of the plant. Numerical parameters of the plant are given in Table 3.2.

Table 3.2: *Numerical parameters of the AMB system I*

	Value		Value
Mass of the rotor m_r [kg]	12.4	Length of the rotor l_r [m]	0.46
Bearing stiffness k_s [N/m]	-2.6e6	Force/current factor k_i [N/A]	280
Air gap s_0 [m]	4.2e-4	Bias current i_0 [A]	5

Although the AMB system is a Multi-Input and Multi-Output (MIMO) system with four inputs and four outputs, it is treated as a Multi-Single-Input and Single-Output (Multi-SISO) system for classic PID-control, i.e., four SISO systems. For a decentralized control

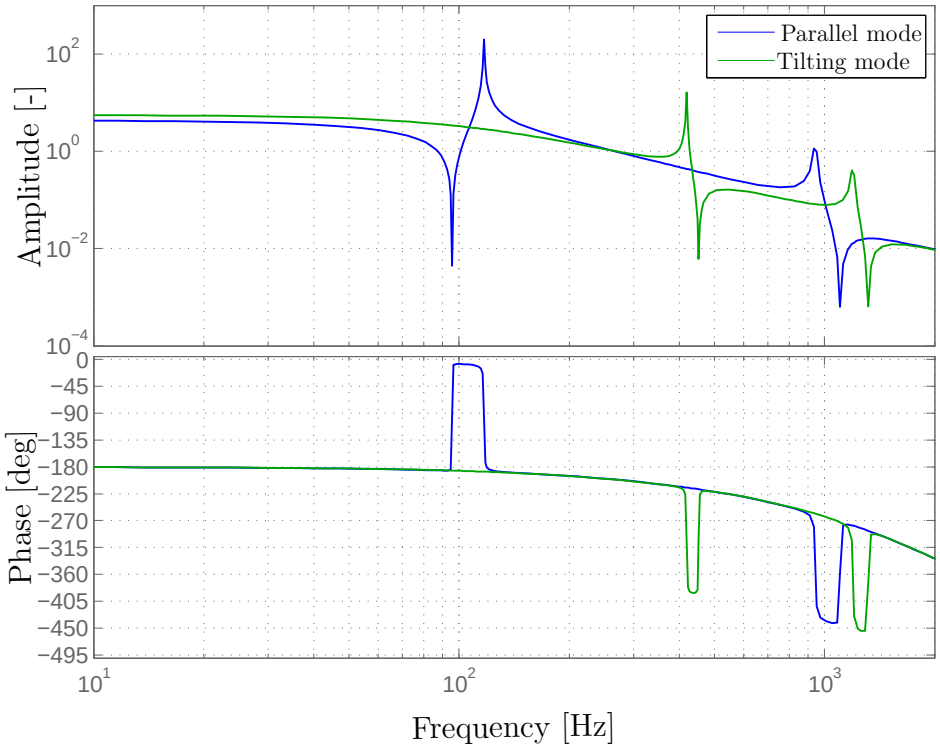

Figure 3.10: *Bode diagram between outputs (displacements, normalized amplitude) and inputs (control currents, normalized amplitude) of the plant of AMB system I [WS12a, WS15]*

configuration, only the diagonal elements in the transfer function matrix are considered in the controller design. For a centralized control configuration, additional off-diagonal elements also have to be considered with the help of transformation matrices. However, only the diagonal elements in the transfer function matrix of the resultant system after transformation are considered in the controller design. These two control configurations will be given in Section 4.1. The centralized control configuration is selected for AMB system I. The Bode diagram of the plant including sensors, rotor, magnetic bearings, AD-converters, DA -converters, and transformation matrices is shown in Figure 3.10. It should be noted that in Figure 3.10 only the transfer functions related to the x-plane because of symmetry in the x- and y-planes are shown. It can be seen that the parallel and tilting modes of the plant are perfectly separated with the transformation matrices because of the rotor symmetry.

3.5.2 AMB System II

For the second AMB system, a real industrial centrifugal compressor rotor (1970 kg, 3.9 m long, 6000 rpm nominal rotational speed) supported by AMBs is considered. The discretized model of the rotor as illustrated in Figure 3.11 is modeled with 96 elements, 97 nodes, and total of 388 DoFs.

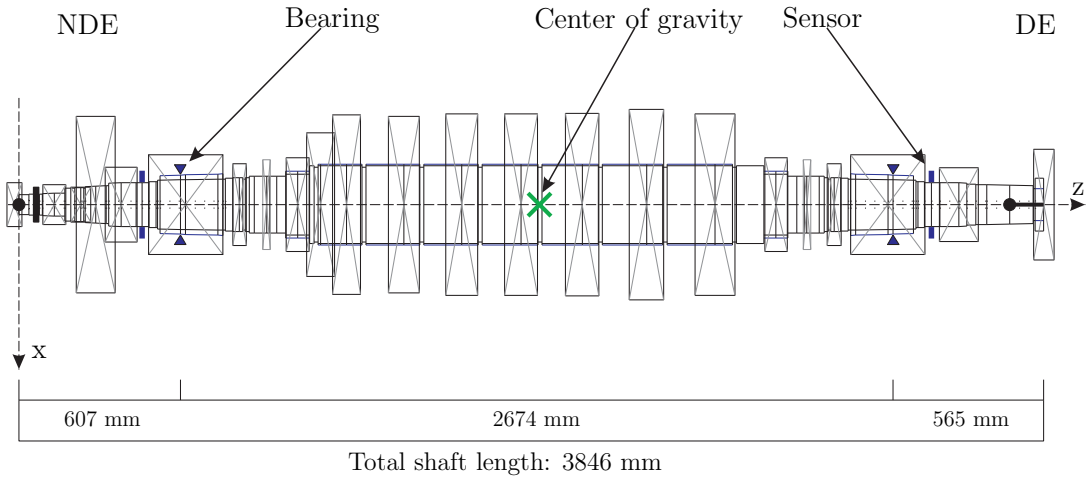

Figure 3.11: *Discretized rotor model from AMB system II*

The model can be transformed easily into a state-space model with 776 states. The bending modes of the rotor are shown in Table 3.3. It can be seen that the rotor is quite flexible. The eigenmodes of the rotor in free-free conditions are close to one another and all eigenmodes up to 2000 Hz have to be considered in the controller design. The controller design is a challenge for the AMB rotor system, because of the closely-located eigenmodes.

Table 3.3: *The bending modes of the rotor system II at standstill*

Mode	Frequency [Hz]
1st bending mode	68
2nd bending mode	158
3rd bending mode	262
4th bending mode	383
...	...
8th bending mode	931

For the actuator of the magnetic bearing, the differential drive configuration (see Figure 3.5) is employed to partially linearize the force-current relation of the magnetic bearing

as mentioned in Section 3.2.2. The entire actuator system, including magnets, amplifiers, and the underlying current controllers, is simplified as a linear relation (referring to Eq. 3.18) between the magnetic force and the control current as well as the displacement of the bearing nodes. The dynamic behavior of the sensors is assumed to be the same as for lowpass filters. The sensors, the rotor, and the simplified actuator models are combined, resulting in the plant model (see Section 3.4.2). The resulting plant possesses $N = 812$ states with four inputs and four outputs. The inputs of the plant are magnetic forces adjusted by the controller. The outputs of the sensors are considered to be the plant outputs.

A decentralized control configuration is selected. The Bode diagram of the transfer functions (in the x-plane) of the plant, including sensors, rotor, and magnetic bearings is shown in Figure 3.12. It can be seen that the frequency response of the Non-Driven-End side (NDE side) and Driven-End side (DE side) of the rotor are different from each other because of the non-symmetry of the rotor.

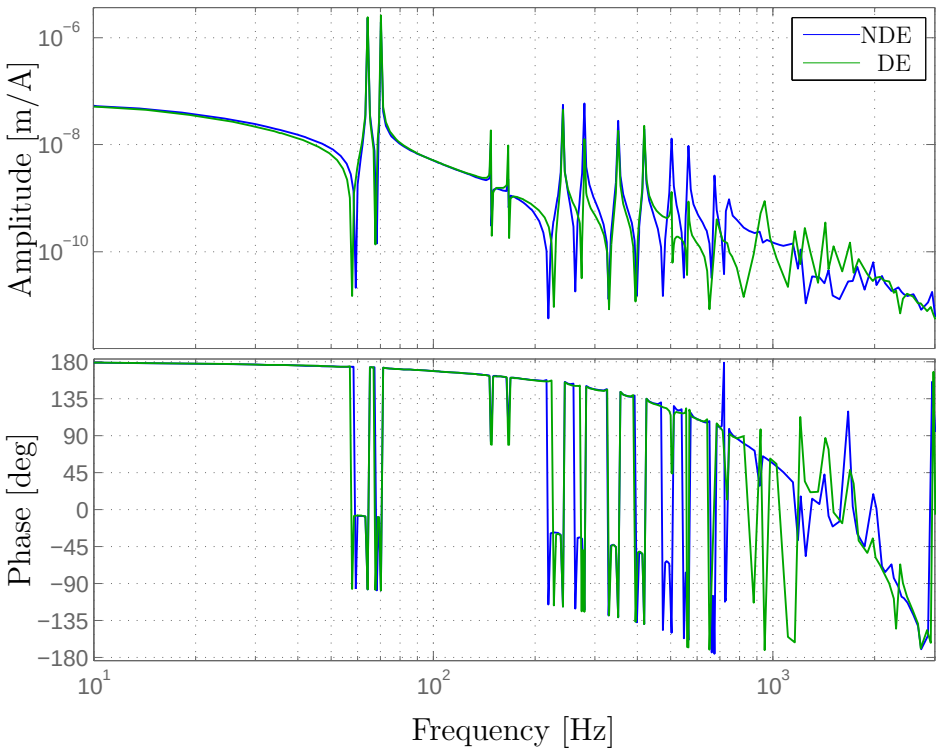

Figure 3.12: *Bode diagram between outputs (displacements at sensor nodes) and inputs (control currents) of the plant at the speed of 6000 rpm [WGS13, WS15]*

For the controller design and optimization, the plant model with an order of 812 shall be reduced. Model reduction is then performed on the rotor model by using the mixed matrix reduction method as described in Section 3.3.2. The simplified plant possesses 236 states. The reduced model is compared with the original model as shown in Figure 3.13. No noticeable difference is observed in low-frequency region. From an engineer's point of view, the model with matrix reduction is sufficient accurate. The reduced model is used for controller design and optimization of the AMB system.

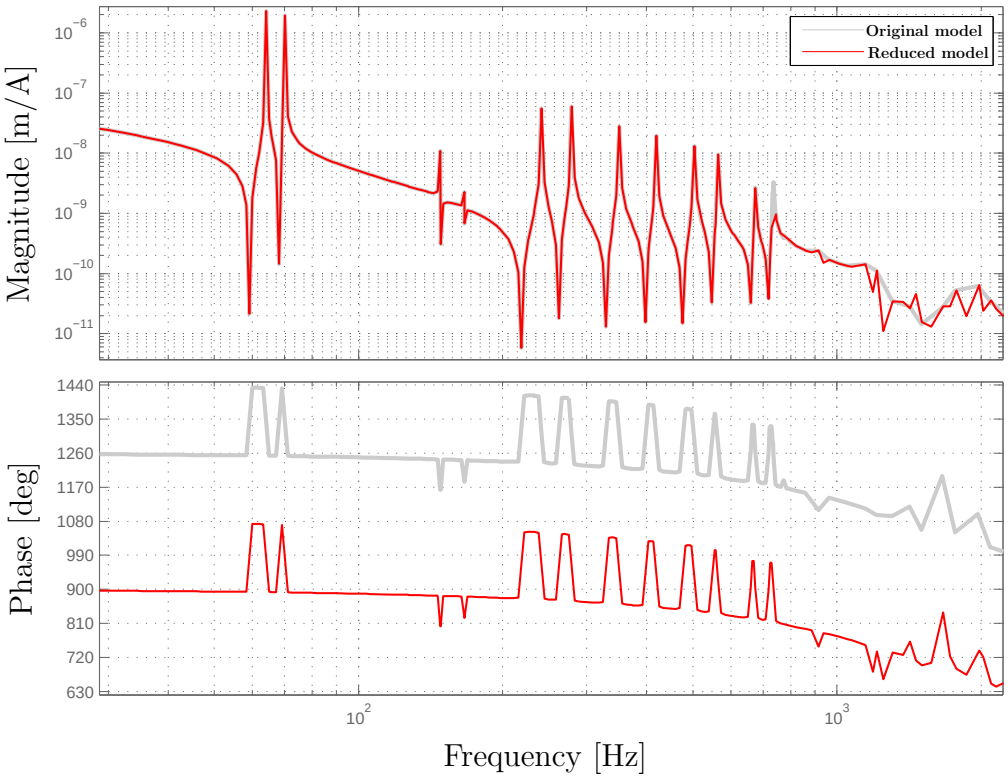

Figure 3.13: *Bode diagram between outputs (displacements at sensor nodes) and inputs (control currents) at NDE side for reduced and original models*

Chapter 4

Controlling of AMB System

In this chapter, the control design with PID-controller for controlling of AMB systems is introduced. In the second part of this chapter, diverse criteria evaluating the performance and requirements for magnetic supported rotor systems in turbomachinary are discussed. It should be noted that the material about PID-controller structure has been partially published in author's previous publication [WS12a, WS15].

4.1 PID-Control and Controller Design for the Two AMB systems

For an AMB system, the inherent negative stiffness causes instability of the open loop of the system; therefore, a feedback control loop is employed to stabilize the rotor system. So the controller design becomes a central task for designing the AMB system. Most industrial AMB systems are controlled by PID-like controllers including diverse filters. Rotor systems and the related AMB controller designs are becoming more complex. This is because of the higher energy density, higher speed, more complex rotor structure, etc. It is difficult for a typical PID-controller using three design parameters (K_P, T_n, and T_v) to achieve the various requirements. A more complex controller structure is therefore necessary, e.g. PID-controller with notch, lag-lead, and low-pass filters.

Two controller configurations are usually used to control AMB rotor systems: decentralized and centralized control (or translation-tilting mode control). If the rotor (relating to the modeshapes) is more or less symmetrical with respect to the rotor midspan, centralized control is preferred [BCK+09]. In this control configuration, the parallel and conical mode of the rotor, as well as the corresponding controller design, can be separated. For the decentralized control configuration, two controllers are necessary to stabilize the rotor in

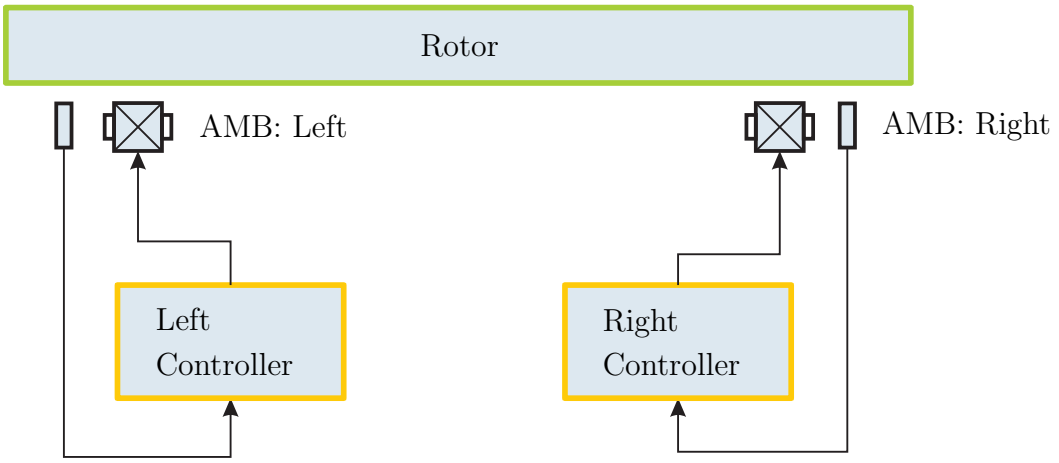

Figure 4.1: *Decentralized control configuration*

the x- or y-plane: one for the left and one for the right side as shown in Figure 4.1, so no transformation of the sensor and bearing coordinates is necessary. This type of control configuration is selected for AMB system II. For the centralized control configuration, two controllers with two transformation matrices are required to control the translation and tilting modes. Before the sensor signals are transfered to the DSP control unit, they have to be transformed from sensor coordinates into modal coordinates to separate the rotor modes into parallel and tilting modes, i.e.

$$\underbrace{\begin{bmatrix} x_\mathrm{p} \\ y_\mathrm{p} \\ x_\mathrm{t} \\ y_\mathrm{t} \end{bmatrix}}_{\text{Modal coordinates}} = \underbrace{\frac{1}{2}\begin{bmatrix} 1 & 0 & 1 & 0 \\ 0 & 1 & 0 & 1 \\ -1 & 0 & 1 & 0 \\ 0 & -1 & 0 & 1 \end{bmatrix}}_{\text{Transformation matrix: } T_\mathrm{in}} \underbrace{\begin{bmatrix} x_\mathrm{left} \\ y_\mathrm{left} \\ x_\mathrm{right} \\ y_\mathrm{right} \end{bmatrix}}_{\text{Sensor coordinates}} . \tag{4.1}$$

Analogously, the control signals (calculated by performing the control algorithm) have to be transformed from modal coordinates into bearing coordinates, i.e.

$$\underbrace{\begin{bmatrix} i_\mathrm{left,x} \\ i_\mathrm{left,y} \\ i_\mathrm{right,x} \\ i_\mathrm{right,y} \end{bmatrix}}_{\text{Bearing coordinates}} = \underbrace{\begin{bmatrix} 1 & 0 & -1 & 0 \\ 0 & 1 & 0 & -1 \\ 1 & 0 & 1 & 0 \\ 0 & 1 & 0 & 1 \end{bmatrix}}_{\text{Transformation matrix: } T_\mathrm{out}} \underbrace{\begin{bmatrix} i_\mathrm{p,x} \\ i_\mathrm{p,y} \\ i_\mathrm{t,x} \\ i_\mathrm{t,y} \end{bmatrix}}_{\text{Modal coordinates}} . \tag{4.2}$$

This can be visualized as illustrated in Figure 4.2.

The structure of PID-controllers as illustrated in Figure 4.3 using in AMB systems com-

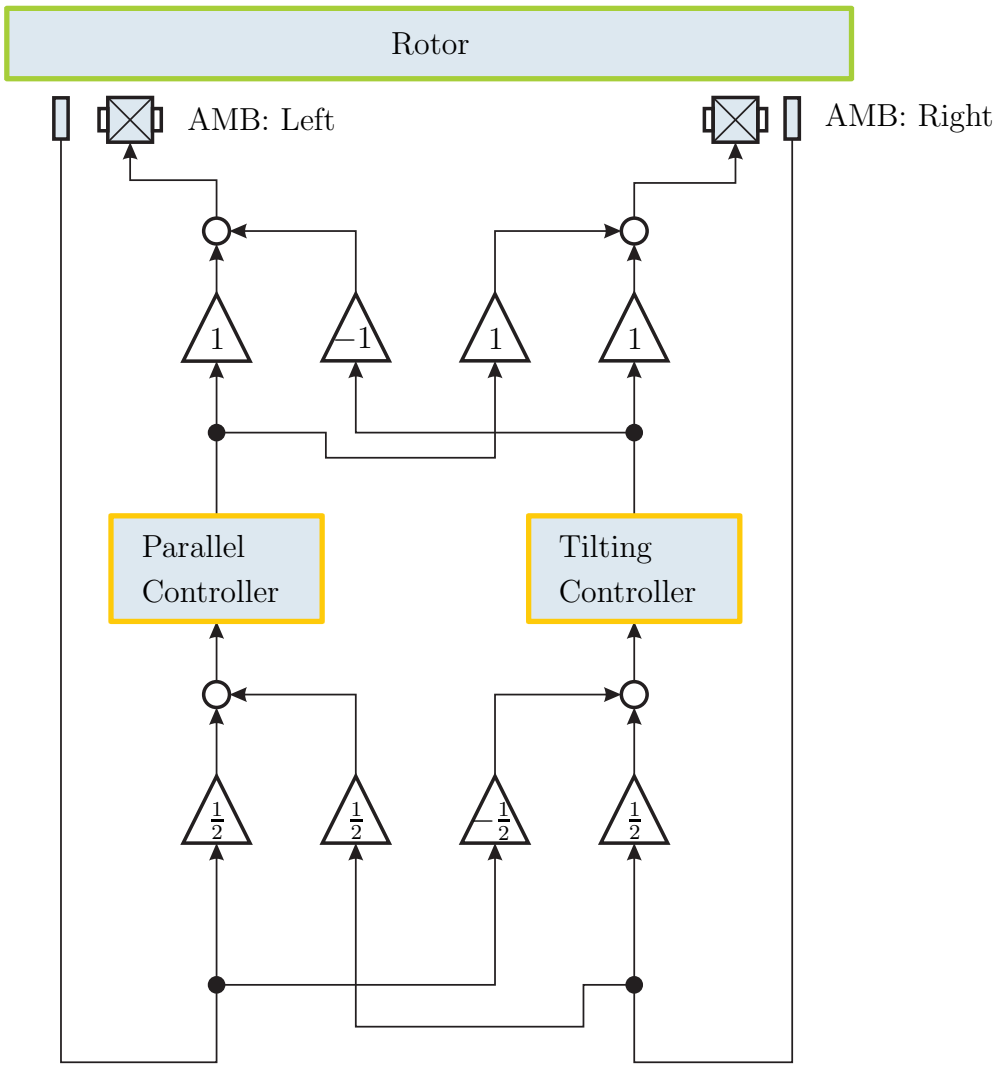

Figure 4.2: *Centralized control configuration*

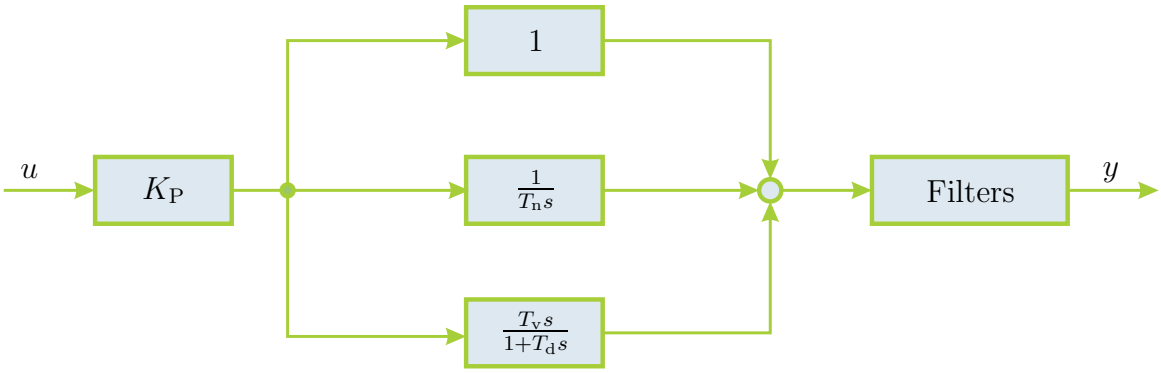

Figure 4.3: *Structure of commonly used PID-controllers in AMB systems*

monly consists of a PID-part connected with several filters

$$K = \underbrace{K_{\mathrm{P}}(1 + \frac{1}{T_{\mathrm{n}}s} + \frac{T_{\mathrm{v}}s}{1 + T_{\mathrm{d}}s})}_{\mathrm{PIDT_1}} \underbrace{\prod_{i=1}^{k} F_i}_{\mathrm{Filters}} . \tag{4.3}$$

The parameters of the PID-controller are defined as given in Table 4.1.

Table 4.1: *Parameters of the generalized PID-controllers*

Parameter	Description
K_{P}	Controller gain
T_{n}	Integral time
T_{v}	Derivative time
T_{d}	Time constant of the first order low pass filter
F_i	The i-th filter
k	Number of filter

Depending on the complexity of the rotor structure, the structure of the controllers can be very different, i.e. the number and the type of the filters change for controlling different rotor system.

Table 4.2: *Commonly used filters and their parameters*

Filter No.	Structure	Parameter	Description
1	$\frac{1}{\frac{s}{\omega_{\mathrm{d}}}+1}$	ω_{d}	Low-pass filter, First order, Roll-off
2	$\frac{1}{(\frac{s}{\omega_{\mathrm{d}}})^2+2\xi_{\mathrm{d}}\frac{s}{\omega_{\mathrm{d}}}+1}$	ω_{d}, ξ_{d}	Low-pass filter, Second order, Roll-off
3	$\frac{\frac{s}{\omega_{\mathrm{n}}}+1}{\frac{s}{\omega_{\mathrm{d}}}+1}$	ω_{n}, ω_{d}	First order filter, Phase lead or lag
4	$\frac{(\frac{s}{\omega_{\mathrm{n}}})^2+2\xi_{\mathrm{n}}\frac{s}{\omega_{\mathrm{n}}}+1}{(\frac{s}{\omega_{\mathrm{d}}})^2+2\xi_{\mathrm{d}}\frac{s}{\omega_{\mathrm{d}}}+1}$	ω_{n}, ξ_{n}, ω_{d}, ξ_{d}	Second order filter, Phase lead or lag
5	$\frac{(\frac{s}{\omega_{\mathrm{d}}})^2+1}{(\frac{s}{\omega_{\mathrm{d}}})^2+2\xi_{\mathrm{d}}\frac{s}{\omega_{\mathrm{d}}}+1}$	ω_{d}, ξ_{d}	Notch filter, Band-stop
6	$\frac{(\frac{s}{\omega_{\mathrm{a}}})^2-2\xi_{\mathrm{a}}\frac{s}{\omega_{\mathrm{a}}}+1}{(\frac{s}{\omega_{\mathrm{a}}})^2+2\xi_{\mathrm{a}}\frac{s}{\omega_{\mathrm{a}}}+1}$	ω_{a}, ξ_{a}	All-pass filter, Phase shifting

In Table 4.2 the commonly used filters and their corresponding parameters are given. They are used to tune the controller with respect to the described functions [NSS99, BCK+09, Oga10]. In practice, in order to manage the AMBs working within their bandwidths so

that no saturation occurs, a roll-off is necessary. Moreover, a roll-off element can cancle sensor noise which often appears at high-frequency region. The first and second order Low-pass filters are normally employed as roll-off elements for controller design. The first and second order filters are used to tune the phase of controller, i.e. phase lead or lag. A notch filter can be used as a band-stop element. If an eigenmode of the rotor shall be neglected by a controller, a notch can be added to the controller in such a way that the eigenmode is located within the narrow stop-band of the notch filter. An all-pass filter is employed to produce a phase shift of ±180 degree at a specified frequency.

4.1.1 Controller Design for the AMB System I

As mentioned in Section 3.5.1, the rotor is symmetrical with respect to the rotor midspan, thus the centralized control configuration is selected to control this AMB system. After transformation, the parallel modes and tilting modes of the rotor allow to be decoupled as shown in Figure 3.10. As a result, the controller design can be achieved separately for the parallel mode and the tilting mode.

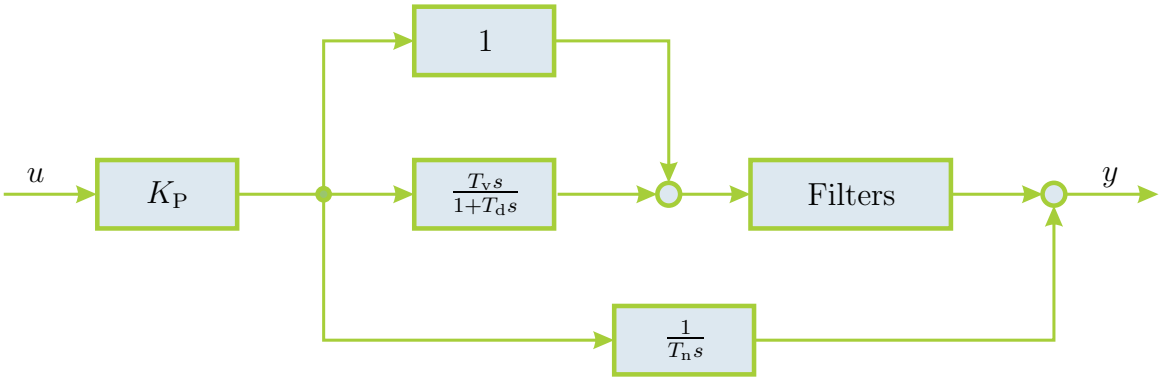

Figure 4.4: *The structure of the PID-controllers in AMB system I [WS15]*

For parallel and tilting mode control, the same controller structure is used. Due to the limitation of the DSP system used in test rig, the PID-controller differs a litte bit from the commonly used PID-controller structure as given in Eq. 4.3. The PID-controller as shown in Figure 4.4, consists of two parts: a PDT_1 elements with filters and an integrator. The first part is limited to be an order of seven due to hardware requirement. It can be written as

$$K_{\mathrm{PD}} = \underbrace{K_{\mathrm{P}} \frac{\frac{s}{\omega_{\mathrm{n0}}} + 1}{\frac{s}{\omega_{\mathrm{d0}}} + 1}}_{\mathrm{PDT}_1} \cdot \prod_{i=1}^{3} F_i, \tag{4.4}$$

with

$$\omega_{\mathrm{n0}} = \frac{1}{T_{\mathrm{v}} + T_{\mathrm{d}}} \quad \text{and} \quad \omega_{\mathrm{d0}} = \frac{1}{T_{\mathrm{d}}}.$$

The three filters F_1–F_3 are second order filters (i.e. No. 4 in Table 4.2).

Furthermore, adding an integrator term to the part K_{PD} gives the final PID-controller structure

$$K = K_{\mathrm{PD}} + \frac{K_{\mathrm{I}}}{s} = \mathrm{PDT}_1 \cdot \prod_{i=1}^{3} F_i + \frac{K_{\mathrm{I}}}{s}, \tag{4.5}$$

with

$$K_{\mathrm{I}} = \frac{K_{\mathrm{P}}}{T_{\mathrm{n}}} = K_{\mathrm{P}} \cdot 2\pi \cdot 1.$$

It can be seen that the controller uses 15 parameters as it will be listed in Table 5.3. For the parallel and tilting mode control, two PID-controllers with the same controller structure as mentioned above are needed. The overall system considering x- and y-plane motions requires four PID-controllers, i.e. two controllers (parallel and tilting mode) for each plane. Therefore, the controller design of the AMB system I requires 30 parameters to be carefully adjusted. The parameters of two controllers (parallel and tilting mode) will be determined and optimized in the next chapter.

4.1.2 Controller Design for the AMB System II

The decentralized control configuration is selected for the controller design, i.e. each side of the rotor requires an individual controller. For both sides (NDE and DE) two controllers need to be designed.

For both sides, the same controller structure is used. Using the controller structure (referring to Eq. 4.3), the controller includes five filters: two second order filters (No. 4 in Table 4.2), one all-pass filter (No. 3), and two low-pass filters of second order(No. 2).

It can be seen that 18 controller parameters are used to construct the controller, 14 from the filters and four from the PIDT_1-part. For both controllers total of 36 parameters shall be determined and optimized. This will be detailed in the next chapter.

4.2 Design Criteria

In this section, criteria related to controller design for AMB-supported rotor system are presented. The criteria are divided into two groups: frequency domain criteria and time

doman criteria. The criteria are introduced from the point of view of control theory. These criteria can be considered in the optimization as it will be shown in the next chapter.

4.2.1 Frequency Domain Criteria

Stability

For any control system, a basic requirement is that the controller shall ensure the stability of the plant. A continuous system is defined as stable if all eigenvalues of the system lie in the left half s-plane. Stability requirement can be considered in the optimization by miniming the stability degree of the system. The stability degree is defined as the maximal real part of the eigenvalues

$$F = \max(\Re(\lambda_i)), \quad \text{for} \quad i = 1 : n, \quad n : \text{number of the eigenvalues},$$

where $\Re$ represents the real part of an eigenvalue. It can be see that the stability of the system is guaranteed, if $F < 0$. According to this definition it can be assumed that the smaller the value of F is, the more stable the system is.

It should be noted that the stability criteria defined here differs from the stability margin defined in the ISO standard ISO-14839 [ISO06], which considers the robustness of the control design. The stability margin will be discussed in detail in the form of sensitivity function in the following.

Damping

For a rotor system equiped with AMBs, an appropriate controller design shall provide sufficient damping level for these eigenmodes within the speed range from zero to maximal operation speed. This ensures that the machine can pass the resonance speeds during run-up or shutdown process without any problem. This objective can be defined to maximize the minimal damping ratio of the eigenvalues within a defined frequency region. Since optimization is defined as minimization as is the case in this contribution, the inverse minimal damping ratio can be defined as a fitness function

$$F = \frac{1}{\min(\zeta_i)} \quad \text{for} \quad i = 1 : k,$$

where ζ_i is the damping ratio of the i-th eigenvalue and k is the number of the eigenvalues in the considered frequency region.

Sensitivity Function

Sensitivity function S gives a measure of robustness of a control system. This can be visualized with the help of a Nyquist plot (also called polar plot) as shown in Figure 4.5. In the Nyquist plot, the smallest distance between the transfer function of the open loop G_0 and the critical point (-1, 0), D_{min}, defines the stability margin of the corresponding closed loop. The larger the distance D_{min}, the more robust the system. The smallest

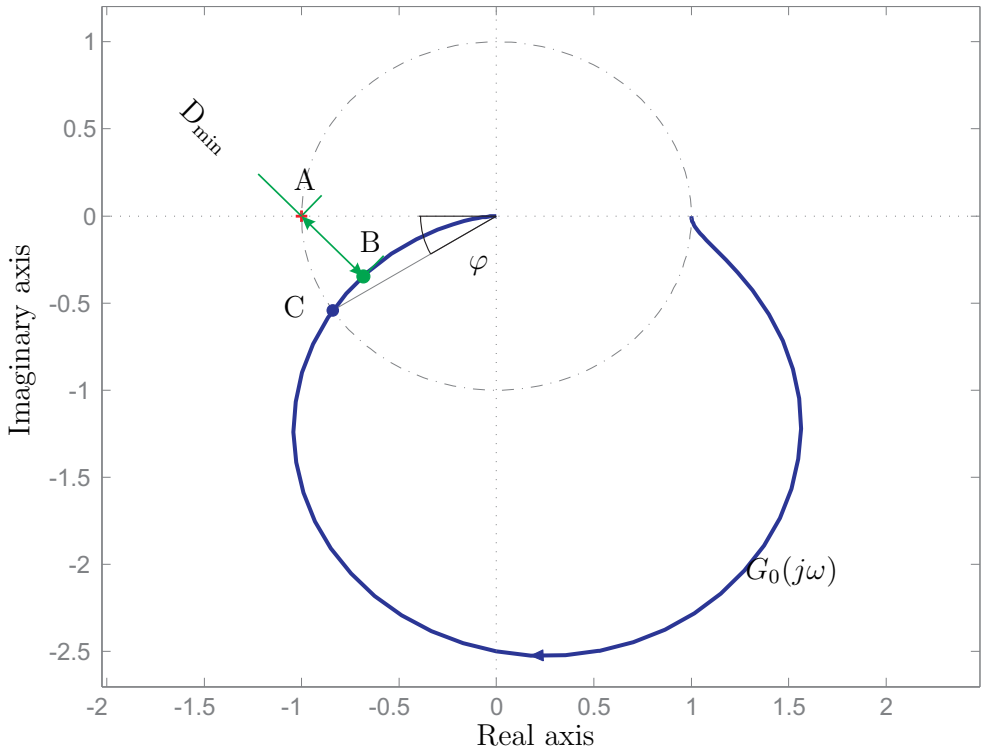

Figure 4.5: *Nyquist plot of a PT2-system with eigenfrequency $f = 10$ Hz and damping ratio $\zeta = 0.2$.*

distance D_{min} is defined by the smallest gain of the transfer function $1+G_0$. Alternatively, it can be determined by calculating the upper bound value of the inverse of the transfer function, i.e. the maximal singular value of the sensitivity function S,

$$F = \max(\sigma(S)) \quad \text{with} \quad S = \frac{1}{1+G_0}.$$

A small value of the maximal singular value indicates that the system has a good robustness. According to ISO-14839 [ISO06], AMB systems can be categorized into four

zones with respect to their sensitivity function values as shown in Table 4.3. Systems with a small peak value of sensitivity function (zone A and B) are expected to have a good robustness. As pointed out in [ISO06], the peak value of sensitivity functions for newly commissioned machines should be located in zone A. Machines with peak values of their sensitivity functions located in zone B are considered as acceptable for long-term operation. An AMB system with a large peak value of sensitivity functions (e.g. in zone C and D) is normally considered as unsatisfactory for long-term continuous operation.

Table 4.3: *ISO-14839 Peak sensitivity at zone limits*

Zone	Peak sensitivity boundaries
A	$\max(\sigma(S)) < 3$
B	$3 \leq \max(\sigma(S)) < 4$
C	$4 \leq \max(\sigma(S)) < 5$
D	$5 \leq \max(\sigma(S))$

An AMB system is a MIMO system, the sensitivity value shall be considered for all axes. The MIMO system is then considered as a Multi-SISO system. For example for the decentralized control configuration (see Section 4.1), the maximal peak values of sensitivity functions both AMBs at left- and right- side shall be considered, i.e.

$$F = \max(\sigma(S_{\text{left}}), \sigma(S_{\text{right}})).$$

4.2.2 Time Domain Criteria

In time domain, the most used design objectives for control system include overshoot, rise time, settling time, and error related cost functions, e.g., the Integrated Squared Error (ISE), the Integrated Absolute Error (IAE), and the Integrated Time Absolute Error (ITAE) [HLX98]. In this contribution, overshoot, settling time, and rise time are taken into account in the optimization, since they can be easily calculated with the help of a step response of the control system. Other objectives (e.g. ISE) can be chosen as fitness functions in the optimization when nonlinear behavior of the control system shall be considered, however, determining these values is expected to be very computationally intensive. In the following, the definations of these terms used in this contribution will be given.

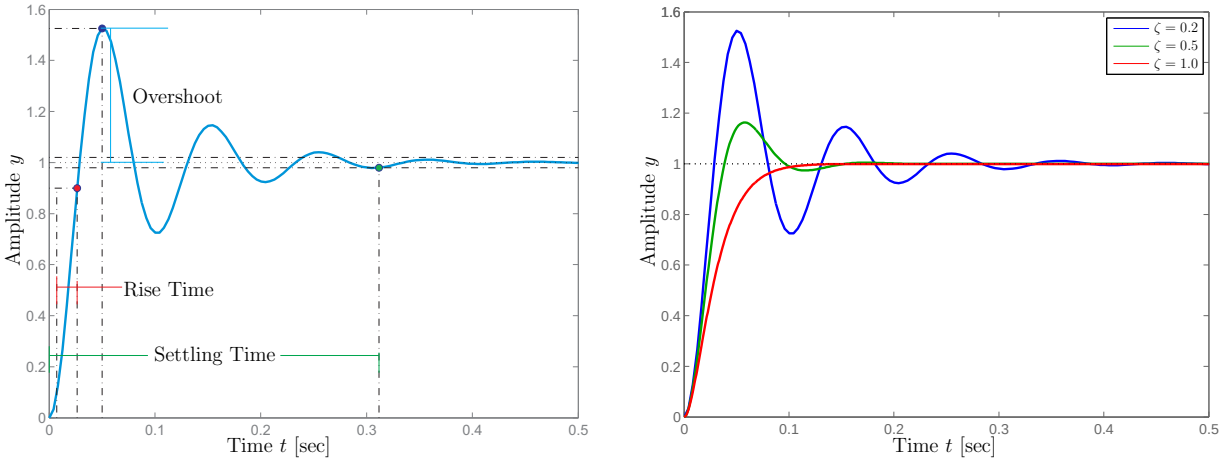

(a) Time domain performance

(b) Effect of damping ratio

Figure 4.6: *Step response of a PT2-system with eigenfrequency $f = 10$ Hz. The damping ratio in plot (a) is set as $\zeta = 0.2$.*

Overshoot

As illustrated in Figure 4.6 (a), overshoot A_{os} is defined as the percentage difference between the maximum peak value from a step response and the final steady-state value [Oga10], i.e.

$$A_{\text{os}} = \frac{y_{\max} - y(\infty)}{y(\infty)} \times 100\%.$$

Overshoot gives an indication how well the system is damped. As shown in [Oga10], the overshoot of a PT2-system is a function of the damping ratio. Figure 4.6 (b) illustrates again the relation between overshoot and damping. A large value of overshoot indicates that the system is poorly damped. A well-damped system behavior can be expected by minimizing the overshoot.

Settling Time

Settling time t_{s} defines the time required for a dynamic system to reach its final steady state and stay within a predefined range (normally 2%) about the final steady-state value [Oga10] as shown in Figure 4.6 (a). Settling time measures how fast the system passes its transient response and reaches its steady state. It is related to the damping ratio [Oga10] as can be seen in Figure 4.6 (b). Obviously, it is desirable for a control design that the controller can regulate the controlled system to reach its steady state as fast as possible, i.e. with a short settling time t_{s}.

Rise Time

Rise time t_r defines the time required for a system to rise from 5% to 95% of its final steady-state value [Oga10]. Rise time measures how fast the system react to the input signal. A short rise time is desired for a control system. As shown in [Oga10], however, the two objectives (minimization of rise time and overshoot of a system) conflict with each other.

Chapter 5

Optimization of the Controller Design for AMB System

In this chapter, various optimization algorithms are reviewed. Special attention is paid to genetic algorithm since the optimization task in this work is performed by using a multi-objective genetic algorithm. A hierarchical evaluation process for evaluating fitness functions is illustrated that it intends to accelerate the optimization process. In order to overcome difficulties from optimization, e.g. optimization with too many decision parameters, sensitivity-based parameter reduction is introduced into optimization. Finally, the optimization results for the two AMB systems are discussed. It should be noted that the material about optimization strategy, optimization ressults, and simulation results has been partially published in author's previous publications [WS12a, WGS13, WS15].

5.1 Introduction to Optimization

5.1.1 Defination

Mathematically, optimization can be defined by

$$\begin{aligned} \text{minimize/maximize} \quad & \mathbf{y} = \mathbf{f}(\mathbf{x}) = [F_1(\mathbf{x}), F_2(\mathbf{x}), ..., F_l(\mathbf{x})]^T, \\ \text{subject to} \quad & \mathbf{g} = [g_1(\mathbf{x}), g_2(\mathbf{x}), ..., g_m(\mathbf{x})]^T \leq \mathbf{0}, \\ \text{where} \quad & \mathbf{x} = [x_1, x_2, ..., x_n]^T \in \mathbf{X}, \text{and} \\ & \mathbf{y} = [y_1, y_2, ..., y_l]^T \in \mathbf{Y}. \end{aligned} \tag{5.1}$$

In an optimization, fitness functions (or objective functions) containing in the fitness vector $\mathbf{y}$ shall be minimized or maximized with design parameters (or decision variables) $\mathbf{x}$

in a search space (or decision space) $\mathbf{X}$, which is subject to the constraint functions containing in the constraint vector $\mathbf{g}$. In this work, without loss of generality, optimization is asummed to be minimization of fitness function(s) unless specified otherwise. Maximization problems can be converted to minimization problems, for example by simply multiplying their original objective functions by -1.

Feasible region (or feasible set) of an optimization problem corresponds to the search space in which all constraints $\mathbf{g}(\mathbf{x})$ are satisfied, i.e.

$$\mathbf{X}_\mathrm{f} = \{\mathbf{x} \in \mathbf{X} \mid \mathbf{g}(\mathbf{x}) \leq \mathbf{0}\}. \tag{5.2}$$

Obviously, the optimization goal is to determine the global optimum for a single objective optimization or the Pareto front for a multi-objective optimization problem within the feasible region.

When there is only one fitness function to be optimized, this type of problem is called single objective optimization problem, otherwise this is a multi-objective optimization problem. Unlike single objective optimization, the result of a multi-objective optimization is a set of optimal solutions, known as Pareto-optimal set or Pareto front. This set of solutions is non-dominated by any other solutions. For multi-objective optimization, two important definations are made as follows [Fon95]:

Definition 1 (Pareto dominance)**.** *A fitness vector* $\mathbf{u} = [u_1, u_2, ..., u_n]^T$ *is said to dominate* $\mathbf{v} = [v_1, v_2, ..., v_n]^T$ *if and only if at least one element* u_i *from* $\mathbf{u}$ *is less than* v_i *from* $\mathbf{v}$ *and all other elemens from* $\mathbf{u}$ *are not larger than the ones from* $\mathbf{v}$*, i.e.*

$$\exists i \in \{1, ..., n\} : \; u_i < v_i \quad \wedge \quad \forall i \in \{1, ..., n\} : \; u_i \leq v_i.$$

Definition 2 (Pareto optimality)**.** *A solution* $\mathbf{x}_u$ *(*$\mathbf{x}_u \in \mathbf{X}$*) with its fitness vector* $\mathbf{u}$ *is said to be Pareto-optimal if and only if it does not exist any solution* $\mathbf{x}_v$ *(*$\mathbf{x}_v \in \mathbf{X}$*) with fitness vector* $\mathbf{v}$ *for which* $\mathbf{v}$ *dominates* $\mathbf{u}$*.*

The relation between solutions in terms of dominance can be visualized as illustrated in Figure 5.1. It shows an optimization problem with the two objectives F_1 and F_2. Taking the red-colored solution R in the middle of the plot as a reference point, it splits the objective space into four quarters. According to the Definition 1, it can be seen that the solution R dominates all solutions located in the peachpuff-colored quarter, since the solution R is better than those solutions in the peachpuff-colored quarter at least in one objective function while it is at least equally good relating to the other objective functions.

On the other hand, the solution R is dominated by any solution in the darkgreen-colored quarter, meanwhile those solutions located in the other two quarters are indifferent to the solution R with consideration of the both objectives. Especially, when compared with those green-marked points, no solution dominates them, in other words, those greed-marked solution are non-dominated by any other solution. They are Pareto-optimal according to Defination 2. All non-dominated solutions together construct the Pareto front (green curve) as shown in Figure 5.1.

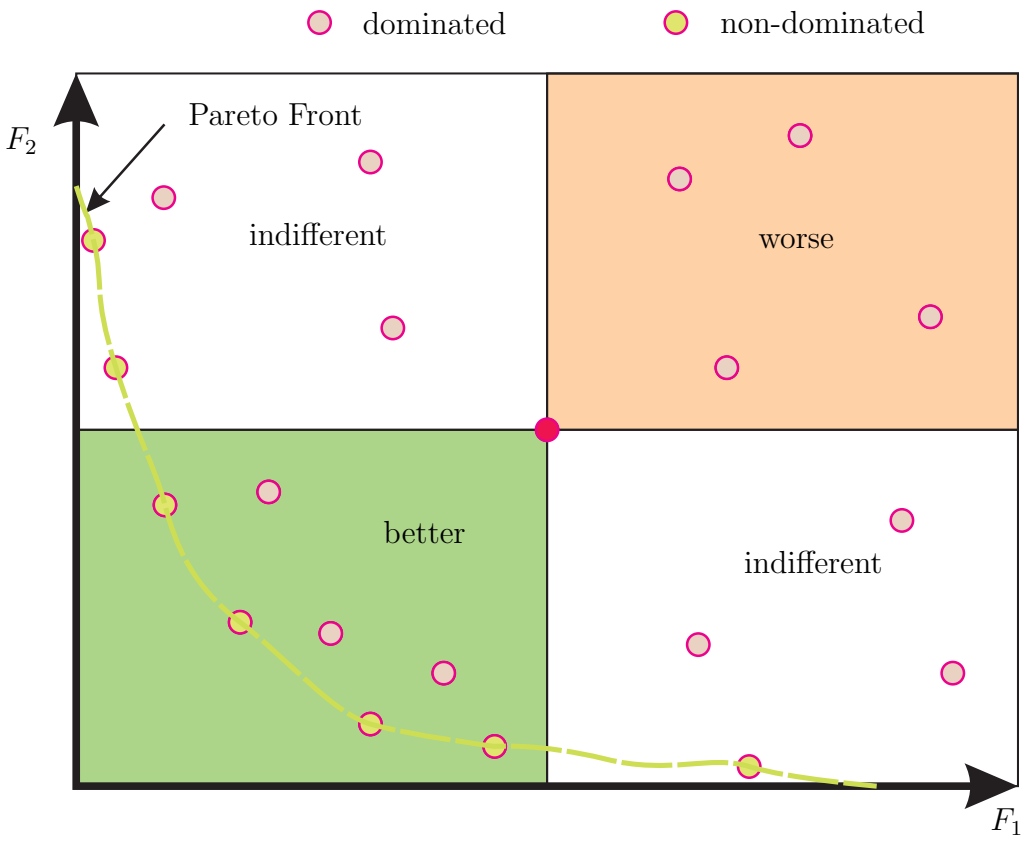

Figure 5.1: *Pareto front of an optimization problem with two objectives*

Most multi-objective optimization algorithms are based on the concept of dominance as illustrated in Figure 5.1. It is clear that multi-objective optimization has two goals [Deb01]:

- to determine the calculated Pareto front as close as possible to the real Pareto front if it exists and
- to maintain the solutions on the calculated Pareto front as diverse as possible.

Traditional optimization methods can be also used to handle multi-objective optimization problem by aggregating the multi-objectives into a single objective (i.e. a scalar function).

The most popular aggregation methods [Fon95,Coe98] include the weighted sum approach and the goal attainment method:

- Weighted sum approach formulates a single objective function F_{sum} with a weighted sum of the original l-objectives, i.e.

$$F_{\text{sum}} = \sum_{i=1}^{l} w_i \cdot F_i,$$

  where the predefined positive coefficient w_i controls the weight (or importance) of the i-th objective. Commonly, the objectives F_i are normalized and the weights are selected so that

$$\sum_{i=1}^{l} w_i = 1.$$

- Goal attainment method introduces a scalar parameter γ and treats the objectives as constraints. The goal is to minimized the scalar parameter γ, i.e.

$$\min_{\gamma \in \mathbb{R},\, \mathbf{x} \in \mathbf{X}} \gamma,$$

  subject to

$$F_i(\mathbf{x}) - w_i \gamma \leq F_i^*,$$

  where coefficients w_i are the weights and parameters F_i^* are the design goals associated with objectives.

When a multi-objective optimization problems are formulated in a single objective problem by using traditional optimization methods, there are a large number of classic deterministic and heuristic optimization methods (see next section) available for solving this single objective problem. These classic methods, especially for deterministic methods, are usually very compuationally efficient and they guarantee a convergence to an optimal solution. However, some drawbacks have to be considered:

- Preference information shall be provided and introduced into optimization problems, for example, with the help of weighting method. How to choose weights for a multi-objective optimization problem is in most cases user-dependent and therefore subjective.

- Most classic optimization algorithms are gradient-based. It is wellknown that they are not suitable for solving multi-modal optimization problems.

- Traditional methods give only a single solution at each run. Therefore they need several simulation runs, for example, by varying the weight coefficients for weighted sum method to generate a Pareto front.

- Some traditional methods (e.g. weight sum method) fail to solve multi-objective optimization problems with nonconvex objective spaces.

In the next section, various optimization algorithms will be given with particular focus on heuristic algorithms.

5.1.2 Optimization Algorithms

Optimization plays a crucial role in various designs of technical systems. Different optimization algorithms are developed during last decades. Solving different optimization problems need different algorthms, e.g. for minimizing or maximizing a single linear fitness function (or objective function) with a set of linear constraints, linear programming (such as simplex algorithm and interior point method) will be the best choice, however this type of algorithms can not be used for solving nolinear optimization problem. No universal algorithm exists, which is suitable for all types of optimization problems.

Optimization algorithms can be roughly divided into two types: classic and heuristic algorithms [Deb01]. The classic algorithms can again be divided into gradient-based methods and direct search methods. Gradient-based methods, such as Newton's method, Quasi-Newton Method (QNM), Gauss-Newton Algorithm (GNA), Levenberg-Marquardt Algorithm (LMA), and Interior Point Method (IPM), use the gradient (the first and/or second derivative of the fitness function) information to guide their search process, therefore these methods are computationally efficient. However the limitation of these methods is that the fitness function has to be continous and differentiable. In direct search methods, e.g. pattern search, only the fitness function value is employed to guide their optimization, thus they are computationally slower than those gradient-based methods.

Heuristic Algorithms

Heuristic algorithms are developed and received more and more attention for solving optimization problems, since they offer some features to overcome those difficulties arising by using classic algorighms, e.g. for solving non-differential fitness function and multi-modal/objective optimization. Heuristic algorithms are somehow between enumerated search and random search [Frö97]. Enumerated search (also called exhaustive search) trys

to find the best solution by evaluating all possible solutions in a predefined search space. Although it always find the global optimum for a single objective optimization problem or the real Pareto front for a multi-objective optimization problem, the computatonal time tends to be unrealistic long for time-consuming evaluations. Random search takes solutions ramdomly and keeps the best solution during search process. Informaton from previous trials which can be used to accelerate the search process and find the global optimum with more confidence, unfortunately, is not used to guide the search direction in this method. Unlike these two methods, heuristic algorithms use some decision mechanisms to steer the optimization procedure and hopefully to reach the optimum. A large class of heuristic algorithms are inspired by phyiscal phenomena or natural processes, i.e. their decision mechanisms mimic some phyiscal phenomena or natural processes. In the following some of these algorithms will be briefly introduced.

Simulated Annealing Simulated Annealing mimics the annealing process in metallurgy and was proposed by Kirkpatrick et al. [KGV83] in 1983. It is observed in metallurgy that forming a crystalline structure of a substance, e.g. growing a single crystal from a meld, is done by annealing, i.e. first heating and melting the substance and then lowering the temperature slowly enough, specially at the temperatures in the vincinity of the freezing point. If this is done, the substance will reach a gobal lowest energy state also called as ground state and form a crystalline solid. Otherwise the resulting crystal retains many defects or even the substance will form a glass. Based on this observaton, the simulated annealing algorithm is developed. In each iteration of this algorithm, a small random change in position is assigned to each atom (indicating a solution of the optimization problem). The resulting energy change ΔE is then calculated. If the energy change $\Delta E \leq 0$, this displacement is directly accepted. For the case $\Delta E > 0$, the Boltzmann distribution is evalutated

$$P(\Delta E) = \mathrm{e}^{\frac{-\Delta E}{\kappa T}}, \tag{5.3}$$

where the parameter κ is known as Boltzmann constant. A random number R_{sa} uniformly distributed in the interval [0 1] is chosen and compared with the Boltzmann distribution $P(\Delta E)$. If $R_{\mathrm{sa}} < P(\Delta E)$, this position change is also accepted. By introducing this randomized acceptance criteria, it allows the solution candidates to escape from a local minimum in order to reach a global minimum.

The main advantages of this algorithm can be summarized as follows:

- easy to implement,
- its global property, and

- no gradient information required.

The disadvangtages are:

- large computational effort and
- inability to deal with multi-objective optimization problems.

Various applications of simulated annealing algorithm can be found in literature. Simulated annealing algorithm was applied to culstering algorithms used in ad hoc networks in [TTEL03]. Simulation results show that with the help of simulated annealing, Weighted Clustering Algorithm (WCA) minimizes the number of clusterheads and improves its performance. Osman et al. [OP89] apply simulated annealing for solving permutation flowshop problem to find a sequence of jobs so that the maximum completion time is minimized. Compared with several other heuristic algorithms, simulated algorithm provides better results in most cases. Gao and Tian [GT07] use an improved simulated annealing algorithm combined with Powell algorithm to optimize the mobile robot path planning. Simulation results indicate the efficiency of the proposed method. In [PFX12], an attitude controller of spacecraft with flywheels supported by magnetic bearings is tuned by using simulated annealing algorithm.

Ant Colony Optimization Ant Colony Optimization (ACO) is inspired by the behavior of ants in searching food source and is proposed by Marco Dorigo et al. [DMC91] in the early 1990s. The basic idee is based on the observation from the entomologist Pierre-Paul Grassé [DBS06]. Grassé observed the mechanism how some species of termites in a colony communicate with each other. Grassé called this type of communication mechanism as "Stigmergy". Stigmergy has the two following main characteristics:

- Indirect: Ants of a colony communicate with each other by using a chemical substance "pheromone" layed in the enviroment by them. In this manner ants indirectly achieve exchanging information.
- Local: The information carried by pheromones is of cause local and it can be only sensed by ants within a small distance near the trail, on which pheromones was layed by other ants.

With the help of stigmergy, ants can achieve tasks such as building nests and searching foods in a very efficient way.

In each iteration of ant colony optimization, the following tasks are performed [DBS06]:

1. Construct ant solutions: each artificial ant from m ants in total constructs a feasible solution from elements of a finite set of available solution components. To construct this solution, an ant searchs and adds a feasible solution components to this solution step by step until this solution is completed. At each step i the probability p_{ij} of choosing the solution component j from the set of the remaining feasible solution components to expand the current solution is guided by the stochastic mechanism

$$p_{ij}^k = \begin{cases} \frac{\tau_{ij}^{\alpha} \cdot \eta_{ij}^{\beta}}{\sum_{c_{il} \text{ is feasible}} \tau_{il}^{\alpha} \cdot \eta_{il}^{\beta}} & \text{if } c_{ij} \text{ is feasible,} \\ 0 & \text{if } c_{ij} \text{ is infeasible,} \end{cases} \tag{5.4}$$

   where the parameters τ and η define the pheromone value and the heursitic information. The parameters α and β give the importance of the pheromone and the heuristic information. The upper index k indicates the k-th artifical ant.

2. Apply local search: The constructed solutions by the ants from last phase will be further improved through a local search.

3. Updata pheromones: Based on the quality (fitness) of the constructed solutions, the pheromone value for next iteration $t+1$ is updated for each solution component

$$\tau_{ij}(t+1) = (1-\rho)\tau_{ij}(t) + \sum_{k=1}^{m} \Delta\tau_{ij}^k, \tag{5.5}$$

   with

$$\Delta\tau_{ij}^k = \begin{cases} \frac{Q_{\text{aco}}}{L_k} & \text{if } c_{ij} \text{ is visited by ant } k, \\ 0 & \text{otherweise,} \end{cases} \tag{5.6}$$

   where parameter ρ controls the evaporation rate of the pheromone and $\rho \in (0\ 1]$. The term $\frac{Q_{\text{aco}}}{L_k}$ introduces the influence of the quality (fitness) of the corresponding solution constructed by the ant k on the pheromone of this solution compoment. Parameter Q_{aco} is a constant and L_k denotes the cost of the solution, e.g. the total distance of a tour in Travel Salesman Problem (TSP).

It can be seen that a pheromone trail (corresponding to a solution) will vanish after several iterations due to evaporation if it corresponds to a poor fitness value. On the other hand, the pheromone value of those trails with a good fitness value will increase. In this manner the artificial ants will find a near optimal solution with an enough large number of iterations. For more infomation about ant colony optimization, reader can reter to [DBS06, DS03].

Ant colony optimization was original proposed for solving combinatorial optimization problem which belongs to the family of discrete optimization. A large number of optimization problems can be formulated as combinatorial optimization problem and be efficiently solved by employing ant colony optimization, such as routing problem [SS03, CCC11], scheduling problem [DZC08, KMF09, CLWL08], assignment problem [DZC08, KMF09], software testing [SS12], and fuzzy controller design [JLLW08]. A survey of application of ant colony optimization in evolvable hardware is given in [DYZF12].

During the last several years, an amount of research has been performed to adapt ant colony optimizatin for solving continous optimization problems [Soc08] and multi-objective optimization problems [IMM01].

Particle Swarm Optimization Particle Swarm Optimization (PSO) and ant colony optimization both belong to swarm intelligence methods. Particle swarm optimization was original developed by J. Kennedy and R. Eberhart [KE95] in 1995 to simulate social behavior. It is inspired by the social behavior of bird flocking and fish schooling. In this algorithm, a set of solutions called as particles fly through the search space of the optimization problem with randomized velocites. Before any termination criterion (e.g. maximal running time, maximal iterations) is met, the positions and velocities of these particles will be adjusted according to their own best position (solution) and the global best position found by the entire population at each iteration, i.e.

$$\begin{aligned} \mathbf{x}_{i,t} &= \mathbf{x}_{i,t-1} + \mathbf{v}_{i,t}, \\ \mathbf{v}_{i,t} &= \mathbf{v}_{i,t-1} + c_1\varphi_1(\mathbf{p}_i - \mathbf{x}_{i,t-1}) + c_2\varphi_2(\mathbf{g}_{\text{pso}} - \mathbf{x}_{i,t-1}), \end{aligned} \tag{5.7}$$

where vectors $\mathbf{x}_i$ and $\mathbf{v}_i$ denote the position and velocity of the i-th particle, respectively. Vectors $\mathbf{p}_i$ and $\mathbf{g}_{\text{pso}}$ define the historical best position of the i-th particle and the global best position found by the entire population, respectively. Parameters c_1 and c_2 are positive numbers and typically they are set to 2, i.e. $c_1 = c_2 = 2$. Parameters φ_1 and φ_2 are two random numbers with uniform distribution in the region of [0 1].

The main advantages of this algorithm are:

- easy to implement,
- very robust,
- its global property,
- utility of parallel computing, and

- no gradient information required.

The disadvantages are the following:

- large computational effort and
- demand on being tuned for different optimization problems.

Several works [BW04, FWX12, Ang98, dNv11] have been performed to compare the two types of optimization algorithm: particle swarm optimization and evolutaionary algorithms. The main result from their comparison can be summarized: Particle swarm optimization has been found to be more effective in terms of convergence than evolutionary algorithms. On the other side, although evolutionary algorithms converge slower to optima than particle swarm optimization does, however it is pointed out in [BW04, FWX12] that they usually obtain a better optimization result than particle swarm optimization does, especially for large number of iterations.

Because of the advantages as mentioned above, particle swarm optimization is applied on solving diverse optimization problems. A literature research [Pol08] is performed by R. Poli. In [Pol08] around 700 papers are counted from over 1100 publications relating to particle swarm optimization found in the IEEE Xplore database until 2007. The most addressed application areas include: Image and video analysis applications (around 7.6% of all application papers), design and restructuring of electricity networks and load dispatching (7.1%), control applications (7.0%), applications in electronics and electromagnetics (5.8%), antenna design (5.8%), power generation, and power systems (5.8%). Numbers of applications of particle swarm optimization to power systems are presented in [dVM+08, YCZ07]. In [dVM+08] diverse variants of particle swarm optimization are summarized. Successful application to antenna design can be found in [RSJ07].

Evolutionary Algorithms Evolutionary algorithms (also called evolutionary computation) are widely used in solving optimization problems. It includes a class of optimization methods which are inspired by natural evolution and based on the principle of natural selection [Dar59]. There are four algorithms belonging to this class: Genetic algorithm, evolution strategy, genetic programming, and evolutionary programming.

Genetic algorithm is the one of the most known heuristic optimization algorithm. It was introduced by R. H. Holland [Hol75] in 1975. In this algorithm, solutions are coded by using chromosome and manipulated with three genetic operators: Selection, crossover, and mutation. Solutions are compared with each other based on their qualities, i.e. fitnesses. Those solutions with a high fitness value have a large chance to survive in the selection

phase and keep as parents to create children by using crossover and mutation. In this manner, the fitness value of the population can be improved through generations. In the next section the detailed optimization mechanism of genetic algorithm will be given.

Evolution strategy was developed by Rechenberg [Rec71] and Schwefel [Sch75] in the mid 1960s. Analogous to genetic algorithm, evolution strategy is also a population-based optimization algorithm using the three operators to improve the fitnesses of solutions. The main difference between both algorithms lies in the selection strategy. In evolution strategy, the so called (μ, λ)-, (μ+λ)-, and ($\mu \overset{+}{,} \lambda$)-selection strategies [BS02] are commonly used. The mainly used selection algorithms in genetic algorithm are roulette wheel selection, rank selection, tournament selection, etc. Moreover, an adaption mechanism is used to adjust the step size of the mutation, although this kind of mutation adaption is later also introduced in genetic algorithm.

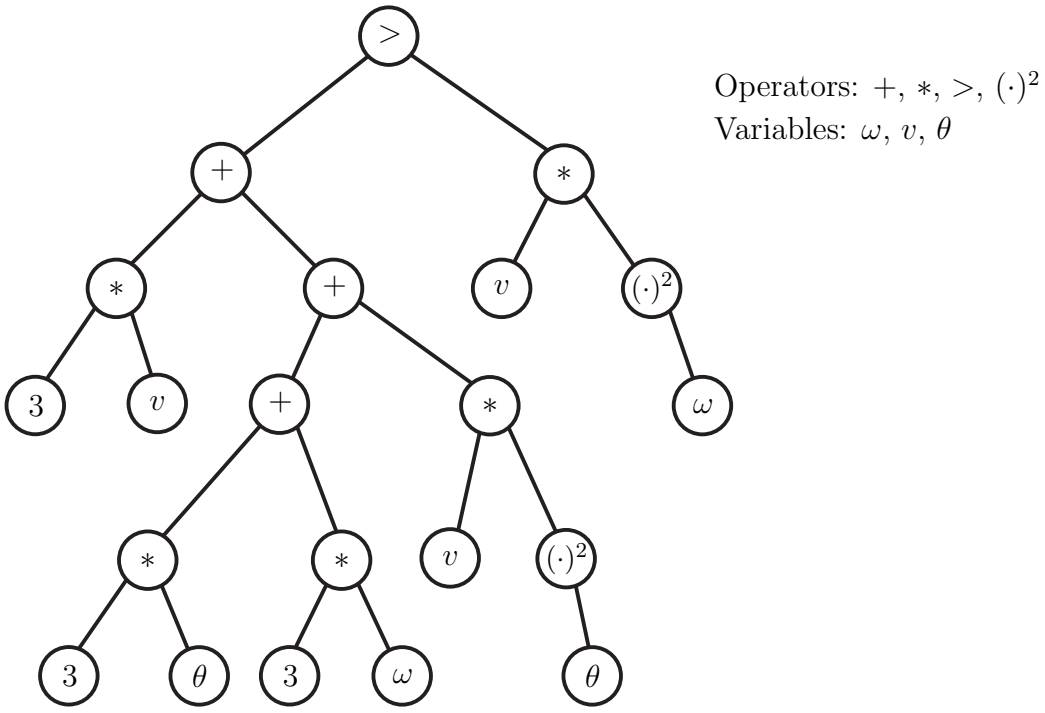

Figure 5.2: *A tree structure representing a control strategy,* $3v + 3\theta + 3\omega + v\theta^2 > v\omega^2$*, for broom balancing problem [Koz90]*

Genetic programming is invented by J.R. Koza [Koz92] in 1992. It was proposed to evolve computer programs. Unlike other evolutionary algorithms, genetic programming uses a tree-like structure to represent a solution (i.e. a program). For instance as shown in Figure

5.2, a control strategy

$$3v + 3\theta + 3\omega + v\theta^2 > v\omega^2,$$

is expressed in form of a tree structure, which is evaluated as $+1$ if this boolean expression (control strategy) is true and -1 for false. The corresponding programs are evaluated based on the efficiency in solving a problem. A fitness value is then assigned to each solution. Based on their fitness values, the solutions representing different programs are selected and the corresponding structures of these programs are modified by means of crossover and mutation.

Evolutionary programming is developed by L.J. Fogel [FOW66] in 1966. Evolutionary programming is quite similar to evolution strategy [BRS93]. They all work in phenotype space (i.e. real-valued search points). They all use a normally distributed randomized and self-adaptable mutation mechanism. However, evolutionary programming employs mutation as a search operator. The fitness values of evolutionary programming are scaled to positive values. Moreover, the selection schema is a tournament selection strategy.

Because of the advantages, e.g., robustness and flexibilty in solving diverse optimization problems, easy to implement, global property, etc., evoluationary algorithms are becoming popular and attracting the attention of practitioners on solving optimizaiton problems. Addtionally, the ability of solving multi-objective optimization problems is an another important reason that makes evolutionary algorithms preferable to other optimization algorithms. During the last three decades, various MOEAs have been developed and successfully applied to numbers of optimization problems. Most of them are based on genetic algorithms. The first study on MOEA was performed by Schaffer [Sch85] in the mid 1980s. Schaffer developed the Vector Evaluated Genetic Algorithm (VEGA). The weighting-based genetic algorithm (HLGA) was developed by Hajela and Lin [HL92] in 1992. Fonseca and Flemming's Multi-objective Genetic Alogrithm (FFGA) [FF93] appeared in 1993. Horn, Nafpliotis, and Goldberg [HN93, HNG94] invented the Niched Pareto Genetic Algorithm (NPGA) in 1993. In 1994, Srinivas and Deb introduced the Nondominated Sorting Genetic Algorithm (NSGA) in [SD94]. Later on, K. Deb et al. improved the NSGA and developed the NSGA-II [DPAM02]. Due to its efficiency, NSGA-II is becoming the most popular optimization algorithm over other MOEAs. The Strength Pareto Evolutionary Algorithm (SPEA) was proposed by Zitzler and Thiele [ZT98, Zit99] in 1998. Q. Zhang and H. Li [ZL07] introduced a decomposition-based algorithm named as MOEA/D in 2007. For the detailed information about MOEAs, the interested reader can refer to the works [Deb01, Coe98, Coe06, FF95, TKK96, KCS06]. Additionally, a repository of MOEA references is maintained by Carlos A. Coello Coello. Over 8000 references in total are collected, including journal and conference papers, Ph.D. theses, books, etc. Statistics

shows that the interest in the area of MOEAs grows rapidly in the last two decades, as illustrated in Figure 5.3.

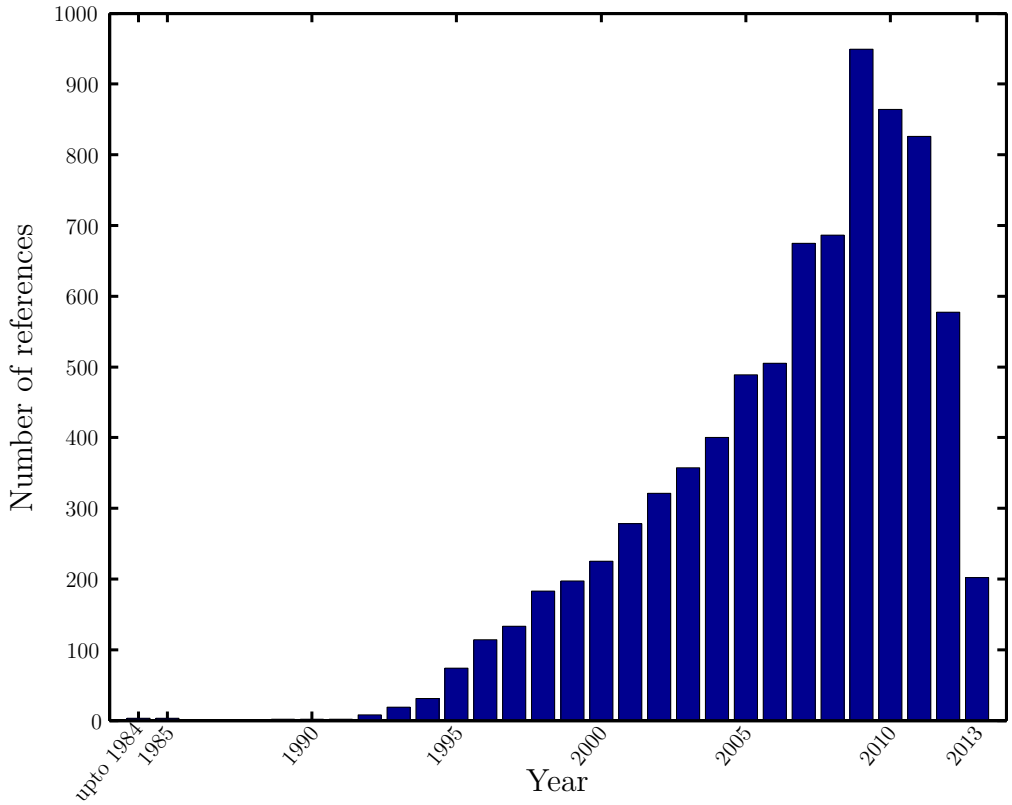

Figure 5.3: *Distribution of the references about MOEAs by year*[1]

Evolutionary algorithms are used in a wide variety of application domains. A survey of application in economics and finance is done by [PJC13]. In [PJC13] it focuses on the application of MOEAs to portfolio optimization problem and the other financial and economics optimization problems such as financial time series, stock ranking, risk-return analysis, financial and trading decision-support tools, and economic modeling. The application of MOEAs in power system optimization problems is summarized in [PSL10]. In [Bak01], genetic algorithm is used to remove overloads and voltage problems in electric power systems. A survey of application of evolutionary algorithm in evolvable hardware is given in [LH06]. The examples contain evolvable hardware consist of FPGA hardware evolution, evolution of analog circuits and optics, evolved robots, evolved Sony AIBO

[1]Statistics of the evolutionary multi-objective optimization repository (by August 5th, 2013): `http://delta.cs.cinvestav.mx/~ccoello/EMOO/EMOOstatistics.html`

Gait, evolution of physical forms, and evolved antenna designs. Yuhui Shi gives a survey [Shi99] of fuzzy system design using evolutionary algorithms in 1999. Surveys of evolutionary algorithms for clusering and decision tree induction are given by E.R. et al. [HCFd09] in 2009 and R.C. Barros et al. [BBdF12] in 2012, respectively. Application in scheduling problems is studied in [SI96, HL10, TNA99]. Furthermore, application in control engineering can be found in a number of literature references. Different types of controller including PID-control [LJS03,CCZ09], robust control [MCGFO06,Fon95,CC98], and LQG-control [MG00], are designed and tuned by using evolutionary alogrithms. Addtionally, evlutionary algorithms are used to tune not only the parameters but also the structure of a controller in [KKY$^+$00, CMN$^+$04, FW06]. A survey on evolutionary algorithms in control engineering is given by P.J. Fleming and R.C. Purshouse [FP02] in 2002. Furthermore, controller design using evolutionary algorithms for magnetic bearing systems is reported in [SGGF01, Bak87].

5.1.3 Genetic Algorithm

Genetic algorithm is a population-based heuristic optimization algorithm inspired by nature evolution and based on the principal of natural selection (i.e. "survival of the fittest") [Dar59]. The concept of genetic algorithm was first introduced by J. Holland from University of Michigan in 1970s.

The algorithm can be illustrated with the help of the flowchart as shown in Figure 5.4. Before the evolution begins, a population of individuals is initialized. The individuals are randomized generated within the predefined search space as well as by satisfying the constraints. The number of individuals is called as population size, which is an important parameter of this algorithm. This population is known as initial population.

After initialization, the members of the initial population will be evalutated based on the used-defined objective function. Each individual is assigned a fitness value according to its quality or cost. The simplest way for fitness assignment is directly taking the objective function values of individuals as their fitness values for a maximization problem. Two other fitness assignment methods are commonly used, namely scaling and ranking [Fon95]:

- Scaling: Raw fitness is defined as a function of the objective function value and then the raw fitness is linearly scaled to give the fitness values of each individuals of the population.
- Ranking: The individuals are sorted base on their cost or objective function values. According to their ranks, fitness values are then assigned to the individues.

Once fitness assignment is completed, the next step is to check the termination criteria. If any termination criteria is fulfilled, the algorithm stops. Otherwise the individials will continue to create new generations and evolve. Typical termination criteria indclude maximal generation number, maximal running time, fitness value limit, and a certain time or number of generations within which no change appears in fitness value.

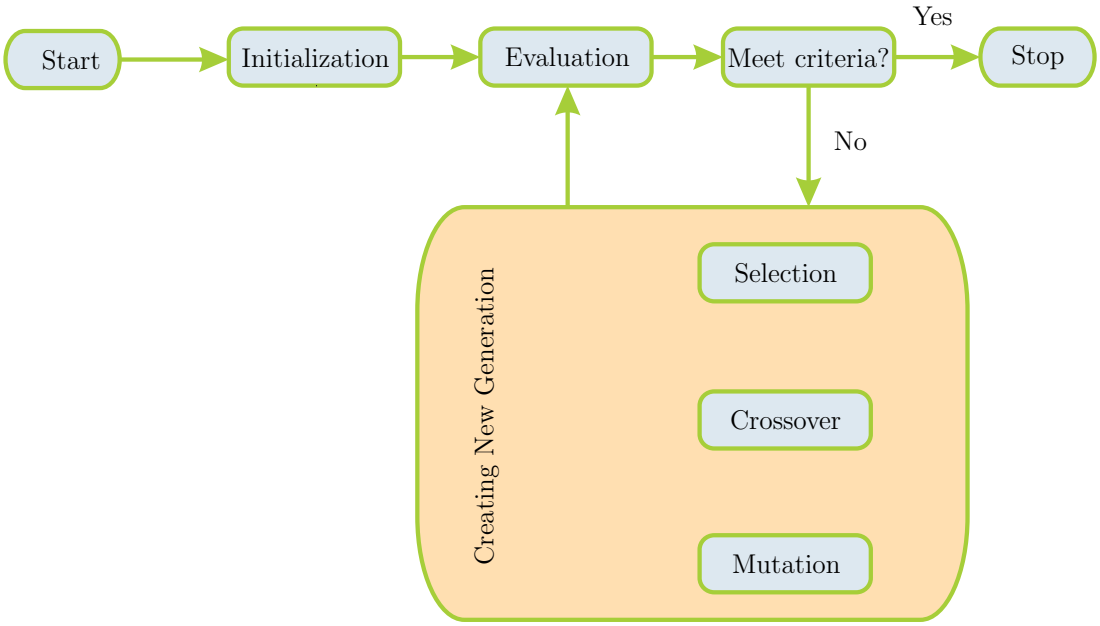

Figure 5.4: *Flowchart of genetic algorithm*

To generate a new population, a certain number of individuals are selected as parents in mating pool. Basically, those indiviuals with good fitness shall have more chance to survive in next generation and be chosen as parents. However a few indiviudes with a low fitness value may be luckily selected in mating pool. Different selection strategies are developed. Roulette wheel selection [Gol89], stochastic universal sampling [Bak87], and tournament selection [Han94] are commonly used.

As illustrated in Figure 5.5, eight parents will be selected from six individuals (A–F) in total. The size of each slot on the roulette wheel indicates the probability of the corresponding individual, e.g. individual A has a probability of 35% which is directly related to its normalized fitness value. For roulette selection, the eight parents are sequentially selected by 8x repeatedly spinning the single pointer on the roulette wheel as shown in Figure 5.5 (a). Obviously the individuals (A, F, and C) have more change being selected. The individuals with low fitness (i.e. B and E) will most likely be eliminated by the selection, thus the fittest one will possibly dominate all the others over time. It leads to an undesirable phenomenon known as genetic drift (i.e. the population tends to evolve

towards a small region). Genetic drift causes loss of diversity and in this case genetic algorithm behaves as a local optimization algorithm.

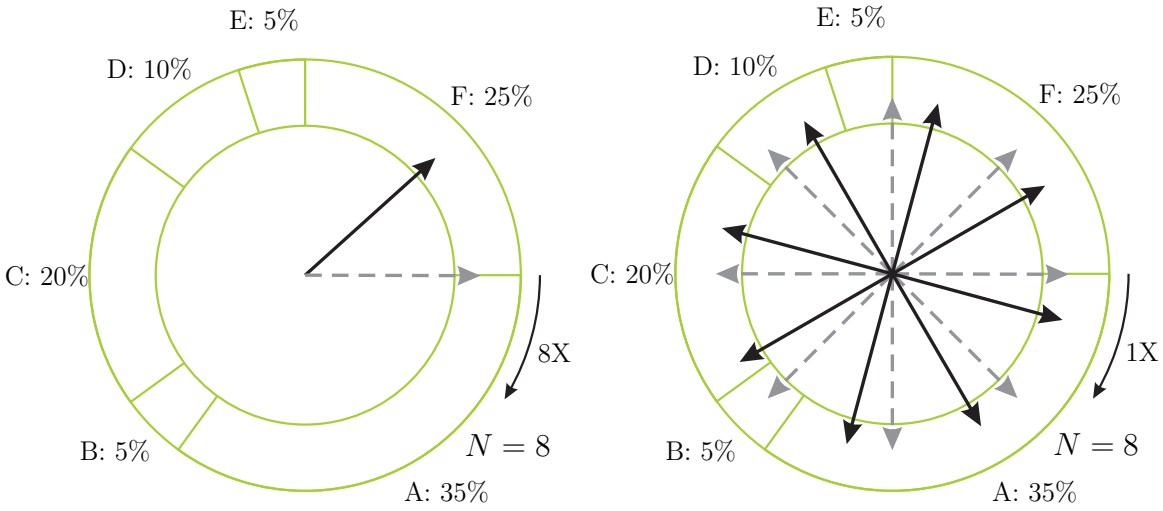

(a) Roulette selection (b) Stochastic universal sampling

Figure 5.5: *Selection strategies of genetic algorithm*

Unlike roulette selection, stochastic universal sampling uses multiple pointers for selection instead of a single pointer. The number of pointers corresponds to the number of individuals to be selected and they equally partition the roulette wheel as shown in Figure 5.5 (b). The selection of the eight parents can be thus achieved by a single spinning of the multiple pointers over the roulette wheel. Obviously, stochastic universal sampling is equivalent to roulette selection in case there is only one single individual to be selected. However in case of selection of multi-individuals, this selection method is undoubtedly superior to the roulette selection method in terms of spread, i.e., it achieves a zero bias (the absolute difference between the actual sampling probability of an individual and the expected value of it) and minimum spread [Bak87].

Tournament selection involves performing N tournaments when N individuals shall be selected. In each tournament, a certain number of individuals (typically two individuals) are randomly chosen and compared with each other. Simply the winner (with the best fitness) in a tournament will be selected as parent in mating pool. A shortcoming of this selection method is that it does not guarantee any particular individual, not even the one with the best fitness, to be actually selected.

When all parents in mating pool are determined by selection, genetic algorithm starts to modify the parents and create new ones known as children or offsprings by using the two genetic operators: Crossover and muation.

Unlike evolution strategy and evolutionary programming, in which the most important operator is mutation, crossover (or recombination) is the most important operator in genetic algorithm. With the help of crossover, genetic algorithm achieves an exploitation of the existing building blocks of the chromosomes from the parents by recombination of these building blocks. It tends to find the superior area from the search space [FP02]. Note that no new building blocks will be introduced with crossover operator, this is namely a task of mutation.

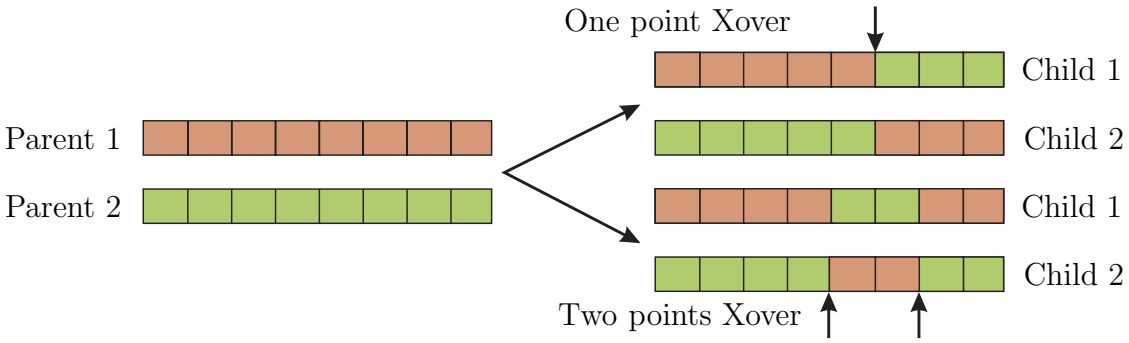

Figure 5.6: *Crossover methods of genetic algorithm*

Crossover is used to generate two children by recombination of a pair of parents. The classic crossover methods are one point crossover and two points crossover. For one point crossover, a point on the chromosomes of the two parents is ramdomly selected. Swapping the part of strings from the both parents behind this point yields the two offsprings as shown in Figure 5.6. Analogously, two points crossover randomly chooses two points on the chromosomes and exchanges the strings between the two points of the two parents to form the two children as illustrated in Figure 5.6. In fact, most of children are generated by using crossover operator and therefore a large probability of crossover is used in genetic algorithms, commonly the crossover probability $p_c \in [0.6 \;\; 0.9]$.

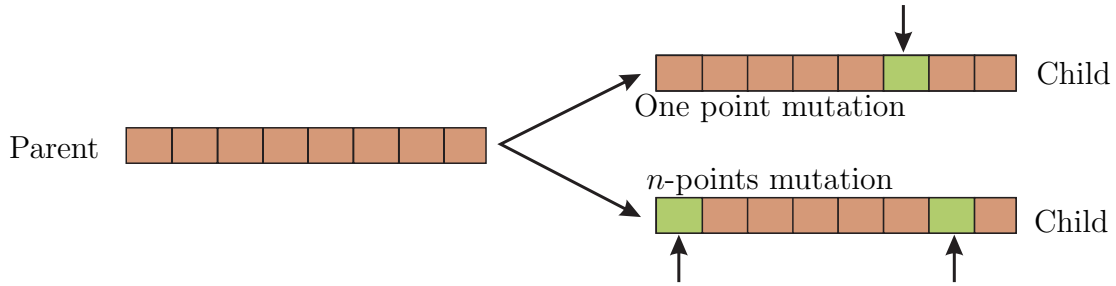

Figure 5.7: *Mutation methods of genetic algorithm*

Mutation is another important operator in genetic algorithms. It allows the optimizer to explore new areas of the search space so that the optimizer can escape from a local

optimum with the help of the mutation operator. This introduces the global property in genetic algorithms.

Mutation chooses one point or n-points on the chromosome of one parent, ramdomly or with a given distribution probability. The corresponding strings are then alterd as shown in Figure 5.7, e.g., by performing a bit flip for a binary string representation. In fact, only a small number of individuals are selected to mutate and usually a small mutation probability is used, commonly mutation probability $p_{\mathrm{m}} \in [0.02 \;\; 0.05]$.

The original genetic algorithm works on the genotypic chromosomes. An individual's genotype is an encoded representation of its original real-valued decision parameters (i.e. phenotype). Before crossover and mutation being performed, all individuals shall be firstly encoded in the genotype, typically in form of bit strings. After a new generation being created, the individuals will be then decoded in their phenotype for evalutation of objective functions. Real-valued genetic algorithms are later developed and become popular, in which no encoding and decoding of decision parameters are needed. Correspondingly, many real-valued crossover and mutation techniques are developed, e.g. Simulated Binary Crossover (SBX), Simplex Crossover (SPX), non-uniform mutation, uniform mutation, gaussian mutation, etc.

5.2 Optimization Strategy

In the last section, various optimization algorithms are introduced. Especially, genetic algorithm is given in detail.

In this contribution, the multi-objective optimization task of the controller design for the AMB systems is performed by using NSGA-II, which is available in several commercial software packages.

Although genetic algorithms are robust and can be applied in a wide variety of optimization problems, their parameters, such as population size, crossover probability, and mutation probability, have to be tuned carefully for different optimization problems. These parameters are often connected.

Deb [Deb01] discusses the significance of the population size used in genetic algorithms with the help of a schema representation. A schema is defined as a set of individuals with the same strings in certain string positions. For example, a schema $\mathcal{H} = [1 \;*\; 0 \;*\; *\; 1\; *]$ represents a set of individuals that have the same strings 1, 0, and 1 at the string position 1, 3, and 6, respectively. The order of a schema defines the number of string positions with the same strings. Clearly, the schema $\mathcal{H}$ has an order of three. A schema can be viewed as

a certain region in the search space. Higher order schemas have a narrower representing region. Deb uses a bimodal optimization (maximization) problem to illustrate the necessity of using a large population size to find the global maximum located at the top of a narrow peak. To locate the maximum point at the top of a narrow peak, the order of the schema should be high enough to represent these narrow regions. The population size is related directly to the order n of these schemata

$$N_{\text{popsize}} = 2^n \cdot \epsilon,$$

and the parameter ϵ denotes the number of individuals needed to represent a region statistically. Higher order schemata have larger population sizes.

Obtaining a balance between exploration and exploitation in the optimization process is another important issue [Deb01]. In genetic algorithms, exploration is controlled by crossover and mutation operators, while the selection operator is responsible for exploitation. Using too large a selection pressure leads to a loss in diversity in the population and causes premature termination of the optimization process. However, genetic algorithms behave like a random search algorithm when too small a selection pressure is chosen.

The above discussion shall be carefully considered in setting the genetic algorithm parameters. These parameters have to be tuned for different optimization problems, i.e., a set of genetic algorithm parameters, which works "well" on most optimization problems, does not exist.

The complexity of the optimization problem may also challenge genetic algorithms. Despite careful consideration, while setting of optimization parameters, genetic algorithms may fail to solve optimization problems because of the high degree of complexity of the problem. Here, a high degree of complexity is described by the properties including the following aspects:

- Objective function of the optimization problem is multi-modal. Multimodality means that a number of local optima exist besides the global optimum.
- Feasible region of the problem is discrete and even random (point-wise) distributed.
- Objective function (or objective space) is non-continuous, non-differentiable, and noisy.
- For multi-objective optimization, different relations between objective functions exist and these relations can even vary within the search domain [PF07].
- The optimization problem belongs to the Non-deterministic Polynomial-time ($\mathcal{NP}$)-complete class.

- The number of objectives to be optimized is high.

The above aspects often lead to crucial problems in optimization, such as the premature convergence to a sub-optimal solution region, loss of diversity, and even failure to solve the optimization problems [Wei09].

With respect to the optimization problem for the controller design of the AMB system, the main difficulty results from the basic requirement on stability. Defining feasible stability regions for the closed-loop AMB system including the aforementioned number of design parameters and requirements leads to randomly distributed, sparse regions within the search space. If the stable region is known in advance, it is preferable to solve the optimization problem directly close to the known solution region. However, determining the stable region of a fixed order controller design (e.g. PID-like controller with fixed structure) is like determining a stable polynomial or matrix in an affine family, which is an $\mathcal{NP}$-hard problem [Pet08, BT00]. In the special case, only two controller parameters are selected as optimization parameters and the D-decomposition method can be used to define their stable region. Considering a linear system with a characteristic polynomial $p(s, \mathbf{k})$, the stability boundary is defined by

$$p(j\omega, \mathbf{k}) = 0, \quad -\infty < \omega < +\infty,$$

where the parameter vector $\mathbf{k}$ ($\mathbf{k} = [k_1, k_2, ...]^T$) contains all unknown parameters (e.g. controller parameters). Evaluating Eq. 5.2 gives two equations, i.e.,

$$\begin{aligned} \Re(p) &= 0, \quad \text{and} \\ \Im(p) &= 0. \end{aligned}$$

The two equations can be solved if the vector $\mathbf{k}$ contains two parameters. The solution curves $k(\omega)$ split the parameter domain into several root invariant regions, within which the number of stable and unstable roots is constant. The stable region can be determined from the region with no unstable roots. It is possible that more than one stable region exists in the parameter domain. This is the basic idea of D-decomposition [GP06].

Known controller design approaches allow for the design of more than two parameters, even for the classic PID-controller that contains three parameters: K_P, T_n, and T_v for the proportional, integral, and derivative parts of the parameters, respectively. Parameter reduction is introduced to ease the optimization due to randomly distributed feasible regions resulting from the stability requirement of the control system with a large number of controller parameters. The main advantages of the parameter reduction can be summarized as follows:

- Reducing the number of optimization parameters reduces the complexity of the optimization problem.
- The continuity of the feasible regions can be improved. Although the problem with the randomly distributed feasible region cannot be removed completely, most feasible candidates will gather together in some regions of the search area.
- The optimization process is accelerated. Some time is taken for genetic algorithms to evaluate sufficiently large number of possible combinations of optimization parameters (i.e., candidates) to gain the heuristic information guiding the optimization direction. The number of combinations is related directly to the number of optimization parameters. Reducing the number of optimization parameters will therefore reduce the necessary number of candidates to be evaluated. This accelerates the optimization process.

In Figure 5.8, an example of the controller design with a different number of tuning parameters for AMB system II is shown. The controller design (including two controllers, one for the DE side and the other for the NDE side), contains 36 controller tuning parameters in total. In Figure 5.8, the feasible region for cases with 36 parameters (5.8a), ten

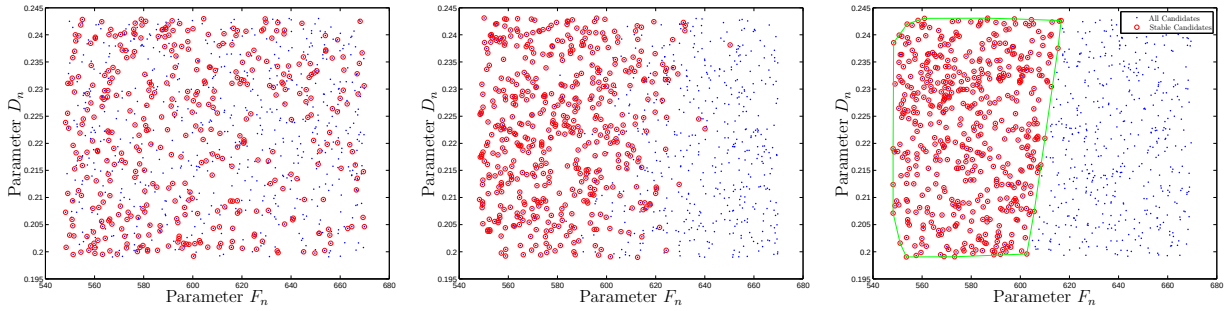

(a) 36 Parameters (b) 10 Parameters (c) 2 Parameters

Figure 5.8: *Feasible region with different number of tuning parameters [WS15]*

parameters (5.8b), and two parameters (5.8c) is illustrated. For each case, a total of 1000 candidates is generated. They are uniformly distributed with a maximal 10% deviation from an initial solution $\mathbf{X}_0$. The feasible ones (i.e., the stable candidates) out of the 1000 candidates are marked by red circles. For the case with two parameters (see Figure 5.8c), the parameters F_n (the zero frequency of a second-order lead-lag filter of the controller from the NDE side) and D_n (the corresponding damping ratio of the zero) are selected as tuning parameters while the other parameters remain constant as the initial solution $\mathbf{X}_0$. For the case with ten parameters (see Figure 5.8b), ten controller parameters including

the two parameters F_n and D_n are selected as tuning parameters. For the case with 36 parameters (see Figure 5.8a), all the 36 controller parameters are considered to be tuning parameters. By comparing the three cases, it can be stated that the feasible candidates will accumulate in certain regions when the number of tuning parameters is reduced. For case a, the feasible candidates are randomly distributed on the D_n-F_n plane. However as described by D-decomposition theory, for case c, the feasible candidates are clearly separated from the infeasible ones and the feasible region can therefore be determined, i.e., the region encircled with green lines as shown in Figure 5.8c. This example shows that reducing the number of optimization parameters can improve the continuity of the feasible region of an optimization problem for controller design.

As a next procedural step, it needs to be determined which parameters should be chosen as design parameters. Intuitively, the parameters that influence the fitness function values significantly, should be selected as optimization parameters. With this assumption, the sensitivity-based parameter reduction strategy is introduced and discussed in the following subsection.

5.2.1 Sensitivity-Based Parameter Reduction for Optimization

Many systems cannot be modeled directly based on an understanding of the working principle or theory behind the systems. Attempts are therefore made to build an empirical model (also called a regression model) in a statistical sense, based on observed data [Mon09]. This procedure is known as regression. When a number of parameters or factors is involved in regression, it is unrealistic to explore all parameter combinations, since each experiment or simulation (corresponding to a parameter combination) can be time-consuming. Sensitivity analysis is therefore introduced to reduce the number of variables required for building a regression model. In [WM09], sensitivity analysis is applied successfully to reduce the number of variables in meta-modeling.

Sensitivity analysis determines the strength of the linear relation between any two variables. For the multivariable case, the elements in the correlation matrix are defined as

$$\mathbf{R}_{\text{corr}}(i,j) = \frac{\text{cov}(x_i, x_j)}{\sigma(x_i)\sigma(x_j)} = \frac{\text{cov}(x_i, x_j)}{\sqrt{\text{cov}(x_i, x_i)\text{cov}(x_j, x_j)}}, \tag{5.8}$$

with

$$-1 \leq \mathbf{R}_{\text{corr}}(i,j) \leq +1,$$

here $\sigma(x_i)$ denotes the standard deviation of the i-th parameter and $\text{cov}(x_i, x_j)$ denotes

the covariance between the i-th and j-th parameter

$$\mathrm{cov}(x_i, x_j) = E[(x_i - \mu_i)(x_j - \mu_j)],$$

with E as expected value and μ as mean value.

A positive value of the correlation coefficient $\mathbf{R}_{\mathrm{corr}}(i, j)$ indicates that both variables are positively linearly correlated, while a negative value means that a negative correlation exists between them.

The idea to reduce the number of regression variables is applied to the optimization problems. As mentioned previously, it is desirable to neglect some of the tuning parameters in the optimization process if they do not influence the optimization result significantly. Only those with a strong influence on the fitness functions are chosen as optimization parameters. The sensitivity analysis is introduced to determine the strength of the relationship between the design parameters (i.e., controller parameters) and the parameters of the objective functions. Using a sensitivity analysis, the design parameters can be ranked based on the strength of their influence on the result of the objective functions. The design parameters with the strongest influence are selected for the optimization, while the remaining design parameters are considered to be constant during the optimization process.

The selection of parameters is intuitive for the case where only one objective is considered. For multi-objective cases, the Goldberg's ranking technique [Gol89], which is used extensively to rank the individuals in one population for Pareto-based multi-objective evolutionary algorithms, is used. In this method, the non-dominated individuals (front 1) of the current population are assigned as rank 1, and the individuals on the next front are assigned as rank 2, and so on. To select the design parameters, the design parameters are ranked based on the sensitivity analysis, then the parameters on the first front are recommended to be selected for further optimization.

To perform the sensitivity analysis, data have to be collected by finite attempts (or more formally called experiments in statistics). Here, the Design of Experiment (DoE) plays a crucial role. Several DoE methods are known. The most widely used DoE is the 2^k (k: number of the variables) factorial design. In this approach, each variable (or factor) is investigated only at two levels. These two levels can be quantitative (e.g. two values of pressure) or qualitative (e.g. with and without optimization). This approach works well only if several design variables are investigated. However, it can become unrealistic if the number of variables increases, e.g. if 30 variables are considered, an unrealistic 1.0737e9 ($= 2^{30}$) experiments are required. To avoid this situation, the randomized method is performed, in which the selected values of each variable are distributed uniformly between

upper and lower bounds.

5.2.2 Results of Sensitivity-Based Parameter Reduction

In the following, two cases are studied illustrating the result of the sensitivity analysis applying on the considered optimization problems of the controller design for AMB system II as given in Chapter 4: single and multi-objective optimization.

Case a: Single Objective

For the sensivity analysis 1e5 controller candidates of the AMB system introduced in Section 3.5.2 are generated randomly in a local search space. The local search space is defined based on an initial solution $\mathbf{X}_0$. The candidate is distributed uniformaly with a 20% maximal deviation from the solution $\mathbf{X}_0$. There are 11363 candidates selected for the sensitivity analysis, which result in a stable closed-loop. As an example, the maximal singular value of the sensitivity functions of both sides (DE: S_{de} and NDE: S_{nde})

$$\sigma_{\max}(\mathbf{S}) = \max\{\sigma(S_{\mathrm{de}}), \sigma(S_{\mathrm{nde}})\}$$

is taken as an objective function to be considered.

In Figure 5.9 the results of the applied sensitivity analysis (i.e. correlation matrix) are illustrated using a colored map. The left plot shows the correlation between variables including controller parameters (No. 1–36) and the objective function parameter $\sigma_{\max}(\mathbf{S})$ (No. 37). The correlation matrix is symmetric and its upper triangular part respresents the same information as its lower triangular part. The correlation coefficient between a variable and its self is always equal to 1, therefore the main diagonal elements of the correlation matrix are equal to 1 (i.e. dark-red colored blocks). It can be seen that some of controller parameters are strongly correlated as indicated by the yellow- or dark-blue-colored blocks, e.g. controller parameter pairs No. 5 – 7 and No. 33 – 35. The correlation between controller parameters and the objective function (as shown in the last row or the last column of the correlation matrix) is of interest for the optimization, since it shows the strength of the influence of these controller parameters on the objective function. This result is highlighted in the right plot. The first five controller parameters (5, 19, 9, 7, 17) with the strongest influence on the objective function are also marked. It should be noted that the absolute value of the correlation coefficients $|\mathbf{R}_{\mathrm{corr}}(i,j)|$ are used to sort the controller parameters.

The parameters with the strongest influence can easily be determined based on the sensitivity analysis and selected for further optimization. Since this is a single-objective opti-

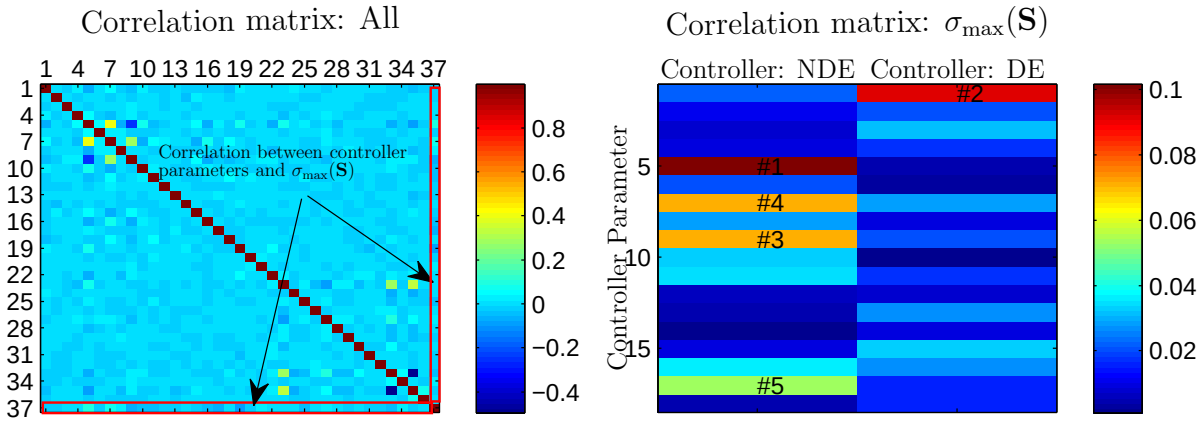

Figure 5.9: *Correlation between controller parameters and the maximal singular value [WGS13]*

Table 5.1: *Optimization results*

Selected parameters		Pattern search		Simulated annealing	
		$\sigma_{max}(\mathbf{S})$	Time [min]	$\sigma_{max}(\mathbf{S})$	Time [min]
Randomly selected	1, 20	3.2712	9	3.2496	165
				3.2496	165
	9, 19	2.93	6	2.9008	165
				2.9006	165
	3, 8, 15, 24, 31	2.264	42	2.2639	165
				2.2585	165
	1, 13, 19, 23, 33	2.1625	43	2.2126	141
				2.2022	141
With all parameters	1–36	2.069	416	2.0949	707
				2.1254	708
Acc. to sensitivity analysis	5, 19	2.7674	10	2.28	165
				2.285	165
	5, 19, 9, 7, 17	2.0596	50	2.0627	166
				2.0392	166

mization problem, instead of using genetic algorithm, two other optimization algorithms are selected for optimization: Pattern search and simulated annealing. The optimization is carried out in the local search space around the initial solution $\mathbf{X}_0$ mentioned above. The only objective function is to minimize the maximal singular value $\sigma_{max}(\mathbf{S})$. The maximal singular value obtained from the initial solution $\mathbf{X}_0$ is about 60. Due to the

randomized characteristic of simulated annealing algorithm, two runs are performed for each case. Parameter reduction is considered in two cases: with two and five parameters. In order to show the efficiency of sensitivity-based parameter reduction, optimization is also performed with randomly selected parameters. For the cases with randomly selected parameters, each case is repeated with different selected parameters, e.g. for optimization with two randomly selected parameters, the optimization is performed in two subcases: a) with parameters No. 1 and 20; b) with parameters No. 9 and 19. Meanwhile, optimization is also performed for the case with all 36 controller parameters. The optimization results are presented in Table 5.1. The optimization result with sensitivity-based selected parameters is clearly superior to the one with randomly selected parameters. Comparing the two optimization algorithms, pattern search is more efficient that simulated annealing, since they give solutions with more or less the same quality while pattern search needs obviously less computational time than the one simulated annealing needed. It should be mentioned that the optimization process for pattern search is terminated by reaching its predefined tolerance of mesh-size, while for simulated annealing is by reaching its maximal optimization time. For the optimzation with all 36 parameters, a larger maximal optimization time is assigned. Theoretically, it should provide the best results. However, it can be seen that the results obtained with the five controller parameters (5, 19, 9, 7, 17) are even better (smaller max. singular value $\sigma_{\max}(\mathbf{S})$ and shorter computing time) than that with all 36 controller parameters. It should be noted that the optimization with all controller parameters shall give the best result by increasing e.g., the time limit and decreasing the mesh size.

From the optimization results given in Table 5.1, it can be seen that the optimization process is accelerated in case of parameter reduction. Moreover, with sensitivity-based parameter selection, it gives a better result than those optimization result with randomly selected parameters.

The result presented above is for the optimization case with a single objective. In the following, the result for the more common case, namely mult-objective optimization, is discussed.

Case b: Multi-Objective

For the multi-objective case, sensitivity analysis is carried out based on the data of 5473 feasible (stable) candidates from the 5e4 randomized generated candidates around the initial solution $\mathbf{X}_0$. The AMB system and controllers are identical to the case with single objective. However, the number of objectives is increased to four:

1. The maximal singular value of the sensitivity function $\sigma_{\max}(\mathbf{S})$ should be minimized.

2. The maximal real part of the eigenvalue of the closed loop, which is related to the degree of stability of the closed loop, should be minimized.

3. The damping of the eigenvalues from 0 to 140 Hz, in which the two rigid modes and the first bending mode of the rotor system are located, should be maximized.

4. The damping of the eigenvalues from 140 to 1000 Hz should be maximized.

It should be noted that the optimization is defined to minimize the objective functions. Therefore, objectives 3 and 4 are reformulated in order to minimize the corresponding inverse damping.

The result of the sensitivity analysis is shown in Figure 5.10. Based on the correlation matrix as shown in the left plot and with the help of the color map (here the absolute values of the correlation coefficients are shown on the color map), the controller parameters that have a strong influence on one objective, can be chosen easily, e.g. parameter 1 for objective 3. However, those parameters that have a medium influence on all objectives, will also be considered in the optimization. These parameters can be determined using Goldberg's ranking method. As an example, the ranking result is illustrated in the right plot (objective 1 versus 4). The parameters are ranked resulting in three fronts. For the optimization, it is recommended that the parameters for front 1 (e.g., the blue asterisks in the right plot) be considered.

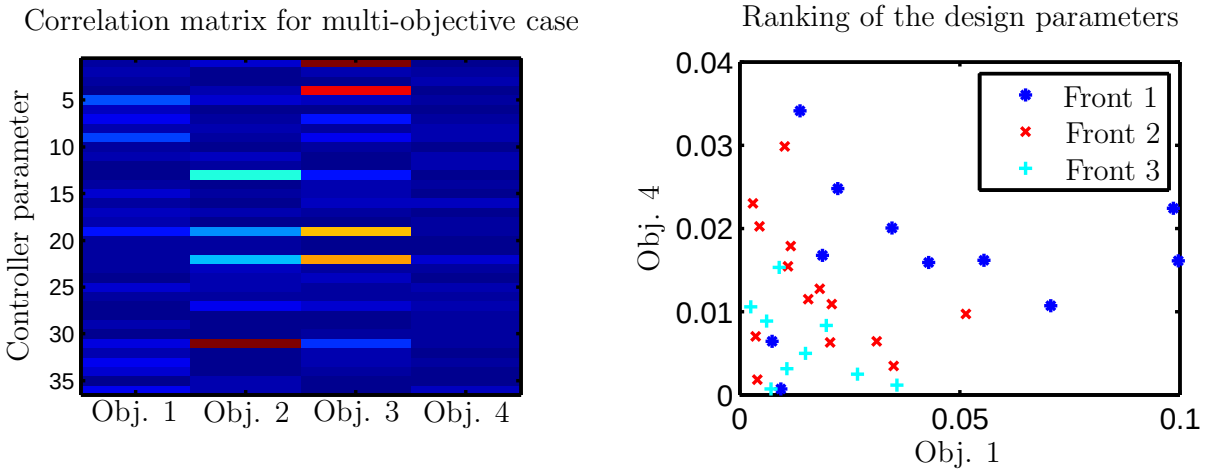

Figure 5.10: *Left: Correlation between controller parameters and the objective functions; Right: Ranking of the design parameters (Plane: Objective 1 versus objective 4) [WGS13, WS15]*

To show the efficiency of the parameter selection method, simulations are performed for the following four cases:

Case 1: All design parameters (36 in total) are considered in the optimization.

Case 2: The parameters on the first front (12 in total) are selected for the optimization.

Case 3: The parameters on the second front (14 in total) are used in the optimization.

Case 4: The parameters on the third front (nine in total) are considered for the optimization.

All 36 parameters are ranked with four fronts. Here, only one parameter (controller parameter number 20) is located on the fourth front. This parameter will not be considered and the fourth front is therefore not shown in the right plot in Figure 5.10. For each case, the optimization is performed several times. A typical evolution of the best fitness values (for the first 100 generations) is shown in Figure 5.11.

Based on the results shown in Figure 5.11, the following conclusions can be made:

- Theoretically, optimization using all parameters should give the best result. Because of the limitation of the optimization routine used (genetic algorithm), this is not always true, as shown in Figure 5.11. The optimization with parameters on front 1 (case 2) for objectives 1 and 3 (see upper-left and lower-left plot) gives a better result than that with all parameters (case 1).

- The result of the optimization for case 2 (with parameters on front 1) is superior to that for cases 3 (on front 2) and 4 (on front 3) and approaches that for case 1 (with all 36 parameters). This can be expected when using the ranking technique. However the result for case 3 is inferior to that for case 4. This may result from the random nature of the optimization routine (MOGA) and the sensitivity analysis (randomized method for DoE).

- The convergence of the optimization process mainly depends on the number of design parameters and their degree of influence. A smaller number of design parameters with lower degree of influence results in a more rapid convergence of the optimization process. For example, within 15 generations, the optimization for case 2 reaches its optimal value (1.94) for objective 1 (maximal singular value of the sensitivity function), however, this process needs 50 generations for case 1. This result demonstrates the usefulness of parameter reduction for the practical application of genetic algorithms.

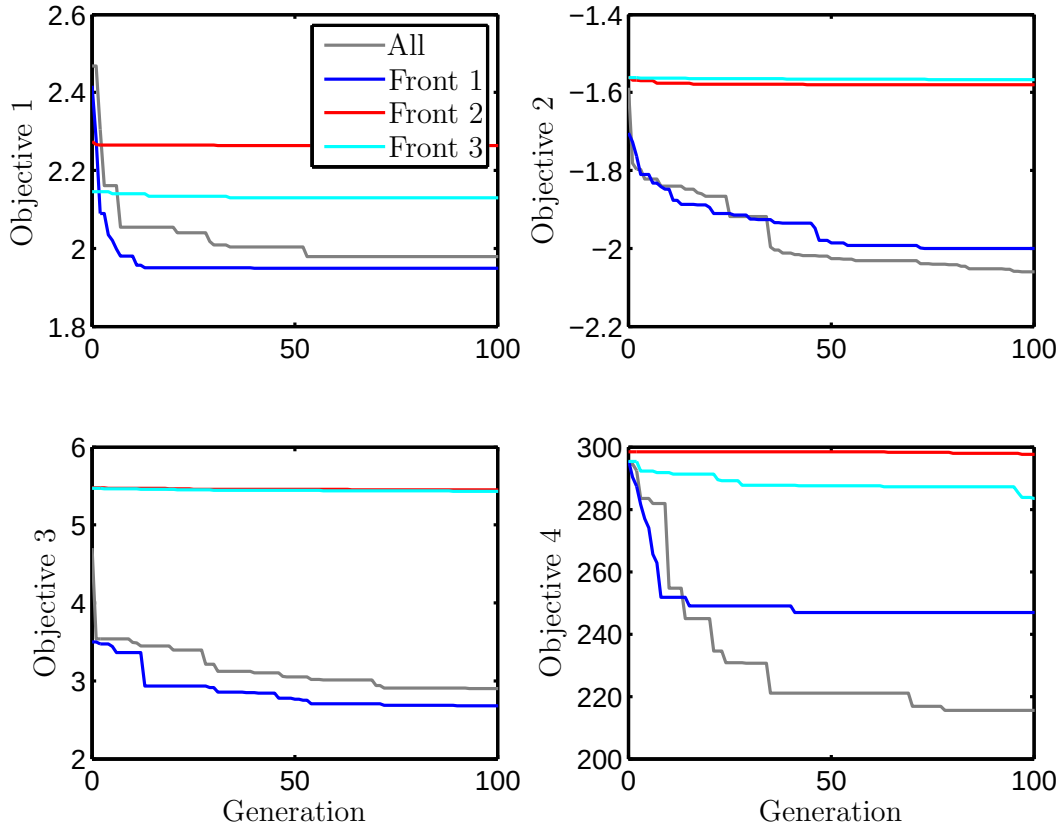

Figure 5.11: *Evolution of the best fitness values [WGS13, WS15]*

The result above serves as an example of the efficiency of the parameter reduction strategy used for optimization. The optimization result will be presented in Section 5.3.2. In the next section, a procedure to evaluate fitness functions to be used within optimization strategies is suggested.

5.2.3 Evaluation of Fitness Functions

In the previous subsection, the sensitivity-based parameter reduction strategy was introduced to reduce the complexity of the optimization problem. In this part, an evaluation of the fitness function will be illustrated using a controller design example for AMB system I.

Diverse criteria have to be formulated as objectives (also called fitness functions). Some of these criteria can be considered as constraints. This is another crucial point to use

MOGA. The optimization problem can be solved quite efficient with well-defined fitness functions, on the contrary the optimization can fail due to non-convengence.

The challenge arising from the control problem is the requirement for stability of the closed-loop as mentioned previously. The stability requirements of the closed-loop of the AMB system can be treated either as a constraint during the optimization process or as an objective to maximize the stability degree d defined as

$$d = 0 - \max\{\Re(\lambda_i)\}, \quad \text{for} \quad i = 1 : n,$$

with $\Re(\lambda_i)$ denoting the real part of the i-th eigenvalue and n denotes the number of the eigenvalue of the linear system.

A strategy using a hierarchical evaluation of the fitness functions for MOEAs and MOGAs is given in the following. With this strategy, the optimizer tries to shift the candidates to the stable region of the closed-loop of the AMB system in the beginning period of the optimization process. Once this step is successful, the other objectives (including time and frequency domain criteria/performance ratios) become available to be optimized. There are two advantages following this strategy:

1. The optimization process is accelerated, since more feasible (stable) candidates will be found (if possible) in the beginning period of the optimization process for further optimization.

2. The probability that the optimization process will converge, increases.

Due to their randomized character (e.g., in case that the feasible region is isolated (too small) in the defined search space), it should be noted that in principle a convergence can not be guaranteed for those MOEAs and MOGAs. Certainly finding global optimum even local optimum can not be guaranteed for each objective.

In the following, the recommended evaluation strategy of the fitness functions is given in detail. Hereby, the optimization of the controller design of the AMB system I is taken as an example to show the procedure of evaluation of the fitness functions. Totally five objectives are formulated as fitness functions for the optimization of this controller design. The maximal singular value of the sensitivity function $\sigma(S_{\mathrm{pt}})$ is treated as the first objective. It is defined as the larger one of the maximal singular value of parallel and tilting mode (see Section 4.1) sensitivity function (S_{p} and S_{t}), i.e.,

$$F_1 = \sigma(S_{\mathrm{pt}}) = \max\{\sigma(S_{\mathrm{p}}), \sigma(S_{\mathrm{t}})\}.$$

The damping ratios of the eigenvalues in the frequency region [0..300] Hz and (300..1000] Hz are considered separately as two objectives, which are denoted as $\zeta_{[0-300]}$ and $\zeta_{(300-1000]}$.

The first frequency region shall include the rigid body modes and the first bending mode. The second frequency region contains other bending modes up to 1000 Hz. Since the optimization goal is defined to minimize the fitness functions, an objective to be maximized has to be reformulated as an objective to be minimized. Therefore, instead of maximizing the damping ratio of eigenvalues, the inverse damping ratio is defined as fitness function by

$$F_2 = \zeta_{\text{inv},[0-300]} = \frac{1}{\min(\zeta_i)}, \quad \text{for} \quad i = 1:k \quad \text{and} \quad \lambda_i \in [0-300] \text{ Hz},$$
$$F_3 = \zeta_{\text{inv},(300-1000]} = \frac{1}{\min(\zeta_j)}, \quad \text{for} \quad j = 1:m \quad \text{and} \quad \lambda_j \in (300-1000] \text{ Hz}.$$

These three fitness functions mentioned above are related to frequency domain performance. For controlling the AMB system, time domain performance is also important and has to be carefully considered. Hereby, the overshoot A_{os} and the settling time t_{st} of the step response of the AMB system are taken into account; So two fitness functions corresponding to the time domain performance,

$$F_4 = A_{\text{os}} \quad \text{and} \quad F_5 = t_{\text{st}}$$

are used.

The five fitness functions are evaluated with the strategy mentioned above for each individual in current population as follows:

Step I: The sensitivity function matrix **S** and complementary-sensitivity function matrix **T** are calculated, as well as their eigenvalues λ_i. If the closed-loop is stable, the evaluation process continues with **Step II**, otherwise

$$F_1..F_5 = \max\{\Re(\lambda_i)\} + \text{constant A}$$

is used to evaluate the fitness functions.

Step II: The maximal singular value of the sensitivity functions for the parallel and tilting mode (which can be directly obtained from **S**) are evaluated and the singular values of the sensitivity function $\sigma(S_{\text{pt}})$ is defined. The inverse damping ratio of the eigenvalues is determined. Calculating the step response of the closed-loop gives the overshoot A_{os} and the settling time t_{st}. If the values of $\sigma(S_{\text{pt}})$, $\zeta_{\text{inv},[0-300]}$, $\zeta_{\text{inv},(300-1000]}$, A_{os}, and t_{st} are not larger than a special suitable choosen number (so that those solutions with extreme large objective values will be rejected), the procedure continues and goes to **Step III**, otherwise

$$F_1..F_5 = \max\{\Re(\lambda_i)\} + \text{constant B}$$

is used.

Step III: If the conditions

$$\sigma(S_{\mathrm{pt}}) \leq 50, \quad \zeta_{\mathrm{inv},[0-300]} \leq 100, \quad \text{and} \quad A_{\mathrm{os}} \leq 1000$$

are fulfilled, the objective functions are defined as

$$\begin{aligned}
F_1 &= \sigma(S_{\mathrm{pt}}), \\
F_2 &= \begin{cases} \zeta_{\mathrm{inv},[0-300]} & \text{if } \zeta_{\mathrm{inv},[0-300]} \geq F_2^*, \\ F_2^* & \text{if } \zeta_{\mathrm{inv},[0-300]} < F_2^*, \end{cases} \\
F_3 &= \begin{cases} \zeta_{\mathrm{inv},(300-1000]} & \text{if } \zeta_{\mathrm{inv},(300-1000]} \geq F_3^*, \\ F_3^* & \text{if } \zeta_{\mathrm{inv},(300-1000]} < F_3^*, \end{cases} \\
F_4 &= \begin{cases} A_{\mathrm{os}} & \text{if } A_{\mathrm{os}} \geq F_4^*, \\ F_4^* & \text{if } A_{\mathrm{os}} < F_4^*, \end{cases} \quad \text{and} \\
F_5 &= \begin{cases} t_{\mathrm{st}} & \text{if } t_{\mathrm{st}} \geq F_5^*, \\ F_5^* & \text{if } t_{\mathrm{st}} < F_5^*, \end{cases}
\end{aligned} \tag{5.9}$$

otherwise

$$F_1..F_5 = \max\{\Re(\lambda_i)\} + \text{constant C}$$

is used.

The constants A, B, and C control the threshold levels with A $\gg$ B $\gg$ C. The purpose of using the threshold levels is to try to collect more feasible solutions at the initial phase of the optimization process and prevent genetic drift.

"Optimal" values F_2^*–F_5^* are defined for the fitness functions F_2–F_5 with the intention to accelerate the optimzation process. If the fitness function reaches its related "optimal" value, then this fitness function does not need to be considered in the optimization process, therefore the optimizer focuses only on the other objectives. This again accelerates the optimization process. The optimal values of the fitness functions are given in Table 5.2. It can be seen that the optimal values for the inverse damping ratio are chosen as 2 and 20, which correspond to a damping ratio of 50% and 5%, respectively. So the system are considered as well-damped with a damping ratio of 50% for the first three lowest eigenfrequencies, which are under the maximal rotation speed. For the high-frequency region, no great influence of AMB system on the eigenfrequencies of the rotor system

can be expected, therefore a small value for the damping ratio in high-frequency region is chosen as optimal value. In time domain, the system with an overshoot of 100% and a settling time of 0.3 second are considered as well-behaved. The first objective, i.e. the maximal singular value of the sensitivity function, is the most essential objective. No optimal value is assigned to it so that this objective shall be improved as well as possible. In fact, no optimal values shall be assigned to those objectives, which are most essential and can be hardly improved.

Table 5.2: *Predefined optimal values of the fitness functions*

Objective parameter	"Optimal" value	Description
$F_2 : \zeta_{\text{inv},[0-300]}$	$F_2^* : 2 \quad (= 50\%$ Damping ratio)	Inverse damping ratio
$F_3 : \zeta_{\text{inv},(300-1000]}$	$F_3^* : 20 \quad (= 5\%$ Damping ratio)	Inverse damping ratio
$F_4 : A_{\text{os}} \quad [\%]$	$F_4^* : 100$	Overshoot
$F_5 : t_{\text{st}} \quad [\text{sec}]$	$F_5^* : 0.3$	Settling time

This section presents a procedure to evaluate fitness functions. In the last section, a sensitivity-based parameter reduction strategy is introduced. The optimization results for the both AMB systems will be shown in the next section.

5.3 Optimization Results

In the previous section, sensitivity-based parameter reduction and evaluation procedure of fitness functions for MOGAs are introduced. In this section, the optimization results for the controller designs (see Section 4.1) of both AMB systems given in Section 3.5, are discussed. Two solutions for the AMB system I are selected and implemented in a test rig. The experimental result obtained from the test rig will be presented in the next chapter.

5.3.1 Results of Controller Design of AMB System I

As described in Section 4.1, 30 parameters in total for the parallel and tilting mode controller have to be carefully choosen. The search space for the controller parameters of AMB system I are given in Table 5.3. The optimization is finished after reaching the generation limit (i.e. 750) with a population size of 90. The computation time is about 5.6 hours on a standard desktop PC.

It should be noticed that the test rig is designed to work with a maximal rotational speed

Table 5.3: *Search space of controller parameters for AMB system I*

		K_P [A/m]	ω_{n0} [Hz]	ω_{d0} [Hz]	ω_{n1} [Hz]	ξ_{n1} [-]
Parallel mode	Lower bound	9e3	50	100	100	0.05
	Upper bound	3e4	150	2e3	1e3	1.00
Tilting mode	Lower bound	1.5e3	60	100	100	0.05
	Upper bound	4e3	180	2e3	1e3	1.00
		ω_{d1} [Hz]	ξ_{d1} [-]	ω_{n2} [Hz]	ξ_{n2} [-]	ω_{d2} [Hz]
Parallel mode	Lower bound	80	0.05	100	0.05	100
	Upper bound	1e3	1.00	1e3	1.00	1e3
Tilting mode	Lower bound	100	0.05	150	0.05	150
	Upper bound	1e3	1.00	1e3	1.00	1e3
		$\xi_{d2}[-]$	ω_{n3} [Hz]	ξ_{n3} [-]	ω_{d3} [Hz]	ξ_{d3}[-]
Parallel mode	Lower bound	0.05	300	0.05	300	0.05
	Upper bound	1.00	1e3	1.00	1e3	1.00
Tilting mode	Lower bound	0.05	300	0.05	300	0.05
	Upper bound	1.00	1e3	1.00	1e3	1.00

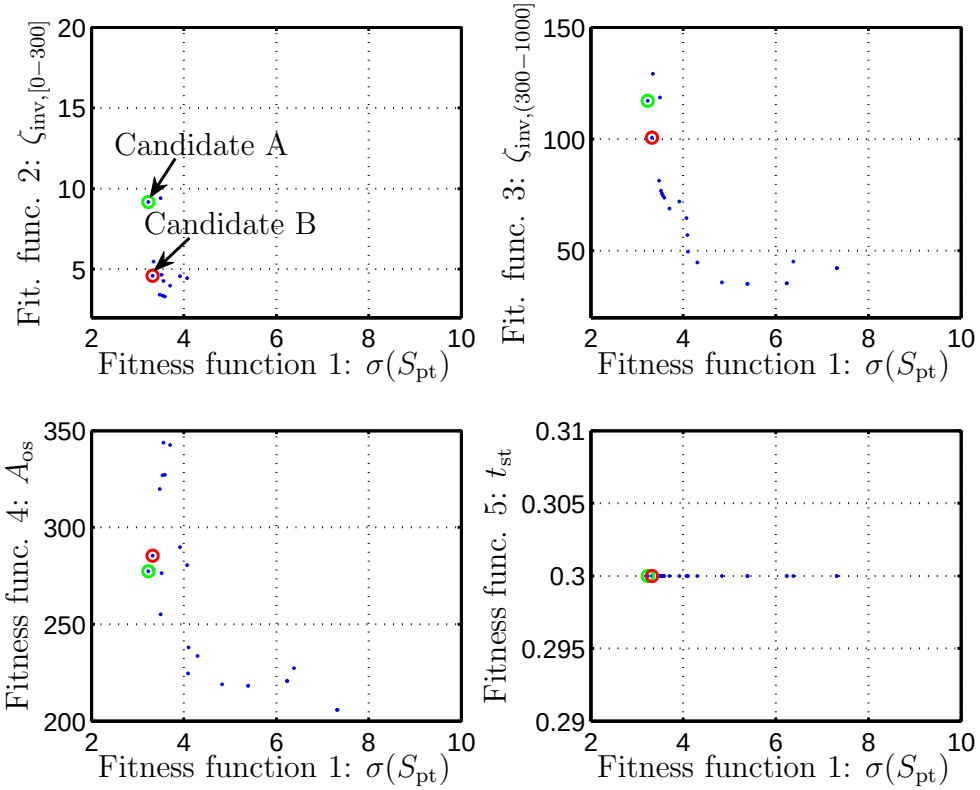

Figure 5.12: *Pareto front of the optimization result for AMB system I [WS12a, WS15]*

of 15000 rpm, thus the rotor model with the rotational speed of 15000 rpm is employed for the controller design and optimization. The fitness functions are given in Section 5.2.3 and evalutated for each individual at current generation during optimization. The rotor system is relative simple for controller design, i.e. the eigenmodes are well separated with each other, thus the optimization are performed without parameter reduction.

Table 5.4: *Objective value of selected candidates*

Objective	Candidate A	Candidate B
#1: Singular value $\sigma(S_{\mathrm{pt}})$	3.23	3.32
#2: Damping ratio [0..300] Hz	11%	21%
#3: Damping ratio (300..1e3] Hz	0.85%	0.99%
#4: Overshoot A_{os}	277%	285%
#5: Settling time t_{st}	0.3 [sec]	0.3 [sec]

Table 5.5: *Parameters of selected controller candidates*

		K_{P} [A/m]	ω_{n0} [Hz]	ω_{d0} [Hz]	ω_{n1} [Hz]	ξ_{n1} [-]
Parallel	Cand. A	1.84e4	137	1.10e3	412	0.40
mode	Cand. B	1.25e4	86	1.47e3	182	0.48
Tilting	Cand. A	2.10e3	119	808	787	0.35
mode	Cand. B	2.08e3	115	683	343	0.71
		ω_{d1} [Hz]	ξ_{d1} [-]	ω_{n2} [Hz]	ξ_{n2} [-]	ω_{d2} [Hz]
Parallel	Cand. A	486	0.56	622	0.38	464
mode	Cand. B	178	0.65	390	0.57	328
Tilting	Cand. A	565	0.67	828	0.75	657
mode	Cand. B	285	0.72	586	0.68	452
		$\xi_{\mathrm{d2}}[-]$	ω_{n3} [Hz]	ξ_{n3} [-]	ω_{d3} [Hz]	ξ_{d3}[-]
Parallel	Cand. A	0.46	667	0.68	652	0.81
mode	Cand. B	0.68	935	0.63	639	0.40
Tilting	Cand. A	0.70	718	0.51	768	0.56
mode	Cand. B	0.59	639	0.51	548	0.39

The optimization results are shown in Figure 5.12. Each point from the Pareto front (see Figure 5.12) respresents an optimal solution, which is not dominated from other candidates. The upper right and lower left plots show that the fitness function $\sigma(S_{\mathrm{pt}})$ is

competing with overshoot A_{os} as well as inverse damping ratio $\zeta_{\mathrm{inv},(300-1000]}$, i.e. minimizing the maximal singular value $\sigma(S_{\mathrm{pt}})$ can only be achieved with increasing the overshoot A_{os} and decreasing the damping ratio of the eigenvalues in the frequency region (300..1000] Hz. The settling time t_{st} reaches the defined optimal value $F_5^* = 0.3$ (see the lower right plot).

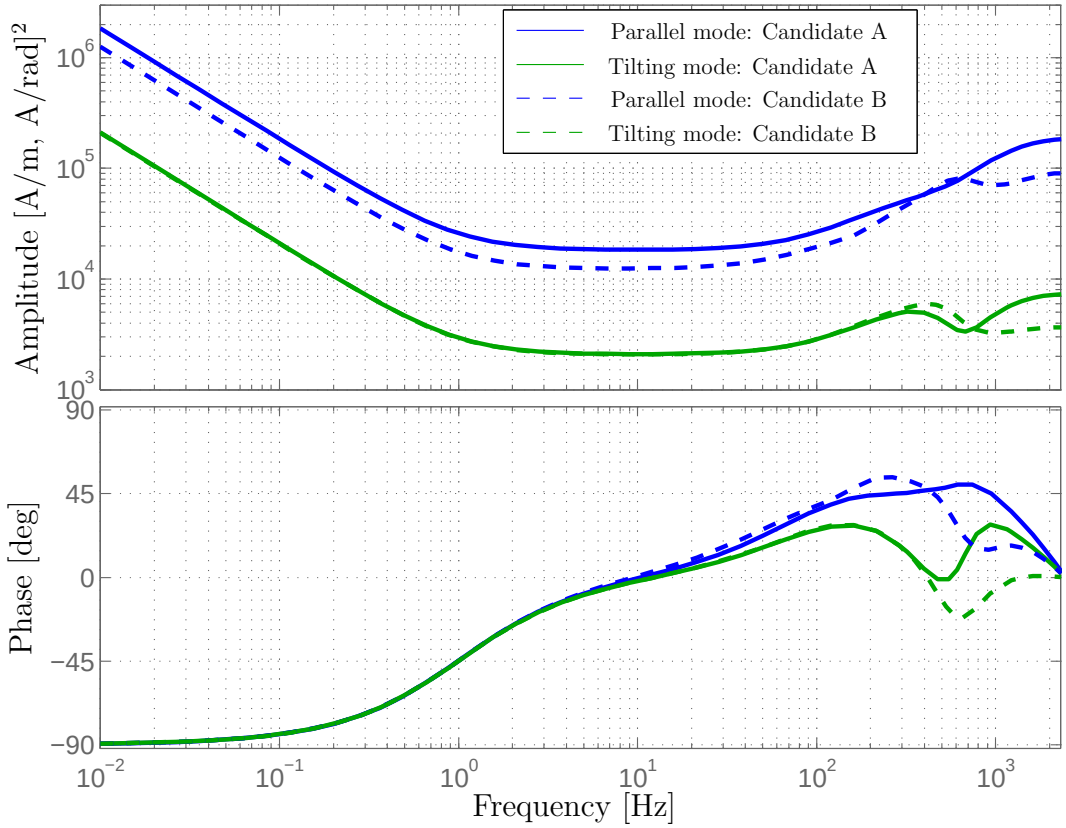

Figure 5.13: *Bode diagram between outputs (control currents) and inputs (displacements) of selected controller candidates [WS12a, WS15]*

Two candidates (A and B) from the Pareto front with the smallest maximal singular value $\sigma(S_{\mathrm{pt}})$ are selected for further simulation and they are implemented in the test rig as it will be shown in the next chapter.

The optimized objective values of the both candidates are given in Table 5.4. The resulting maximal singular values of candidates A and B are corresponding to zone B according to the ISO Stardard 14839-3. All eigenmodes of the closed loop with controller candidate B in the frequency region [0..300] Hz are well damped. It should be noted that a candidate has to be selected carefully from the Pareto front. The optimizer tries to present all

[2]The unit for parallel and tilting mode is [A/m] and [A/rad], respectively.

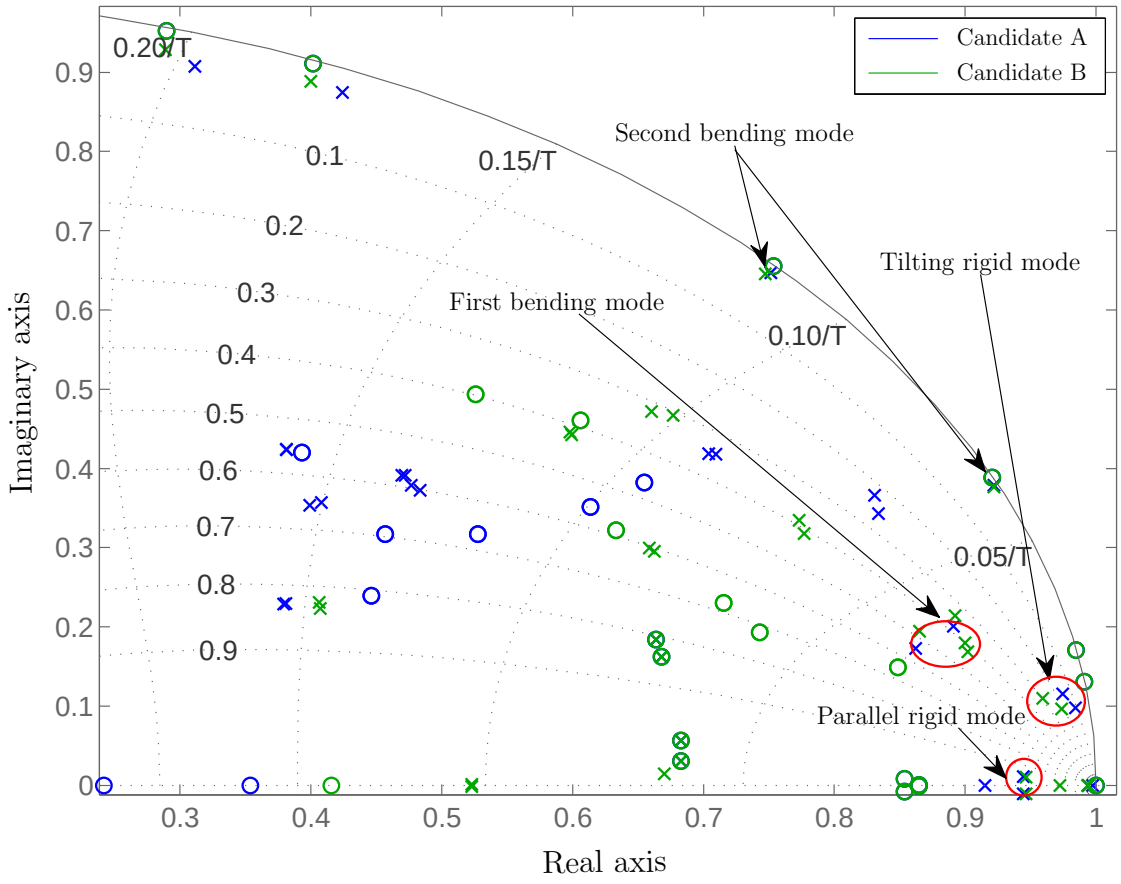

Figure 5.14: *Pole-zero map of the closed-loop with the rotor at the speed of 15000 rpm [WS12a, WS15]*

non-dominated solutions based on the defined fitness functions, consequently, some outlier points are also found by the optimizer to form the entire Pareto front. However, these points are usually unacceptable because of known realization problems.

The corresponding controller parameters of selected candidates are summerized in Table 5.5. The Bode diagram of the controllers (including parallel- and tilting-mode controller) for both candidates is shown in Figure 5.13. The parallel-mode controller of candidate A has a larger P-part (K_P) compared with that of candidate B. The tilting mode controllers are similar at low frequencies but differ at high frequencies.

The pole-zero map of the closed loop is shown in Figure 5.14. The eigenmodes up to the first bending mode are well-damped for both candidates. The first bending mode is damped with more than a 30% damping ratio.

The singular values for the parallel and tilting modes of both candidates are illustrated in Figure 5.15. For the parallel mode, large differences occur at low frequencies. Candidate

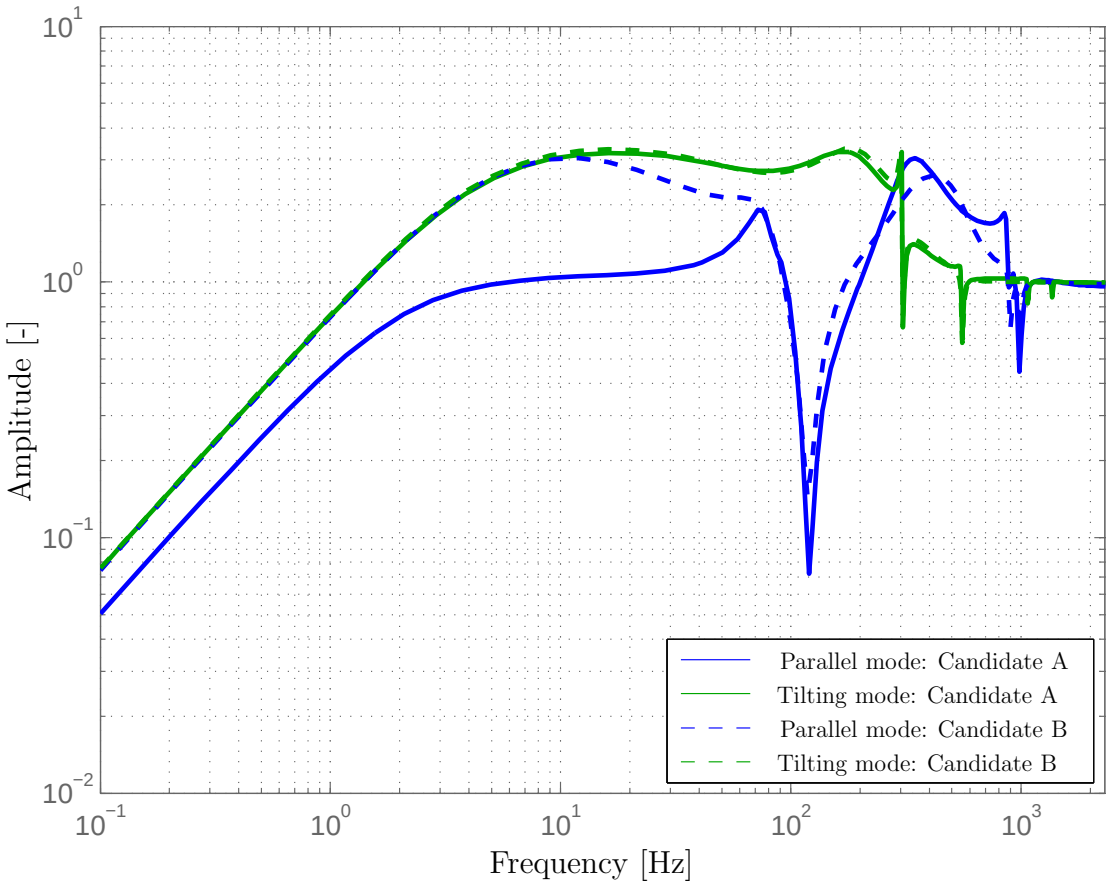

Figure 5.15: *Singular values with the rotor at the speed of 15000 rpm [WS12a, WS15]*

A has a singular value of approximately only 30% of that of candidate B in the region from 2 to 30 Hz. For the tilting mode, no remarkable differences are observed.

Table 5.6: *Objective value of the selected candidates at speed of 0 and 15000 rpm*

		Candidate A		Candidate B	
		0 rpm	1.5e4 rpm	0 rpm	1.5e4 rpm
Parallel mode	Max. sinuglar value	3.08	3.23	3.05	3.32
	Overshoot A_{os}	138%	132%	263%	258%
	Settling time t_{st} [sec]	0.28	0.28	0.15	0.15
Tilting mode	Max. sinuglar value	3.3	3.25	3.37	3.34
	Overshoot A_{os}	275%	277%	283%	285%
	Settling time t_{st} [sec]	0.15	0.15	0.15	0.15
Damping ratio	[0..300] Hz	13.2%	10.9%	25.4%	21.7%
	(300..1000] Hz	1.6%	0.85%	2.2%	0.99%

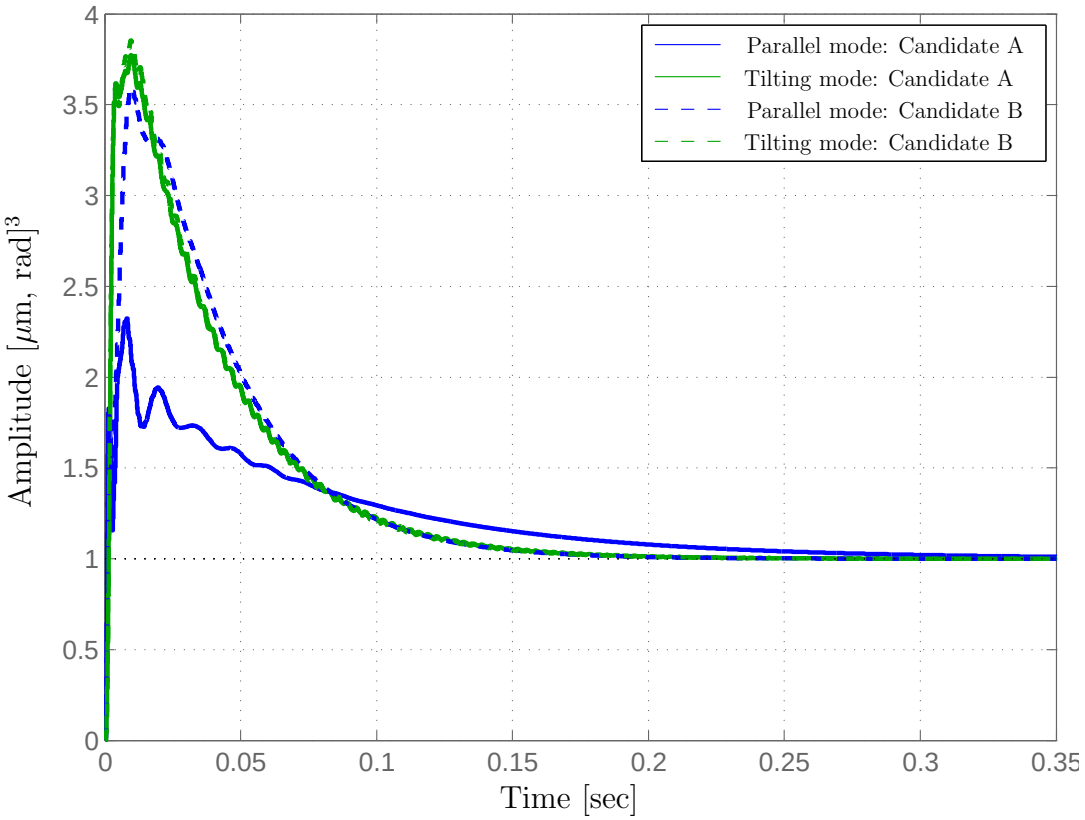

Figure 5.16: *Step response using step input amplitude of 1 μm for parallel mode and 1 rad for the tilting mode for the rotor at the speed of 15000 rpm [WS12a, WS15]*

The step response behavior is presented in Figure 5.16. The parallel mode of candidate A is superior to that of candidate B with respect to the overshoot of the step response, however, the result is similar for the tilting mode. The results above are determined for AMB system I at 15000 rpm. Simulations must be carried out to ensure the stability and performance for the AMB system with a rotor at rest. The simulation results (including the results with the rotor at rest) are summarized in Table 5.6. The system performance does not change noticeably with rotation.

The simulation results of the both candidates will be validated by comparing with the experimental results, which will be given in the next chapter.

5.3.2 Results of Controller Design of AMB System II

The result for the controller design of AMB system II is obtained based on the initial solution $\mathbf{X}_0$. The controller design contains 36 parameters in total. The optimization

[3]The unit for parallel and tilting mode is [μm] and [rad], respectively.

is performed with the MOGA in a local region with a maximal 20% deviation from the initial solution $\mathbf{X}_0$ as mentioned in Section 5.2.2. The optimization result is gained with the parameters on front 1 as optimization parameters, i.e., case 2 from mult-objective case (case b) as presented in Section 5.2.2. The optimization includes four fitness functions as given in Section 5.2.2.

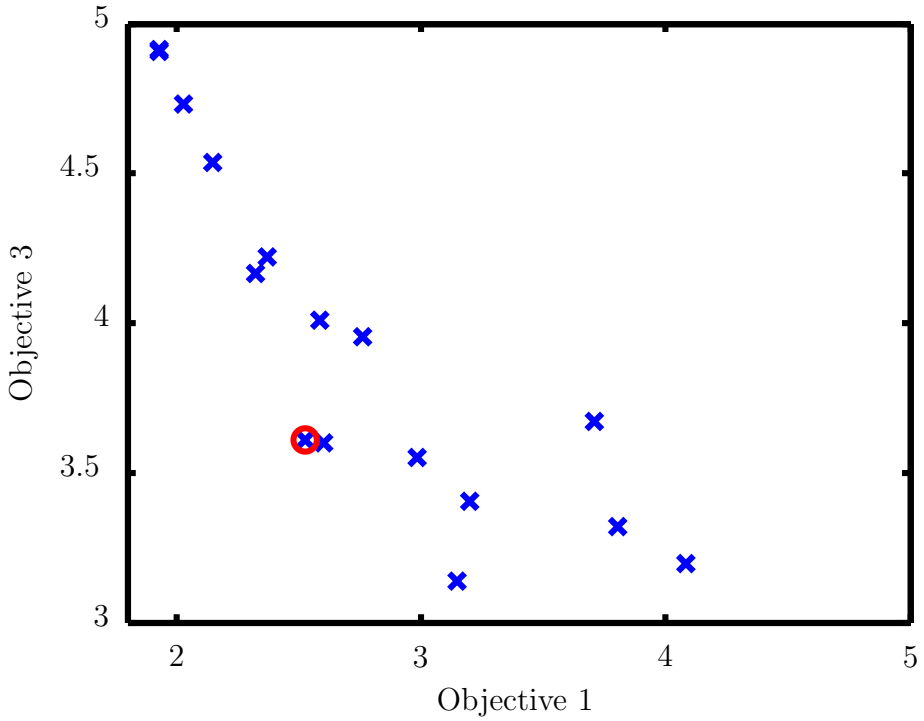

Figure 5.17: *Pareto front (objective 1 versus 3) of the optimization with the parameters on the front 1 based on the sensitivity analysis; the red circled point is the selected solution for controlling the AMB system [WGS13, WS15]*

To illustrate the quality of the optimization, a solution from the optimization result is selected based on the following:

1. The maximal singular value $\sigma_{\max}(\mathbf{S})$ should be less than 3 (i.e., objective 1 < 3);
2. The damping of the eigenvalues of the two rigid modes and the first bending mode of the rotor system should be larger than 20% (i.e., objective 3 < 5).

Accordingly, the solution with $\sigma_{\max}(\mathbf{S}) = 2.53$ and the smallest damping of the eigenvalues from 0 to 140 Hz is selected as shown in the Pareto front in Figure 5.17. The transfer

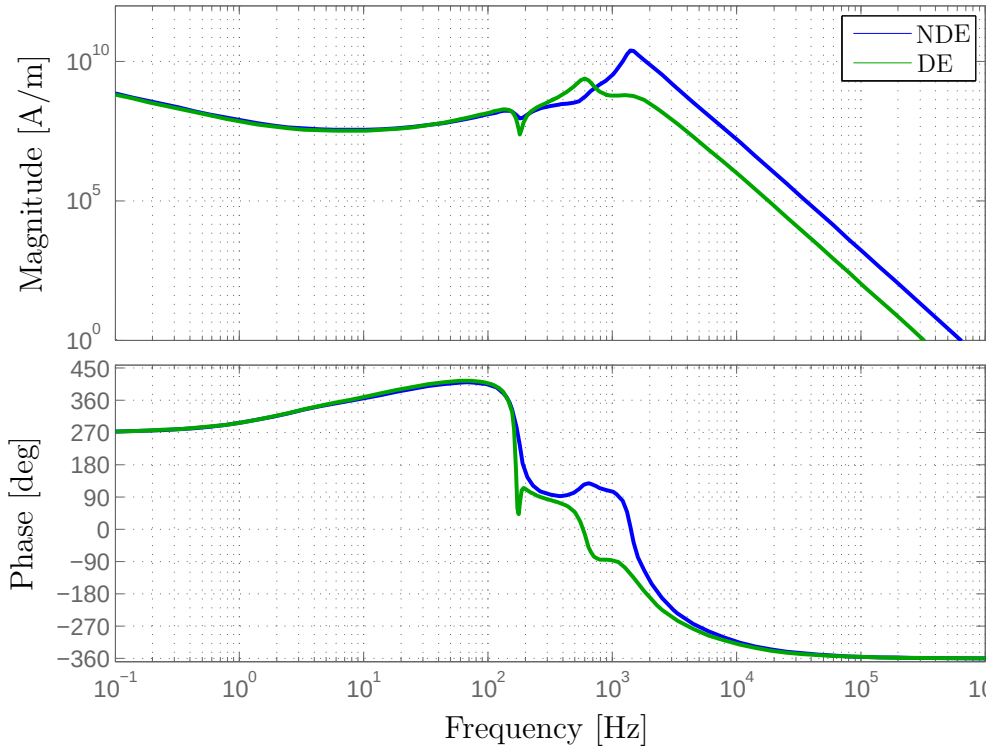

Figure 5.18: *Bode diagram between outputs (control currents) and inputs (displacements) of the controller of both DE- and NDE-sides*

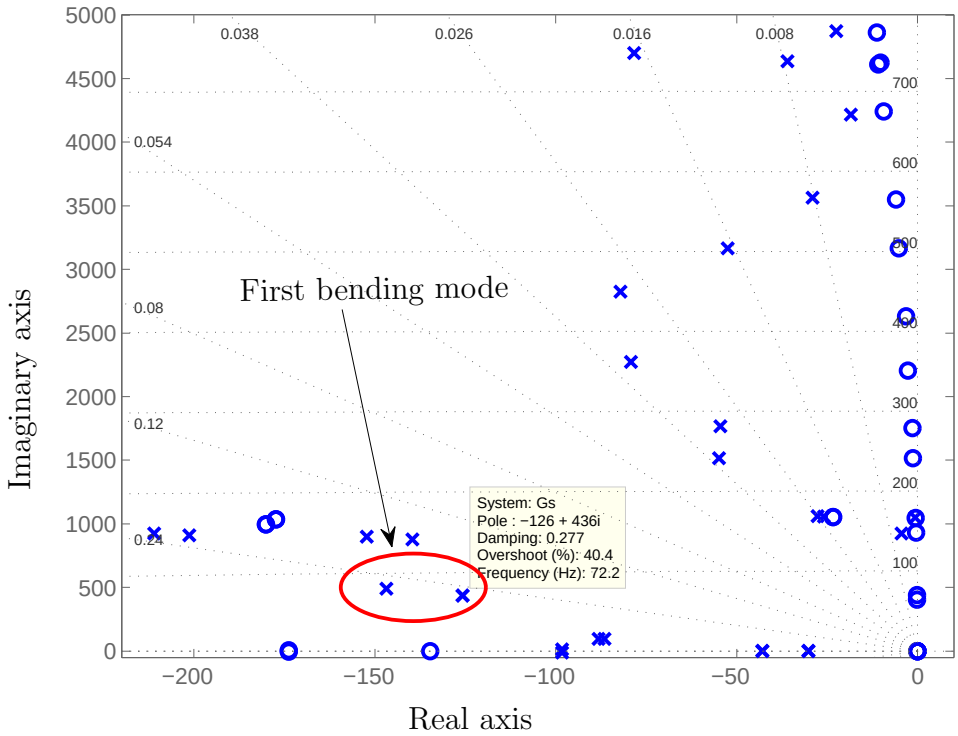

Figure 5.19: *Eigenvalues of the closed loop (speed n=6000 rpm) [WGS13, WS15]*

functions of the resulting controllers are shown in Figure 5.18 in form of Bode diagram. The corresponding sensitivity functions and eigenvalues are shown in Figures 5.20 and 5.19. The damping of the first bending (backward) mode is approximately 27.7% and the maximal singular value of the sensitivity function for the DE and NDE sides is 2.53. This corresponds to zone A according to ISO Standard 14839-3.

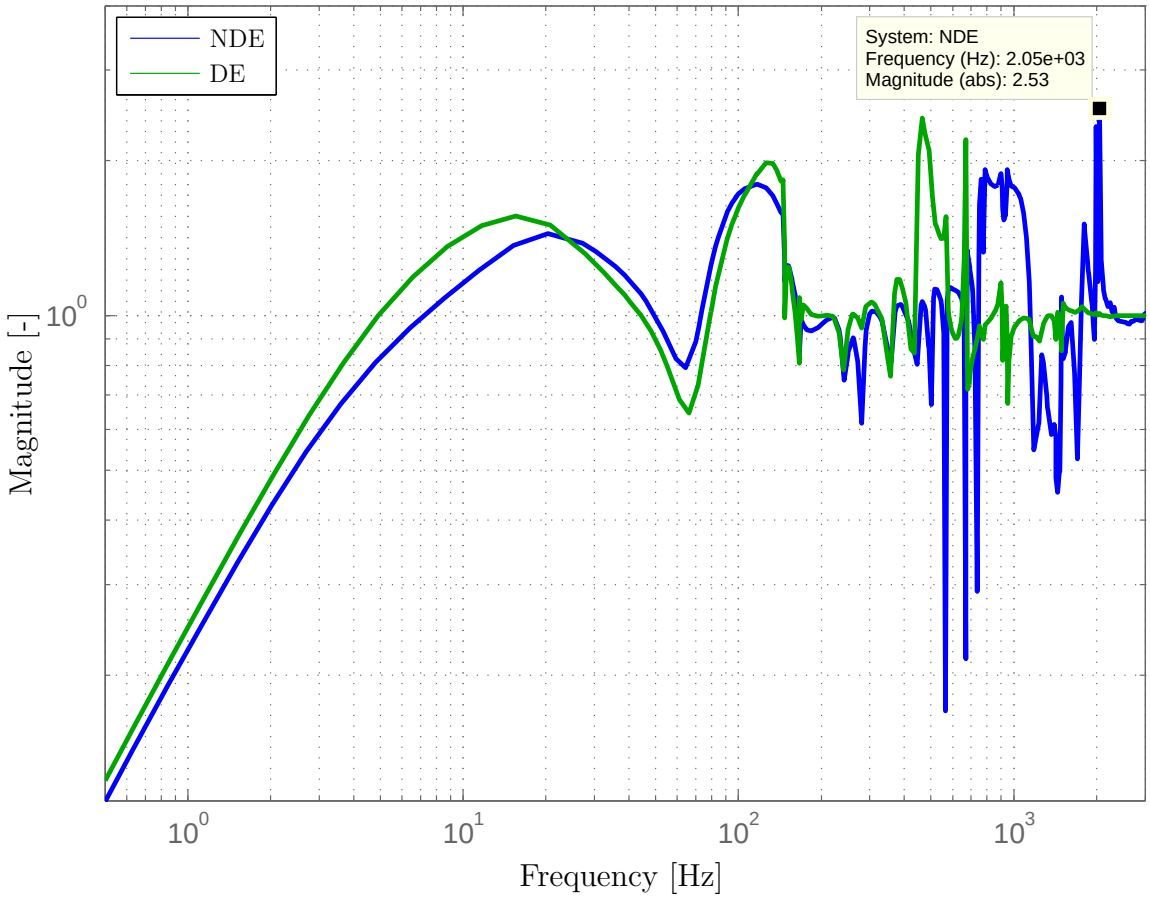

Figure 5.20: *Singular values of the sensitivity functions (speed n=6000 rpm) [WGS13, WS15]*

Chapter 6

Experimental Results

In this chapter, the realization of the selected optimal PID-controllers for AMB system I is focused. Here, the aim is to validate the optimization results by comparing simulation and experimental results. The optimal controller is applied to a test rig with a flexible rotor supported by AMBs. It should be noted that the material about experimental results has been partially published in author's previous publication [WS12b, WS15].

6.1 Test Rig

In this section, the test rig that is used will be described briefly. The test rig, including the driving motor, gear box, coupling, and controller box, is shown in Figure 6.1. The rotor system is driven by a Direct Current (DC) motor (100 kW) with a nominal speed of 2000 rpm. The step-up gear is used to increase the test rotor speed upto a maximal rotational speed of 15000 rpm.

The test rig was originally designed for seal force identification [WS97], therefore the rotor is packaged in a housing as shown in Figure 6.2. The structure of the test rig is detailed in Figure 6.3. The test rotor (steel) is directed connected to the driving rotor, which is supported by two ball bearings. The driving rotor is then connected with the gear box using a coupling. In order to reduce the influence from driving rotor on the lateral vibration of the test rotor, the right side of the driving rotor is constructed so thin that it becomes very elastic as shown in Figure 6.2. The test rotor is installed in the housing of the test rig, which is fixed on the ground. The test rotor is supported by the two AMBs.

In addition to the AMBs, two backup bearings are arranged at both ends of the test rotor, which are ball bearings. In normal case (i.e. the magnetic bearings are active), there is no contact between the test rotor and the backup bearings. The backup bearings work only

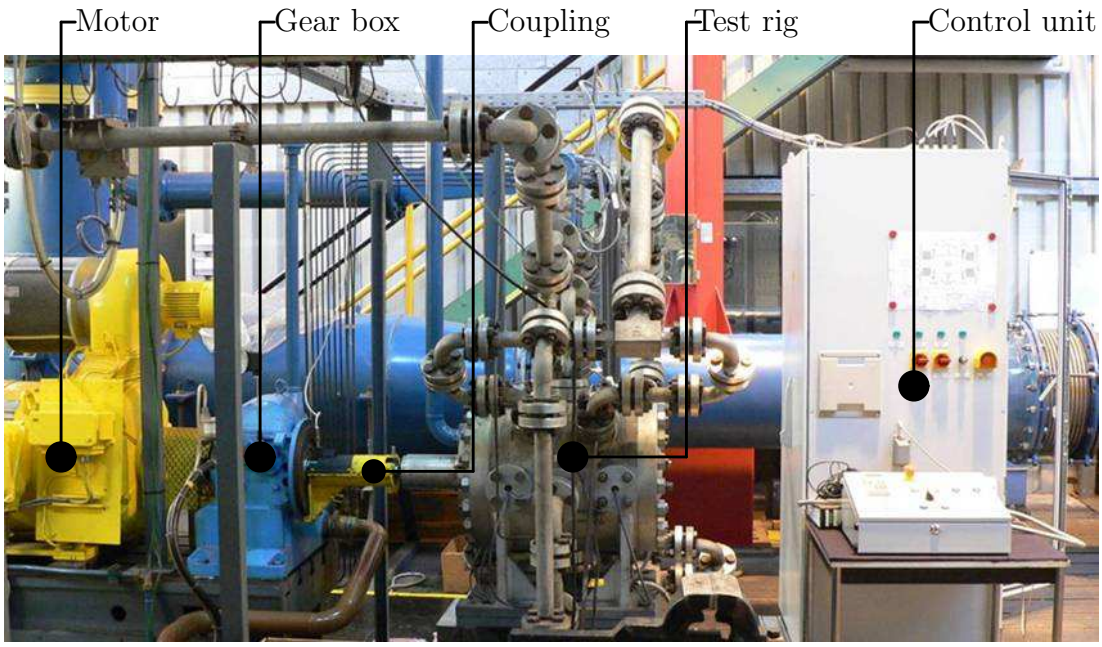

Figure 6.1: *Test rig used (Siemens Energy Sector, Duisburg, Germany) [WS12b, WS15]*

when any AMB is overloaded or power failure (emergency case). In this case, the backup bearings catch the rotor so that no contact occurs between the rotor and the AMBs and it prevents destruction of the AMBs.

The control algorithm is implemented and operated on a DSP unit. A communication tool between a personal computer and the DSP unit is used for data acquisition and parameter modification of the DSP unit. Various functions (e.g. step response, measurement of transfer functions) can be performed with this communication tool.

The two candidates obtained from optimization as given in Section 5.3.1 are then in turn implemented on the DSP unit to control the AMB system. The measured result will be presented in the next Sections.

6.2 Model Validation

To validate the structure model, modal testing and analysis have to be performed. Modal analysis is used to determine the eigenfrequencies and eigenshapes of a real structure such as a rotor. In this subsection, the modal analysis of the test rotor will be discussed. With the help of a communication tool, the transfer functions of the AMB system are measured and compared with the simulation results.

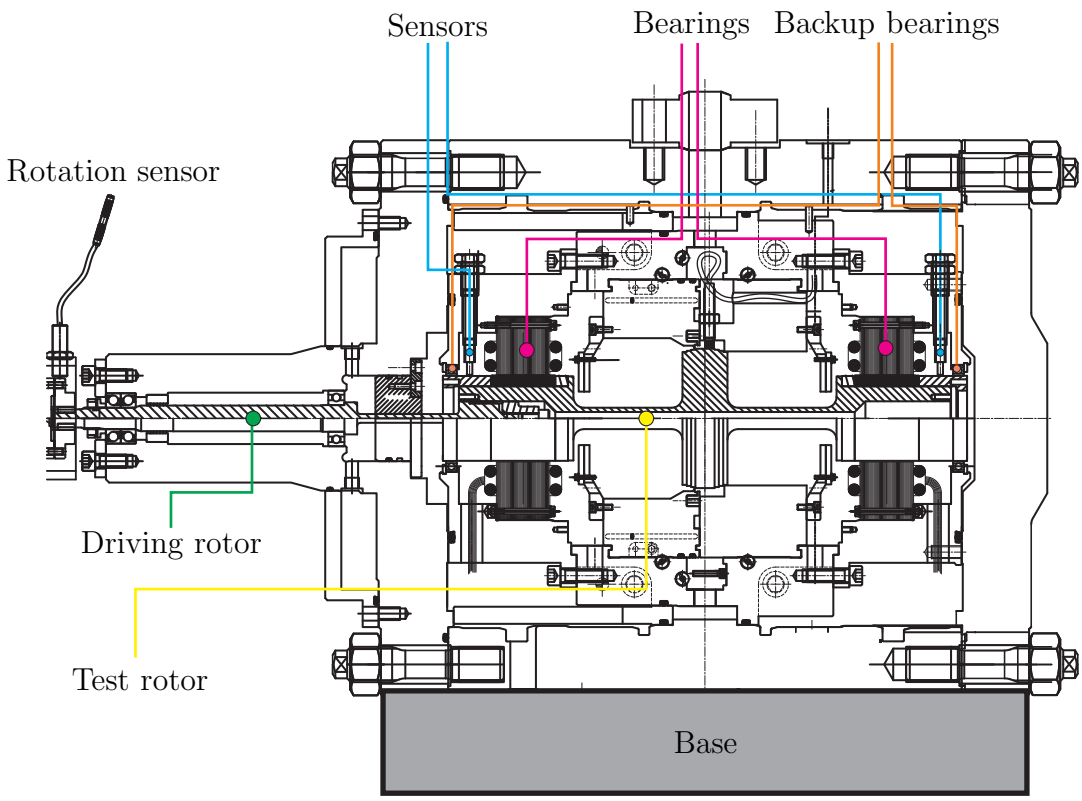

Figure 6.2: *Test rotor mounted in the housing (Siemens Energy Sector, Duisburg, Germany)*

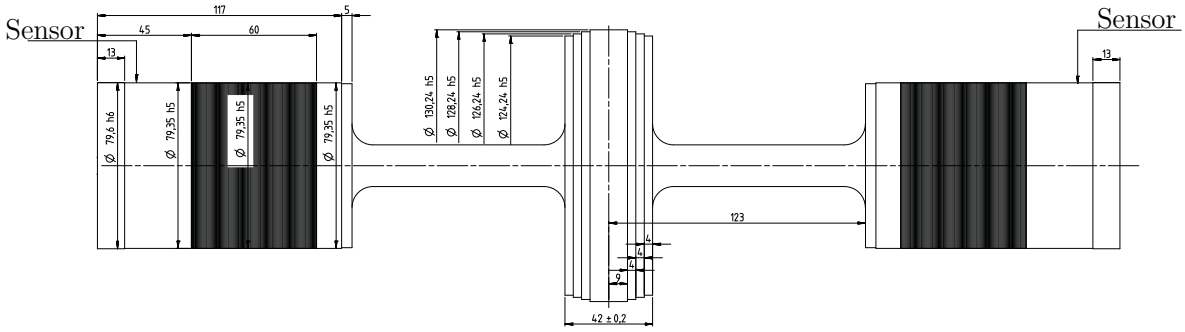

Figure 6.3: *Drawing of test rotor including bearing lamination sheets (Siemens Energy Sector, Duisburg, Germany)*

6.2.1 Modal Analysis

An impact hammer modal testing is performed with 27 measuring nodes. A single accelerometer is used to measure the response from the hammer impact. During the modal testing, the test rotor is hung vertically and is impacted by the hammer at a fixed position while the accelerometer moves from measuring node 1 to 27. The eigenfrequencies and

eigenforms are then calculated. The eigenfrequencies of the modal analysis of the test rotor in free-free condition without AMB are summarized in Table 6.1.

Table 6.1: *Comparison of eigenfrequencies from modal analysis and simulation*

Eigenmode	Modal analysis	Simulation	
		0 rpm	15000 rpm
1st bending mode [Hz]	124	123	107/141
2nd bending mode [Hz]	429	420	311/558
3rd bending mode [Hz]	992	944	900/993

The first two eigenfrequencies (bending mode) are consistent with those resulting from the simulation. The eigenfrequencies obtained from simulation are slightly less than those obtained from modal analysis for the rotor in free-free condition without AMB.

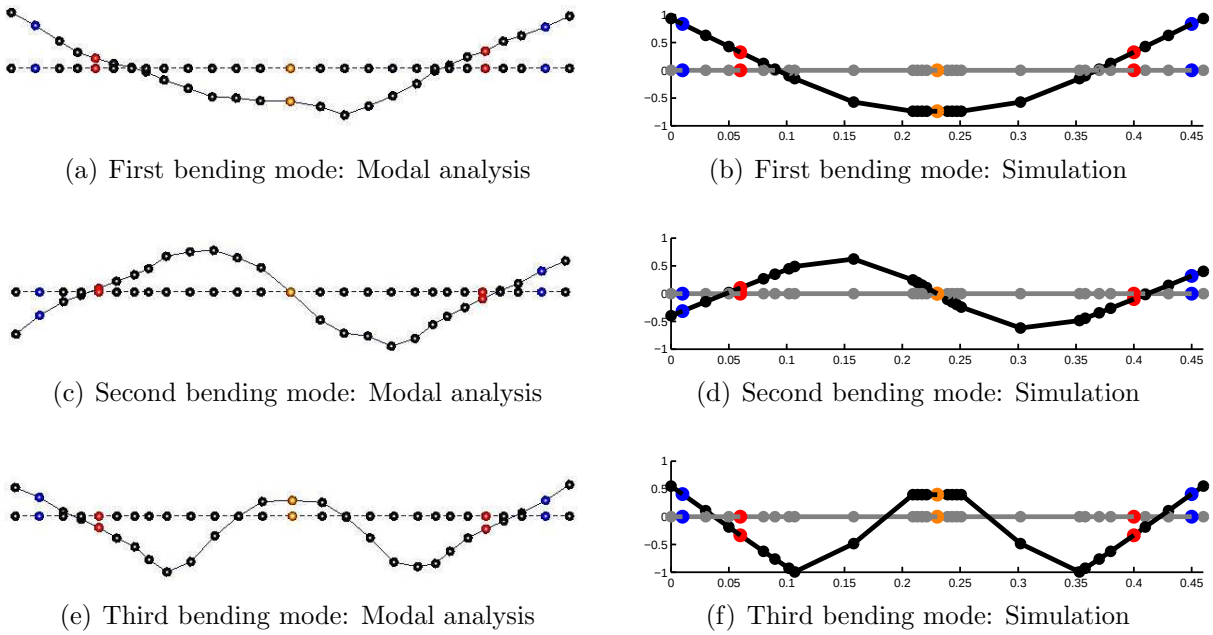

(a) First bending mode: Modal analysis

(b) First bending mode: Simulation

(c) Second bending mode: Modal analysis

(d) Second bending mode: Simulation

(e) Third bending mode: Modal analysis

(f) Third bending mode: Simulation

Figure 6.4: *Comparison of eigenmodes from modal analysis and simulation [WS12b]*

The eigenforms of the modal analysis are shown in Figure 6.4 with 27 nodes. The nodes marked as blue, red, and orange denote the sensor nodes, bearing nodes, and rotor-mid nodes, respectively. The results match the simulation results relatively well.

6.2.2 Transfer Functions of the Plant

The transfer functions (including parallel and tilting modes) of the plant with AMBs (inputs: control currents, outputs: displacements), are measured from 5 to 2000 Hz. The measurements are performed with the test rotor at rest. The results show the effect caused by connecting the driving rotor. It should be noted that in the simulation, only the test rotor is considered, i.e. the test rotor is unconnected to the driving rotor. In Figure 6.5 the measured transfer functions of the parallel mode are shown in form of Bode diagram.

Without connecting the test rotor to the driving rotor (see gray and blue curves), the

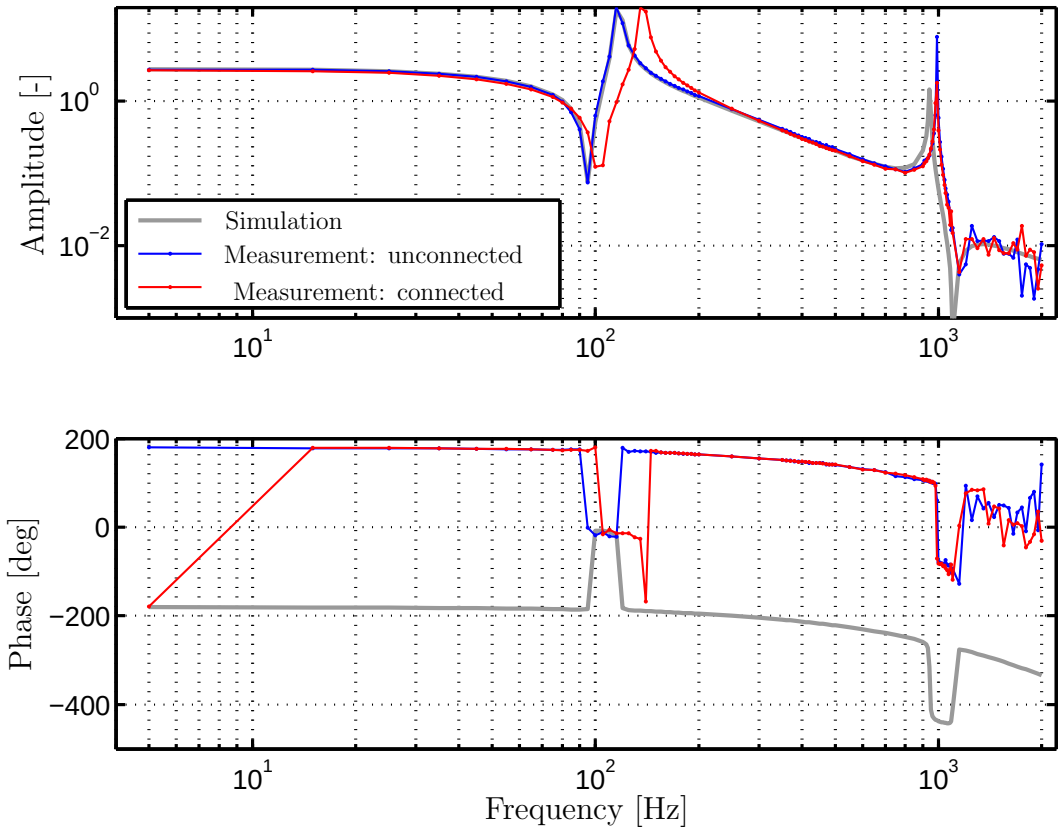

Figure 6.5: *Bode diagram between outputs (displacements in DSP units) and inputs (control current in DSP units) of the plant with AMBs for parallel mode [WS12b, WS15]*

AMB rotor system is modeled accurately with respect to the stationary behavior in the frequency domain using the transfer functions. The dynamics of the test rotor has been influenced significantly by the driving rotor. The eigenfrequency of the first bending mode is shifted to 140 Hz because of the coupling with the driving rotor (see the red curve in Figure 6.5). Obviously the same situation occurs in the case of the tilting mode as shown in Figure 6.6. The DC-gain of the plant with tilting mode increases by approximately 28%

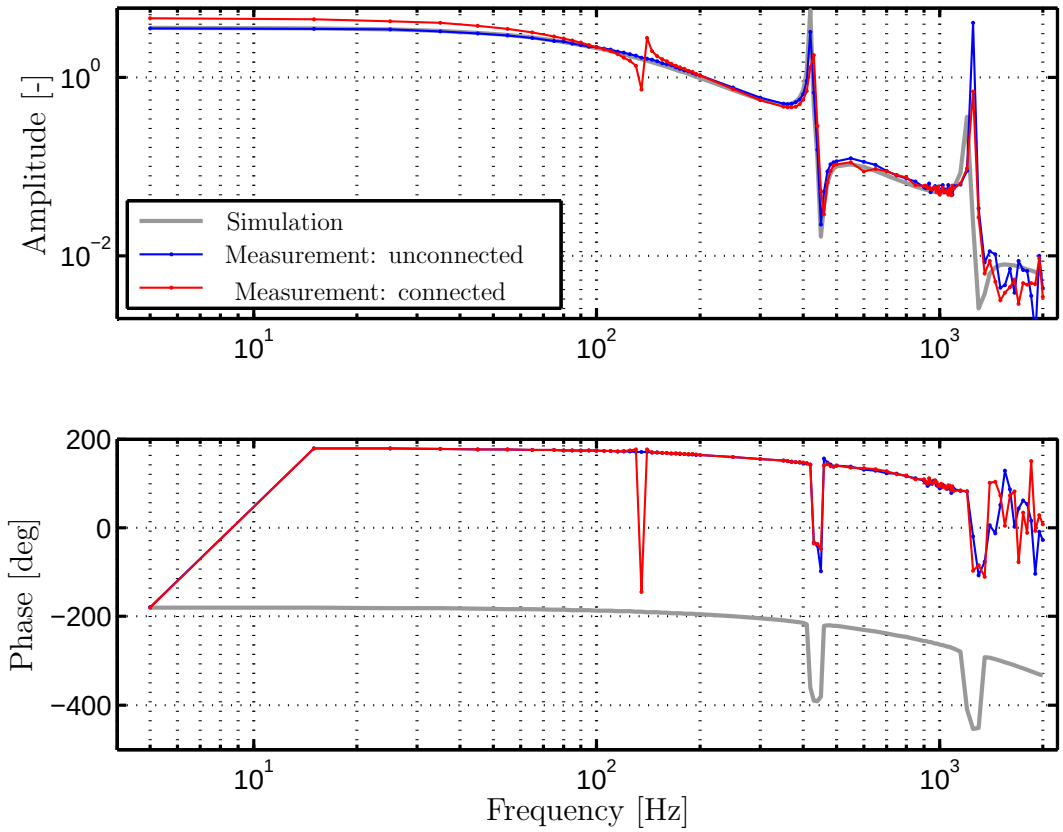

Figure 6.6: *Bode diagram between outputs (displacements in DSP units) and inputs (control current in DSP units) of the plant with AMBs for tilting mode [WS12b, WS15]*

compared with the case without coupling. The first bending mode arises in the case of the tilting mode because of the asymmetry of the test rotor, which is caused by the coupling. For the dynamics at high frequencies, the influence of the coupling is neglected. The effect caused by the coupling changes the performance (e.g. sensitivity) of the selected controller candidates, which is obtained based on the model of the test rotor without coupling. The results will be given in the next section.

6.3 Performance Evaluation

In this section, the two selected controller candidates obtained by the suggested optimization strategy are compared based on the experimental results consisting of the singular values of the sensitivity functions as well as the obtained step responses. Finally, an unbalanced vibration response is measured up to the maximal rotor rotational speed (15000 rpm).

6.3.1 Sensitivity

Because of the existence of uncertainties and nonlinearities in an AMB rotor system, the robustness of the closed loop becomes an essential requirement. The maximal singular value of the sensitivity function serves as a measure of robustness. According to ISO Standard 14839-3, a maximal singular value should be less than four (A/B zone) for the long-term operation of rotor systems supported by AMBs.

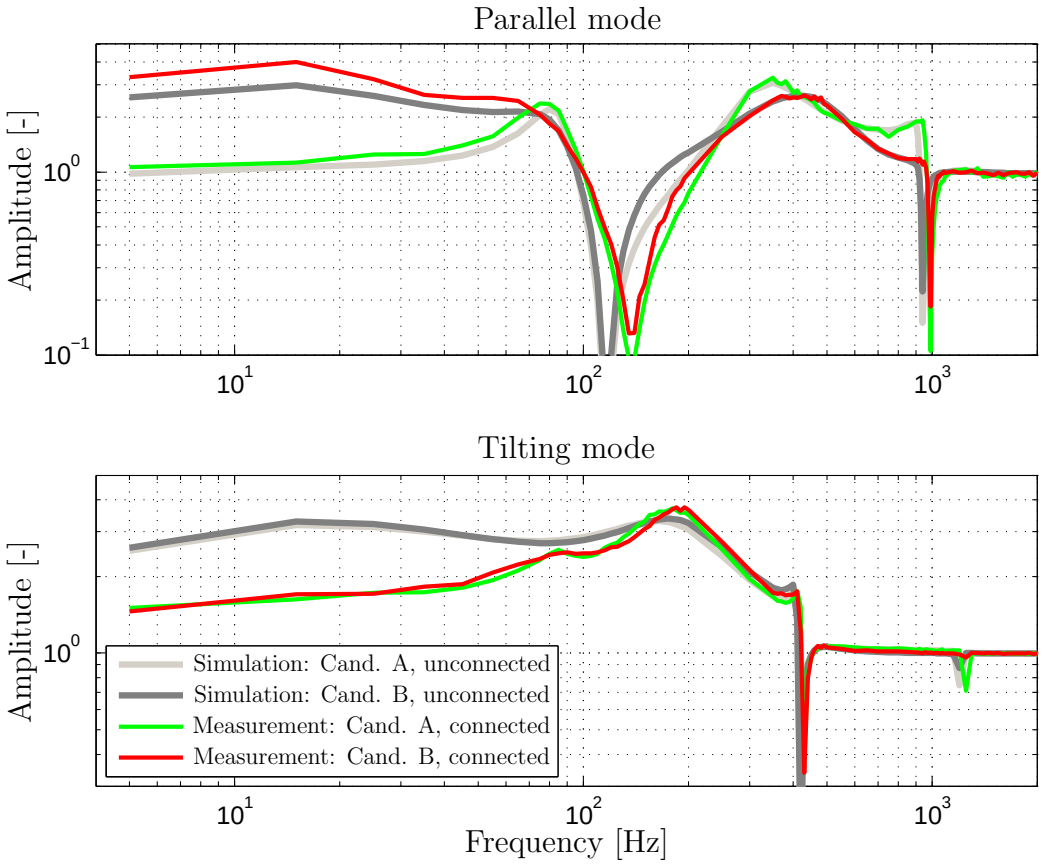

Figure 6.7: *Comparison of the sensitivity from measurement and simulation with the test rotor unconnected to the driving rotor [WS12b, WS15]*

The sensitivity function is measured for the parallel and tilting modes of the AMB rotor system with the rotor at the speed of 0 rpm, i.e. standstill. The measurements are performed with the test rotor connected to the driving rotor. The measured sensitivity functions are compared with the simulation results as shown in Figure 6.7. Note that the simulation results are obtained with the test rotor unconnected to the driving rotor. For the parallel mode, the system with candidate A (green curve) is superior in comparison with that with candidate B (red curve) as indicated by the simulation results. The measured maximal singular value of the parallel mode is approximately 3.3 and 4.0 for

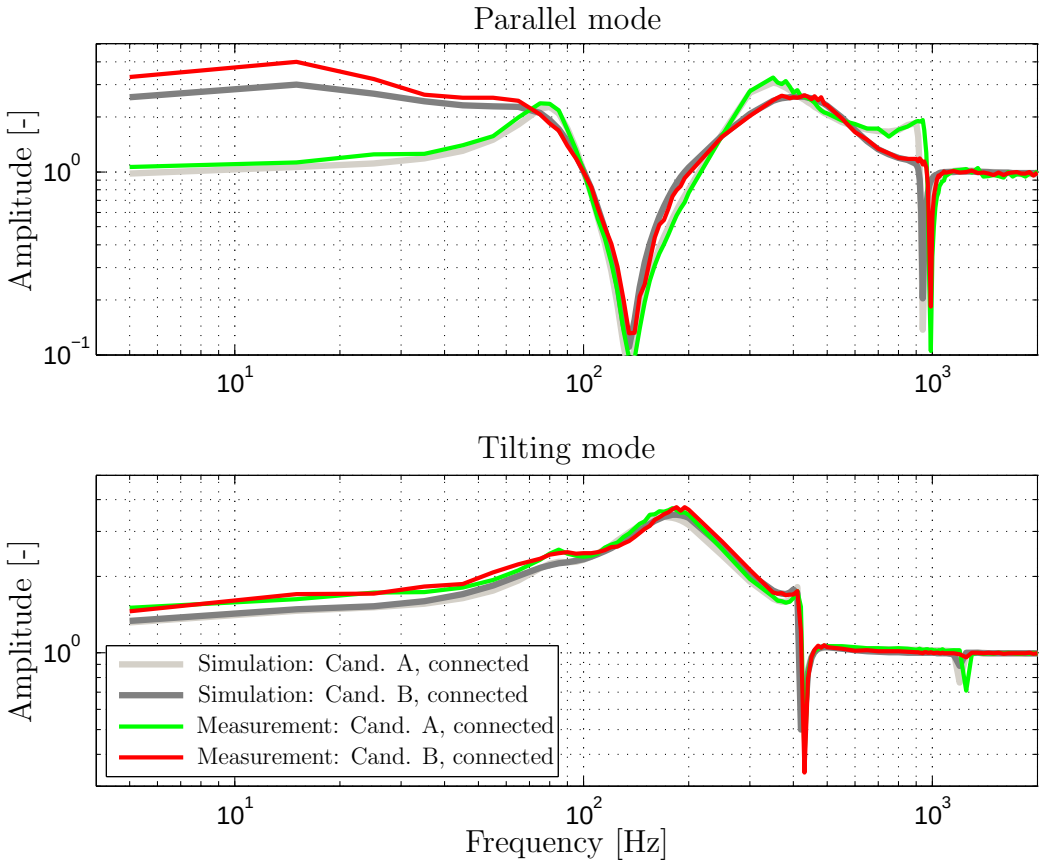

Figure 6.8: *Comparison of the sensitivity from measurement and simulation with the test rotor connected to the driving rotor*

candidates A and B, respectively. Because of the effect of the coupling mentioned in Subsection 6.2.2, the position of the first valley (corresponding to a zero) of the sensitivity function is shifted from 115 to 138 Hz. By comparing the simulation results (no effect of the coupling is considered) with those from the measurement (for the test rotor coupled with the driving rotor), the influence of the coupling for the tilting mode is found to be significant in the low frequency region. The measured maximal singular value for the tilting mode is approximately 3.7 at around 200 Hz for both candidates. In Figure 6.8, the same measured sensitivity functions are compared with the simulation results, which are obtained with the test rotor connected to the driving rotor. The measured results are in agreement with that obtained from simulation, especially for the results relating to the tilting mode, which show a large difference at low frequencies in case that the simulation results are obtained with the rotor unconnected to the driving rotor as shown in Figure 6.7.

6.3.2 Step Response

Step responses have been performed and the measured results are shown in Figures 6.9 and 6.10. The results both for measurement and simulation are obtained with the rotor at standstill and the test rotor are connected to the driving rotor. The step starts at t = 0.05 s with a defined final amplitude value of 50 DSP units (1 DSP = 0.1 [μm] for parallel mode and 1 DSP = 0.1e-6 [rad] for tilting mode).

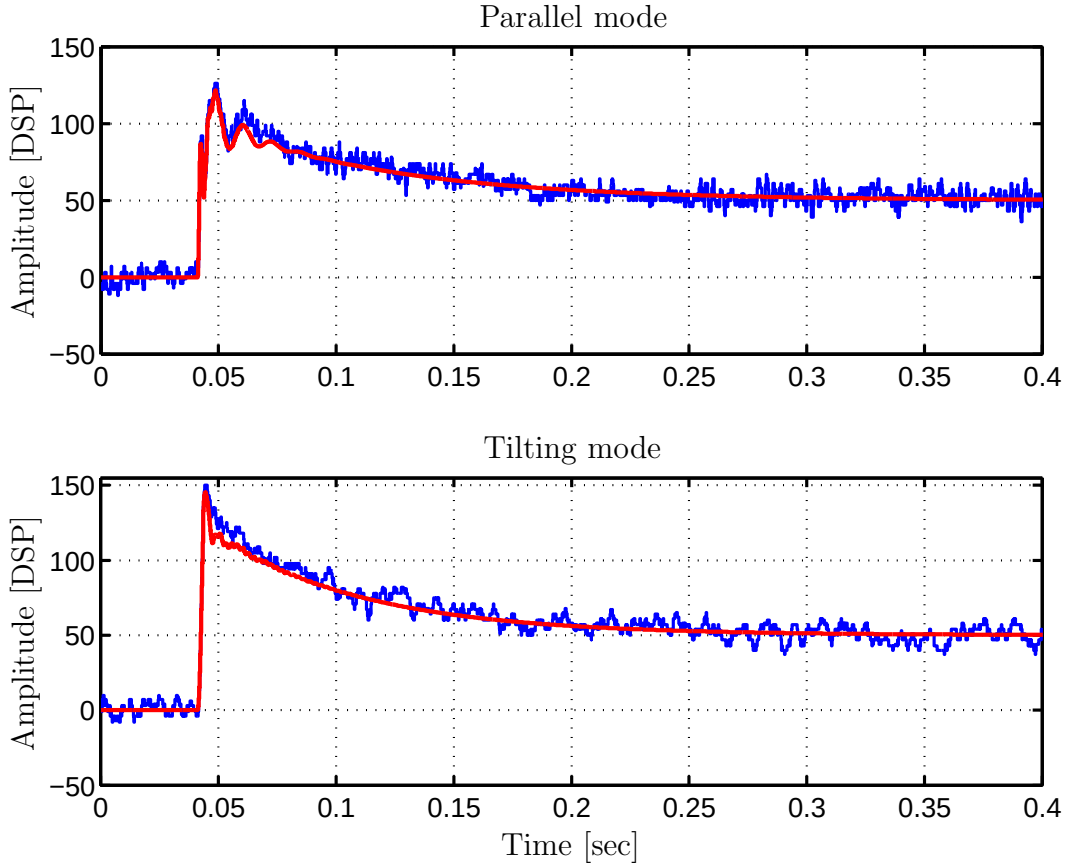

Figure 6.9: *Step response of candidate A from measurement (blue) and simulation (red), 1 DSP = 0.1 [μm] for parallel mode and 1 DSP = 0.1e-6 [rad] for tilting mode*

As shown in Figures 6.9 and 6.10, the simulated step responses for the parallel and tilting modes are consistent with the results obtained by measurement, especially for the case with candidate A. From the measured results, it can be concluded that performance of controller candidate A is better than the that of controller candidate B (smaller overshoot and error). The control current from the step response of the parallel mode is shown in Figures 6.11 and 6.12. Controller candidate A reacts faster and more strongly (but with more noise) on the controller error (as a result of the higher K_P value) than controller candidate B does, e.g., the peak value of the control current is 0.5 A for candidate A and

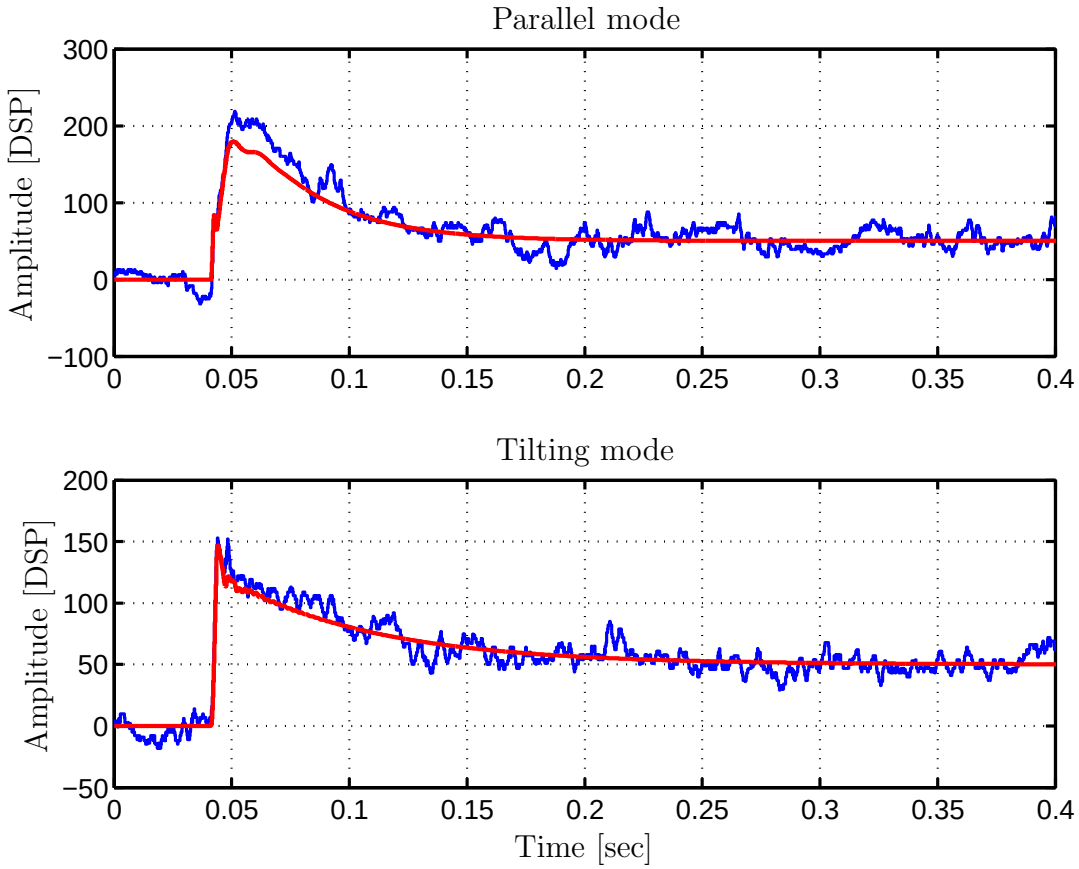

Figure 6.10: *Step response of candidate B from measurement (blue) and simulation (red), 1 DSP = 0.1 [µm] for parallel mode and 1 DSP = 0.1e-6 [rad] for tilting mode*

only 0.25 A for candidate B.

6.3.3 Unbalance Vibration Response

The performance of the controller shall be checked in case with rotating rotor. From the results of sensitivity and step response as shown previously, the controller candidate A is obviously better than candidate B and therefore the candidate A is selected for unbalance response test. This measurement is carried out from 500 to 15000 rpm. For each rotational speed, the peak-to-peak vibrational amplitude in the x- and y-directions (corresponding to the horizontal and vertical direction, respectively) for both sensor nodes (i.e., the DE- and NDE-sides) is determined. The results are presented in Figure 6.13. Critical speeds can be detected easily from Figure 6.13. A peak appears at approximately 5300 rpm because of the rigid tilting mode with a damping ratio of ca. 15% as indicated in Figure 5.14. The peak-to-peak vibrational amplitude has a maximal value under 50 μm up to the maximal rotational speed. The orbits of the rotor at the two sensor nodes (left plot: NDE, right

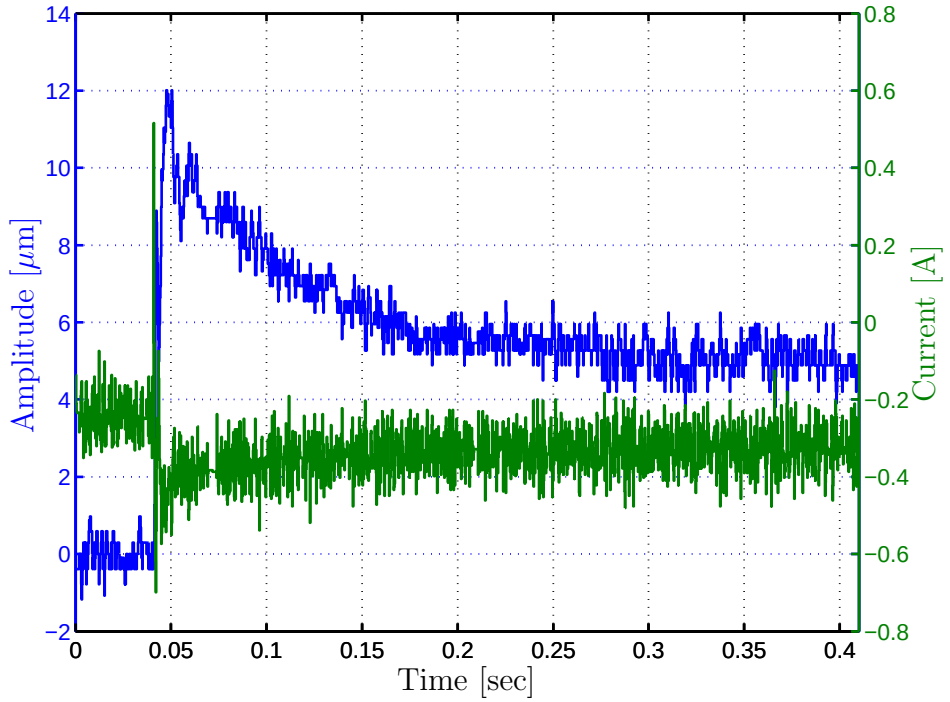

Figure 6.11: *Control current for the controller candidate A for the given step response [WS12b, WS15]*

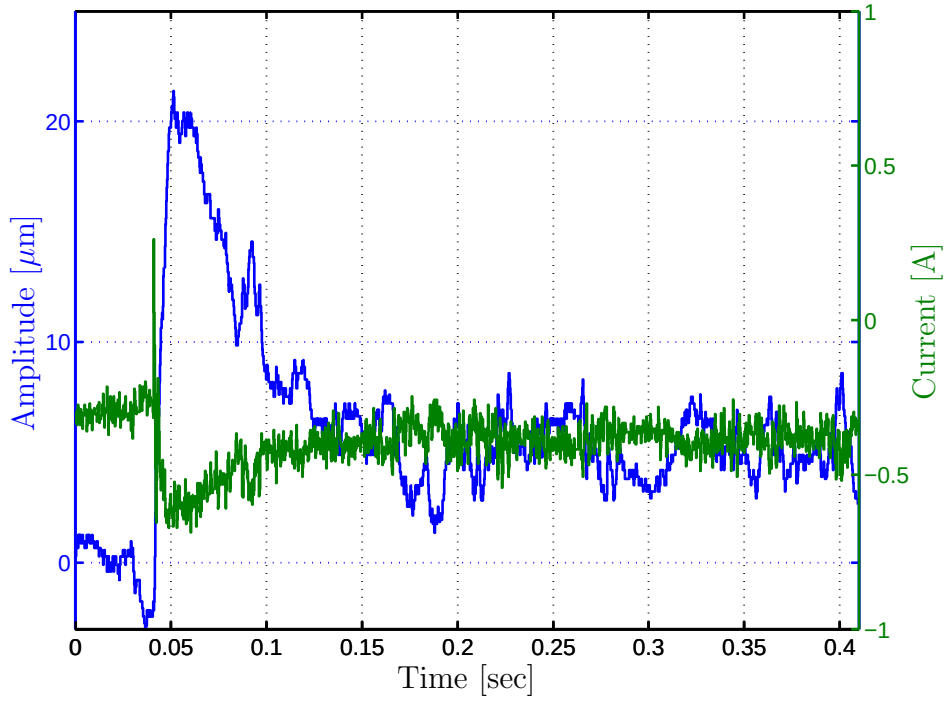

Figure 6.12: *Control current for the controller candidate B for the given step response [WS12b, WS15]*

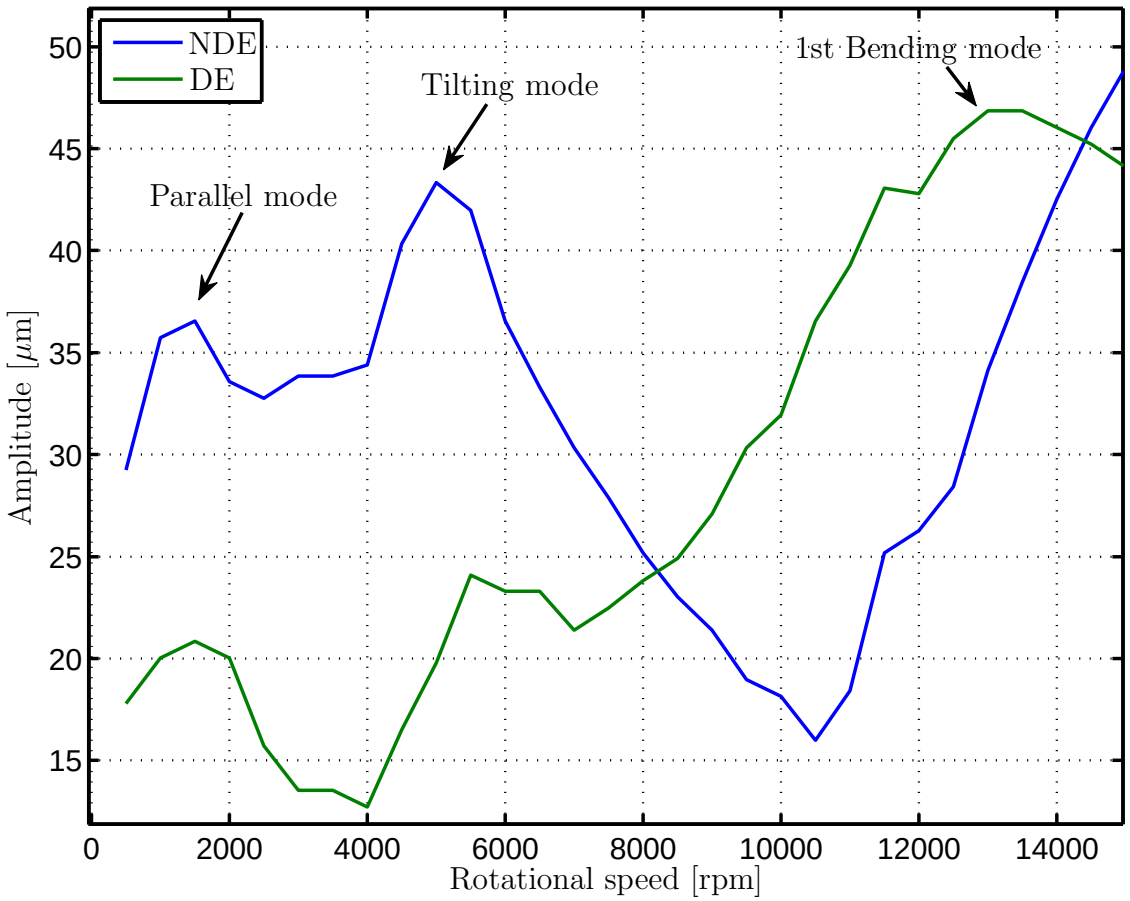

Figure 6.13: *Unbalance vibration response (peak-to-peak) [WS12b]*

plot: DE) at 3000, 9000, and 15000 rpm are illustrated in Figure 6.14. Unlike traditional bearings, both orbits with AMBs are neither elliptical nor circular.

6.4 Summary

This chapter presents the experimental results to validate the optimized controllers by using the suggested optimization approach developed and introduced in last chapter. The results show that the experimental results match the simulation results when the test rotor is not connected with the driving rotor. Otherwise, the dynamics of the AMB rotor system at low frequencies changes caused by connecting to the driving rotor. The controller candidate A performs well (i.e. small maximal singular value, low overshoot, small vibrational amplitude). With this controller, the maximal speed (15000 rpm) is reached. This example shows that a complex PID-controller for the AMB rotor system

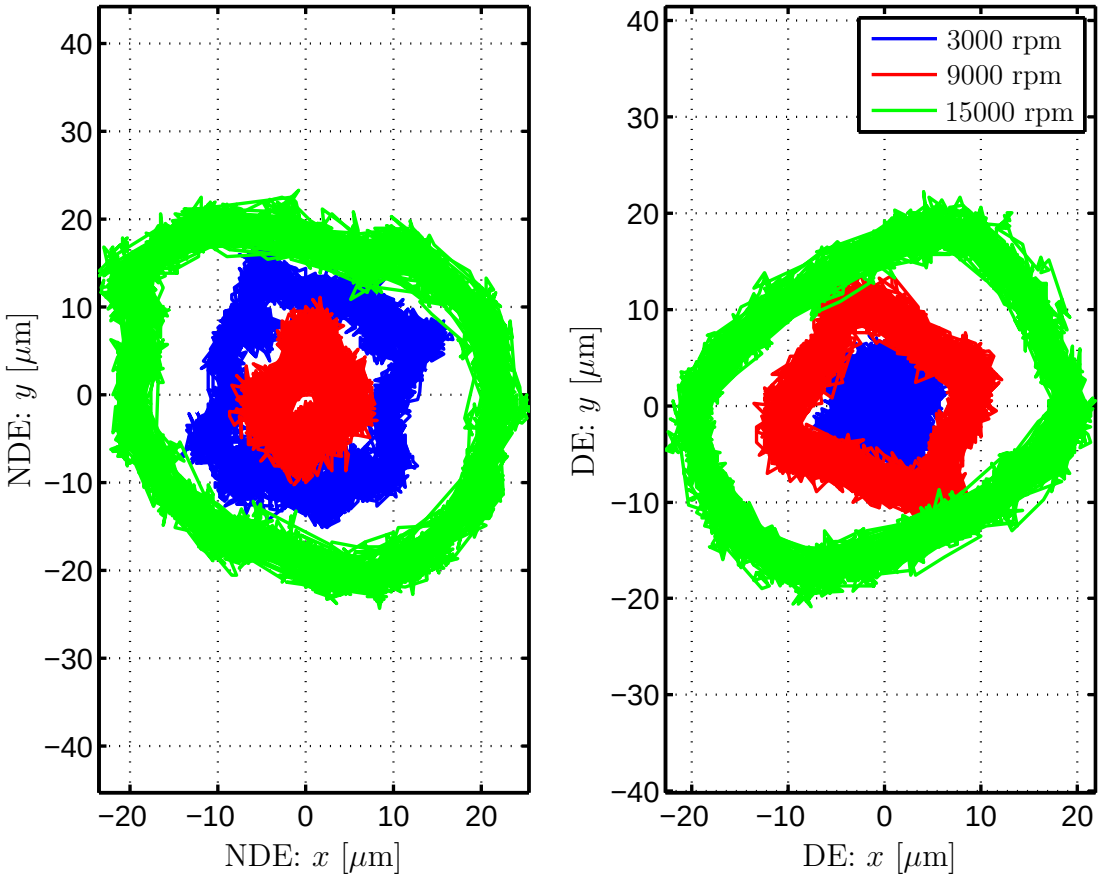

Figure 6.14: *Orbit of the rotor at the rotational speed of 3000, 9000, and 15000 rpm*

can be determined and optimized by using MOGA in combination with the introduced optimization strategy.

Chapter 7

Summary and Outlook

7.1 Summary

Active magnetic bearings as a mature product have been receiving increased attention in industry because of their advantages compared with conventional bearings. They are used extensively in rotor system applications, especially in conditions where conventional bearing systems fail.

However, the inherent negative stiffness of an AMB system causes instability in the open loop of the system; therefore, a feedback control loop is required to stabilize the AMB system. The controller design therefore becomes a central task in AMB system design and requires expert knowledge. Usually, the PID-controller design for AMB systems is tuned manually and iteratively and is a time-consuming process. During the tuning process, a number of objectives are considered and some of these objectives conflict with one another.

Motivated by this situation, an optimization strategy by using MOGAs for the fast and optimal parameter design of complex PID-controllers with respect to given requirements formulated in the time and frequency domain is presented. The challenges that arise when using MOGAs/MOEAs are discussed and a corresponding evaluation procedure of the fitness function and a sensitivity-based parameter reduction strategy are suggested. The simulation results show that a complex PID-controller can be obtained/optimized by using MOGAs with the introduced optimization strategy, considering various criteria and limitations, and performance aspects. Experimental tests have been performed to validate the optimized controllers obtained by using the suggested optimization approach. The results show that the simulation results match the experimental results.

The main contribution of this work can be summaried as follows:

- Literatures related to magnetic bearing technique are reviewed. Research activities in controller design, self-sensing and backup bearing are introduced. Various applications that utilize AMBs are summarized.

- A generalized controller structure is presented, which is suitable for most PID-like controller design for AMB systems. Design criteria related to controller design for AMB system are introduced. It includes design objectives both in time and frequency domain.

- Controller design for AMB systems by means of hand tuning is time-consuming and requires expert knowledge. In order to avoid this situation and reduce the effort to tune the controller, multi-objective optimization with genetic algorithm is introduced to design and optimize the AMB controller. In the optimization, criteria both in time and frequency domain are considered. A hierarchical fitness function evaluation procedure is used to accelerate the optimization process and to increase the probability of convergence. For the first AMB system, which contains a rotor with relative simple structure, the optimization with the introduced evaluation procedure provides satisfactory results. It should be noted that the results for the AMB system are obtained without specific requirements related to initial solutions.

- Multi-objective optimization is introduced. The drawbacks of traditional methods solving multi-objective optimization problem are discussed. Heuristic algorithms are reviewed. Their advantages and disadvangtages are summarized. Complexity of an optimization problem is discussed:

  - Objective function of the optimization problem is multi-modal.
  - Feasible region of the problem is discrete and even random (point-wise) distributed.
  - Objective function (or objective space) is non-continous, non-differentiable, and noisy.
  - In case of multi-objective optimization, different relations between objective functions exist and these relations can even vary within the domain of the search [PF07].
  - The optimization problem belong to the class of $\mathcal{NP}$-complete.
  - The number of objectives to be optimized is large.

  The above aspects often lead to crucial problems in optimization, such as premature convergence to sub-optimal solution region, loss of diversity, and even failure of

solving optimization problems. The challenges/difficulties that arise when using multi-objective genetic algorithms for AMB controller design include:

- Parameters of genetic algorithm have to be carefully tuned for different optimization problems.
- The number of objectives to be optimized is large. The objectives can conflict with one another.
- The number of optimization parameters is large. This increases the complexity of the optimization problem.
- The requirement of stability of the AMB system leads to the feasible region being randomly and even point-wise distributed in the search space as shown in Figure 5.8. Determining the feasible region is an $\mathcal{NP}$-hard problem.

In order to overcome the difficulties above, a strategy reducing the number of optimization parameters in an optimization is developed, which is based on a sensitivity analysis of the controller parameters. This strategy reduces directly the complexity of the optimization problem and accelerates the optimization process. The second AMB system is designed for a real turbo-compressor. The rotor structure is relative complex. The introduced parameter reduction strategy is applied for the controller design of this AMB system. The controller design is optimized in the search space around an initial solution. Optimization results show the efficiency of the introduced strategy. A solution is selected from the optimization results (Pareto front), which provides a damping ratio of 27.7% and a peak value of sensitivity functions about 2.5 (corresponding to zone A according to ISO 14839-3).

- Experimental tests for the first AMB system have been performed to validate the optimized results. The results show that the simulation results match the experimental results when the test rotor is not connected with the driving rotor. Otherwise, the dynamics of the AMB rotor system at low frequencies changes because of the coupling effect when connecting the test rotor to the driving rotor. One controller candidate obtained by using MOGAs performs well (small maximal singular value, low overshoot, small vibrational amplitude through the entire rotation region). With this controller, the maximal speed (15000 rpm) for the test rig is reached.

7.2 Outlook

In future works, experimental tests for the second AMB system (turbo-compressor) shall be carried out to validate the optimization results.

Although the AMB systems are assumed to be linear time invariant in this work, the suggested optimization strategy can be used for nonlinear systems by introducing time domain objectives into the optimization, in which nonlinear behaviors are considered. The performance of the optimization strategy for nonlinear systems shall be investigated.

Based on the optimization results for the two AMB systems, the evaluation procedure for fitness functions and the sensitivity-based parameter reduction strategy show a good performance for optimization of controller design, however, this cannot be generalized to other optimization problems and the evaluation procedure and the parameter reduction stategy shall be tested for other AMB systems and optimization tasks and shall be continuously improved.

A question remains open: how many tuning parameters shall be considered in the optimization? It was recommended that at least the parameters on the first Pareto front based on the sensitivity analysis shall be taken as design parameters. A possible way might be to consider the percentage of correlation coefficents of the selected parameters as a parameter and to find out the best suitable value of this parameter in a statistical manner.

The multi-objective genetic algorithm is employed to optimize the controller designs. Other multi-objective optimization algorithms, e.g. particle swarm optimization, could be an alternative option to perform the optimization task.

Bibliography

[Ahr96] Ahrens, M.: *Zur magnetischen Lagerung von Schwungrad-Energiespeichern*, Eidgenössische Technische Hochschule Zürich, Dissertation, 1996

[Ang98] Angeline, P. J.: Evolutionary Optimization Versus Particle Swarm Optimization: Philosophy and Performance Differences. In: *Proceedings of the Seventh International Conference on Evolutionary Programming VII*. London, UK : Springer-Verlag, 1998 (EP '98), pp. 601–610

[Ant84] Anton, E.: *Stabilitätsverhalten und Regelung von parametererregten Rotorsystemen*, Technische Universität München, Dissertation, 1984

[Bak87] Baker, J. E.: Reducing Bias and Inefficiency in the Selection Algorithm. In: *Proceedings of the Second International Conference on Genetic Algorithms and Their Application*. Cambridge, Massachusetts, USA : L. Erlbaum Associates Inc., 1987, pp. 14–21

[Bak01] Bakare, G. A.: *Removal of Overloads and Voltage Problems in Electric Power Systems Using Genetic Algorithm / Expert System Approaches*, Gerhard-Marcator-Universität - Gesamthochschule Duisburg, Dissertation, 2001

[BBdF12] Barros, R. C. ; Basgalupp, M. P. ; de Carvalho, A. C. P. L. F. ; Freitas, A. A.: A Survey of Evolutionary Algorithms for Decision-Tree Induction. In: *IEEE Transactions on Systems, Man, and Cybernetics* 42 (2012), Nr. 3, pp. 291–312

[BCK+09] Bleuler, H. ; Cole, M. ; Keogh, P. ; Larsonneur, R. ; Maslen, E. H. ; Nordmann, R. ; Okada, Y. ; Schweitzer, G. ; Traxler, A. ; Schweitzer, G. (Hrsg.) ; Maslen, E. H. (Hrsg.): *Magnetic Bearings:*

Theory, Design, and Application to Rotating Machinery. Springer-Verlag Berlin Heidelberg, 2009

[BGH+94] Bleuler, H. ; Gähler, C. ; Herzog, R. ; Larsonneur, R. ; Mizuno, T. ; Siegwart, R. ; Woo, S. J.: Application of Digital Signal Processors for Industrial Magnetic Bearings. In: *IEEE Transactions on Control Systems Technology* 2 (1994), Nr. 4, pp. 280–289

[Ble84] Bleuler, H.: *Decentralized Control of Magnetic Rotor Bearing Systems*, Swiss Federal Institute of Technology Zurich, Dissertation, 1984

[BRS93] Bäck, T. ; Rudolph, G. ; Schwefel, H.-P.: Evolutionary Programming and Evolution Strategies: Similarities and Differences. In: Fogel, D. B. (Hrsg.) ; Atmar, J. W. (Hrsg.): *Proceedings of the Second Annual Conference on Evolutionary Programming.* La Jolla, CA : Evolutionary Programming Society, 1993, pp. 11–22

[BS02] Beyer, H.-G. ; Schwefel, H.-P.: Evolution Strategies: A Comprehensive Introduction. In: *Natural Computing* 1 (2002), pp. 3–52

[BT00] Blondel, V. D. ; Tsitsiklis, J. N.: A Survey of Computational Complexity Results in Systems and Control. In: *Automatica* 36 (2000), pp. 1249–1274

[BW04] Boeringer, D. W. ; Werner, D. H.: Particle Swarm Optimization Versus Genetic Algorithms for Phased Array Synthesis. In: *IEEE Transactions on Antennas and Propagation* 52 (2004), Nr. 3, pp. 771–779

[CC98] Chen, B.-S. ; Cheng, Y.-M.: A Structure-Specified H_∞ Optimal Control Design for Practical Applications: A Genetic Approach. In: *IEEE Transactions on Control Systems Technology* 6 (1998), Nr. 6, pp. 707–718

[CCC11] Correia, S. L. O. B. ; Celestino Jr., J. ; Cherkaoui, O.: Mobility-Aware Ant Colony Optimization Routing for Vehicular Ad Hoc Networks. In: *IEEE Wireless Communications and Networking Conference (WCNC).* Cancun, Quintana Roo, 2011, pp. 1125–1130

[CCD+08] Chen, H. M. ; Chapman, P. A. ; Donahue, A. C. ; Prisco, C. J. ; Walter, T. J.: A Magnetically Levitated Blood Pump Using LCR Circuits. In: *Proceedings of the Eleventh International Symposium on Magnetic Bearings (ISMB 11)*, 2008, pp. 212–216

[CCZ09] Chen, Q. ; Chen, T. ; Zhang, Y.: Research of GA-Based PID for AUV Motion Control. In: *Proceedings of the 2009 IEEE International Conference on Mechatronics and Automation*. Changchun, China, 2009, pp. 4446–4451

[CLWL08] Chen, R.-M. ; Lo, S.-T. ; Wu, C.-L. ; Lin, T.-H.: An Effective Ant Colony Optimization-Based Algorithm for Flow Shop Scheduling. In: *IEEE Conference on Soft Computing in Industrial Applications (SMCIA/08)*. Muroran, Japan, 2008, pp. 101–106

[CMN+04] Cupertino, F. ; Mininno, E. ; N., D. ; Turchiano, B. ; Salvatore, L.: On-Line Genetic Design of Anti-Windup Unstructured Controllers for Electric Drives With Variable Load. In: *IEEE Transactions on Evolutionary Computation* 8 (2004), Nr. 4, pp. 347–364

[Coe98] Coello, C. A. C.: A Comprehensive Survey of Evolutionary-Based Multiobjective Optimization Techniques. In: *Knowledge and Information Systems* 1 (1998), pp. 269–308

[Coe06] Coello, C. A. C.: Evolutionary Multi-Objective Optimization: A Historical View of the Field. In: *IEEE Computational Intelligence Magazine* 1 (2006), Nr. 1, pp. 28–36

[CW10] Chen, S. L. ; Weng, C. C.: Robust Control of a Voltage-Controlled Three-Pole Active Magentic Bearing System. In: *IEEE/ASME Transactions on Mechatronics* 15 (2010), Nr. 3, pp. 381–388

[Dar59] Darwin, C.: *On the Origin of Species*. John Murray, 1859

[DBS06] Dorigo, M. ; Birattari, M. ; Stützle, T.: Ant Colony Optimization: Artificial Ants as a Computational Intelligence Technique. In: *IEEE Computational Intelligence Magazine* 1 (2006), pp. 28–39

[Deb01] Deb, K.: *Multi-Objective Optimization Using Evolutionary Algorithms*. Chichester : John Wiley & Sons, 2001 (Wiley-Interscience Series in Systems and Optimization)

[DMC91] Dorigo, M. ; Maniezzo, V. ; Colorni, A.: Positive Feedback as a Search Strategy / Dipartimento di Elettronica, Politecnico di Milano. Milan, Italy, 1991 (91-016). – Techreport

[dNv11] de Bruyn, K. ; Nitschke, G. ; van Heerden, W.: Evolutionary Algorithms and Particle Swarm Optimization for Artificial Language Evolution.

In: *IEEE Congress on Evolutionary Computation (CEC)*. New Orleans, LA, 2011, pp. 2701–2708

[DPAM02] Deb, K. ; Pratap, A. ; Agarwal, S. ; Meyarivan, T.: A Fast and Elitist Multiobjective Genetic Algorithm: NSGA-II. In: *IEEE Transactions on Evolutionary Computation* 6 (2002), pp. 182–197

[DS03] Dorigo, M. ; Stützle, T.: The Ant Colony Optimization Metaheuristic: Algorithms, Applications, and Advances. In: Glover, F. (Hrsg.) ; Kochenberger, G. (Hrsg.): *Handbook of Metaheuristics* Bd. 57. Springer US, 2003, pp. 250–285

[dVM+08] del Valle, Y. ; Venayagamoorthy, G. K. ; Mohagheghi, S. ; Hernandez, J. C. ; Harley, R. G.: Particle Swarm Optimization: Basic Concepts, Variants and Applications in Power Systems. In: *IEEE Transactions on Evolutionary Computation* 12 (2008), Nr. 2, pp. 171–195

[DYZF12] Duan, H. ; Yu, Y. ; Zou, J. ; Feng, X.: Ant Colony Optimization-based Bio-Inspired Hardware: Survey and Prospect. In: *Transactions of the Institute of Measurement and Control* 34 (2012), Nr. 2-3, pp. 318–333

[DZC08] Du, Y. ; Zhang, Q. ; Chen, Q.: ACO-IH: An Improved Ant Colony Optimization Algorithm for Airport Ground Service Scheduling. In: *IEEE International Conference on Industrial Technology (ICIT 2008)*. Chengdu, China, 2008, pp. 1–6

[DZJG10] Du, H. ; Zhang, N. ; Ji, J. C. ; Gao, W.: Robust Fuzzy Control of an Active Magnetic Bearing Subject to Voltage Saturation. In: *IEEE Transactions on Control Systems Technology* 18 (2010), Nr. 1, pp. 164–169

[FF93] Fonseca, C. M. ; Fleming, P. J.: Genetic Algorithms for Multiobjective Optimization: Formulation, Discussion and Generalization. In: Forrest, S. (Hrsg.): *Proceedings of the Fifth International Conference on Genetic Algorithms*. San Mateo, California, USA : Morgan Kaufmann, 1993, pp. 416–423

[FF95] Fonseca, C. M. ; Fleming, P. J.: An Overview of Evolutionary Algorithms in Multiobjective Optimization. In: *Evolutionary Computation* 3 (1995), Nr. 1, pp. 1–16

[Fon95] Fonseca, C. M.: *Multiobjective Genetic Algorithms with Application to Control Engineering Problems*, The University of Sheffield, Dissertation, 1995

[FOW66] Fogel, L. J. ; Owens, A. J. ; Walsh, M. J.: *Artificial Intelligence through Simulated Evolution*. John Wiley, New York, 1966

[FP02] Fleming, P. J. ; Purshouse, R. C.: Evolutionary Algorithms in Control Systems Engineering: A Survey. In: *Control Engineering Practice* 10 (2002), pp. 1223–1241

[Frö97] Fröhlich, J.: *Evolutionary Optimization for Computational Electromagnetics*, Swiss Federal Institute of Technology Zurich, Dissertation, 1997

[Fum97] Fumagalli, M. A.: *Modelling and Measurement Analysis of the Contact Interaction Between a High Speed Rotor and Its Stator*, Swiss Federal Institute of Technology Zurich, Dissertation, 1997

[FW06] Farag, A. ; Werner, H.: Structure Selection and Tuning of Multi-Variable PID Controllers for an Industrial Benchmark Problem. In: *IEE Proceedings of Control Theory Application* Bd. 153, 2006

[FWX12] Fan, X. ; Wang, X. ; Xiao, Y.: PSO Versus GAs for Fast Object Localization Problem. In: *IEEE Fifth International Conference on Advanced Computational Intelligence (ICACI)*, 2012, pp. 605–609

[GK89] Gasch, R. ; Knothe, K.: *Strukturdynamik Band 2: Kontinua und ihre Diskretisierung*. Springer Verlag, 1989

[Gol89] Goldberg, D. E.: *Genetic Algorithms in Search, Optimization and Machine Learning*. New York, NY, USA : Addison-Wesley Longman Publishing Co., Inc., 1989

[GP06] Gryazina, E. N. ; Polyak, B. T.: Stability Regions in the Parameter Space: D-Decomposition Revisited. In: *Automatica* 42 (2006), Nr. 1, pp. 13–26

[GT07] Gao, M. ; Tian, J.: Path Planning for Mobile Robot Based on Improved Simulated Annealing Artificial Neural Network. In: *The Third International Conference on Natural Computation (ICNC 2007)* Bd. 3, 2007, pp. 8–12

[GU08] Ginzinger, L. ; Ulbrich, H.: Simulation-Based Controller Design for an Active Auxiliary Bearing. In: *Proceedings of the Eleventh International Symposium on Magnetic Bearings (ISMB 11)*, 2008

[Han94] Hancock, P. J. B.: An Empirical Comparison of Selection Methods in Evolutionary Algorithms. In: Fogarty, T. C. (Hrsg.): *Selected Papers from AISB Workshop on Evolutionary Computing* Bd. 865. London, UK : Springer Berlin Heidelberg, 1994, pp. 80–94

[HCFd09] Hruschka, E. R. ; Campello, R. J. G. B. ; Freitas, A. A. ; de Carvalho, A. C. P. L. F.: A Survey of Evolutionary Algorithms for Clustering. In: *IEEE Transactions on Systems, Man, and Cybernetics* 39 (2009), Nr. 2, pp. 133–155

[Hir03] Hirschmanner, M.: *Control of Unbalance and Self-Exciting Forces by Active Magnetic Bearings*, Technische Universität Wien, Fakultät für Maschinenbau, Dissertation, 2003

[HL92] Hajela, P. ; Lin, C.-Y.: Genetic Search Strategies in Multicriterion Optimal Design. In: *Structural Optimization* 4 (1992), pp. 99–107

[HL00] Hong, S.-K. ; Langari, R.: Robust Fuzzy Control of a Magnetic Bearing System Subject to Harmonic Disturbances. In: *IEEE Transactions on Control Systems Technology* 8 (2000), Nr. 2, pp. 366–371

[HL10] Hao, X. ; Lin, L.: Job Shop Rescheduling by Using Multi-Objective Genetic Algorithm. In: *The 40th International Conference on Computers and Industrial Engineering (CIE)*. Awaji, Japan, 2010, pp. 1–6

[HLX98] Ho, W. K. ; Lim, K. ; Xu, W.: Optimal Gain and Phase Margin Tuning for PID Controllers. In: *Automatica* 34 (1998), Nr. 8, pp. 1009–1014

[HN93] Horn, J. ; Nafplioti, N.: Multiobjective Optimization Using the Niched Pareto Genetic Algorithm / Illinois Genetic Algorithms Laboratory, University of Illinois. 1993 (IlliGAL Report 93005). – Techreport

[HNG94] Horn, J. ; Nafpliotis, N. ; Goldberg, D. E.: A Niched Pareto Genetic Algorithm for Multiobjective Optimization. In: *Proceedings of the First IEEE Conference on Evolutionary Computation, IEEE World Congress on Computational Intelligence* Bd. 1. Piscataway, NJ, 1994, pp. 82–87

[Hol75] Holland, J. H.: *Adaptation in Natural and Artificial Systems: An Introductory Analysis with Applications to Biology, Control, and Artificial Intelligence*. University of Michigan Press, 1975

[IMM01] Iredi, S. ; Merkle, D. ; Middendorf, M.: Bi-Criterion Optimization with Multi Colony Ant Algorithms. In: Zitzler, E. (Hrsg.) ; Deb, K. (Hrsg.) ; Thiele, L. (Hrsg.) ; Coello, C. A. C. (Hrsg.) ; Corne, D. (Hrsg.): *Proceedings of the Evolutionary Multi-Criterion Optimization, First International Conference (EMO 2001)* Bd. 1993, Springer Berlin Heidelberg, 2001, pp. 359–372

[ISO06] ISO 14939-3: *Mechanical Vibration — Vibration of Rotating Machinery Equipped with Active Magnetic Bearings — Part 3: Evaluation of Stability Margin.* 2006

[JLLW08] Juang, C.-F. ; Lu, C.-M. ; Lo, C. ; Wang, C.-Y.: Ant Colony Optimization Algorithm for Fuzzy Controller Design and Its FPGA Implementation. In: *IEEE Transactions on Industrial Electronics* 55 (2008), Nr. 3, pp. 1453–1462

[JP09] Jastrzębski, R. P. ; Pöllänen, R.: Centralized Optimal Position Control for Active Magnetic Bearings: Comparison with Decentralized Control. In: *Electrical Engineering* 91 (2009), Nr. 2, pp. 101–114

[KCS06] Konaka, A. ; Coit, D. W. ; Smith, A. E.: Multi-Objective Optimization Using Genetic Algorithms: A Tutorial. In: *Reliability Engineering and System Safety* 91 (2006), pp. 992–1007

[KE95] Kennedy, J. ; Eberhart, R.: Particle Swarm Optimization. In: *Proceedings of IEEE International Conference on Neural Networks* Bd. 4. Perth, WA, 1995, pp. 1942–1948

[KGV83] Kirkpatrick, S. ; Gelatt Jr., C. D. ; Vecchi, M. P.: Optimization by Simulated Annealing. In: *Science* 220 (1983), Nr. 4598, pp. 671–680

[KKY+00] Koza, J. R. ; Keane, M. A. ; Yu, J. ; Bennett III, F. H. ; Mydlowec, W.: Automatic Creation of Human-Competitive Programs and Controllers by Means of Genetic Programming. In: *Genetic Programming and Evolvable Machines* 1 (2000), pp. 121–164

[KMF09] Kato, E. R. R. ; Morandin, O. ; Fonseca, M. A. S.: Ant Colony Optimization Algorithm for Reactive Production Scheduling Problem in the Job Shop System. In: *Proceedings of the 2009 IEEE International Conference on Systems, Man and Cybernetics (SMC 2009).* San Antonio, TX, USA, 2009, pp. 2199–2204

[Koz90] Koza, J. R.: Genetic Programming: A Paradigm for Genetically Breeding Populations of Computer Programs to Solve Problems / Computer Science Department, Stanford University. Margaret Jacks Hall, Stanford, CA 94305, USA, 1990. – Techreport

[Koz92] Koza, J. R.: *Genetic Programming: On the Programming of Computers by Means of Natural Selection*. Cambridge, MA, USA : MIT Press, 1992

[Kär07] Kärkkäinen, A.: *Dynamic Simulations of Rotors During Drop on Retainer Bearings*, Lappeenranta University of Technology, Dissertation, 2007

[KSBC08] Keogh, P. ; Sahinkaya, N. ; Burrows, C. ; Cade, I.: Rotor/Auxiliary Bearing Dynamic Contact Modes in Magnetic Bearing Systems. In: *Proceedings of the Eleventh International Symposium on Magnetic Bearings (ISMB 11)*, 2008

[Lan97] Lang, O.: *Vibration Control of a Self-Excited Rotor by Active Magnetic Bearings*, Technische Universität Wien, Dissertation, 1997

[Lar90] Larsonneur, R.: *Design and Control of Active Magnetic Bearing Systems for High Speed Rotation*, Swiss Federal Institute of Technology Zurich, Dissertation, 1990

[LH06] Lohn, J. D. ; Hornby, G. S.: Evolvable Hardware: Using Evolutionary Computation to Design and Optimize Hardware Systems. In: *IEEE Computational Intelligence Magazine* 1 (2006), Nr. 1, pp. 19–27

[LJS03] Lin, C.-L. ; Jan, H.-Y. ; Shieh, N.-C.: GA-Based Multiobjective PID Control for a Linear Brushless DC Motor. In: *IEEE/ASME Transactions on Mechatronics* 8 (2003), Nr. 1, pp. 56–65

[Lös02] Lösch, F.: *Identification and Automated Controller Design for Active Magnetic Bearing Systems*, Swiss Federal Institute of Technology Zurich, Dissertation, 2002

[MCGFO06] Molina-Cristóbal, A. ; Griffin, I. A. ; Fleming, P. J. ; Owens, D. H.: Linear Matrix Inequalities and Evolutionary Optimization in Multiobjective Control. In: *International Journal of Systems Science* 37 (2006), June, Nr. 8, pp. 513–522

[MG00] Mei, T.X. ; Goodall, R. M.: LQG and GA Solutions for Active Steering of Railway Vehicles. In: *IEE Proceedings - Control Theory and Applications* Bd. 147, 2000, pp. 111–117

[MLA12] Mushi, S. E. ; Lin, Z. ; Allaire, P. E.: Design, Construction, and Modeling of a Flexible Rotor Active Magnetic Bearing Test Rig. In: *IEEE/ASME Transactions on Mechatronics* 17 (2012), Nr. 6, pp. 1170–1182

[MMI06] Maslen, E. H. ; Montie, D. T. ; Iwasaki, T.: Robustness Limitations in Self-Sensing Magnetic Bearings. In: *Journal of Dynamic Systems, Measurement, and Control* 128 (2006), pp. 197–203

[Mon09] Montgomery, D. C.: *Design and Analysis of Experiments*. 7. John Wiley & Sons, Inc., 2009

[MVL+10] Masala, A. ; Vannini, G. ; Lacour, M. ; Tassel, F.-M. ; Camatti, M.: Lateral Rotordynamic Analysis and Testing of a Vertical High Speed 12.5 MW Motorcompressor Levitated by Active Magnetic Bearings. In: *Proceedings of The Twelfth International Symposium on Magnetic Bearings (ISMB 12)*, 2010, pp. 8–13

[Noh96] Noh, M. D.: *Self-Sensing Magnetic Bearings Driven by a Switching Power Amplifier*, University of Virginia, Dissertation, 1996

[NRK+08] Nonami, K. ; Rachmanto, B. ; Kuriyama, K. ; Sato, Y. ; Kondo, K. ; Kubo, A. ; Takahata, R.: AMB Flywheel-Powered Electric Vehicle. In: *Proceedings of the Eleventh International Symposium on Magnetic Bearings (ISMB 11)*, 2008, pp. 232–237

[NSS99] Nijhuis, A. B. M. ; Schmied, J. ; Shultz, R. R.: Rotordynamic Design Considerations for a 23 MW Compressor with Magnetic Bearings. In: *Fluid Machinery for the Oil, Petrochemical and Related Industries - IMechE Conference* Bd. 2, 1999, pp. 129–142

[Oga10] Ogata, K.: *Modern Control Engineering*. 5. Prentice Hall PTR, 2010

[OMN92] Okada, Y. ; Matsuda, K. I. ; Nagai, B.: Sensorless Magnetic Levitation Control by Measuring the PWM Carrier Frequency Component. In: *Proceedings of the Third International Symposium on Magnetic Bearings (ISMB 3)*, 1992

[OP89] Osman, I. H. ; Potts, C. N.: Simulated Annealing for Permutation Flow-Shop Scheduling. In: *Omega* 17 (1989), Nr. 6, pp. 551–557

[Pes13] Pesch, A. H.: *Development of Chatter Attenuation Robust Control for an AMB Machining Spindle*, Cleveland State University, Dissertation, 2013

[Pet06] Petzold, O.: *Modellbildung und Untersuchung eines magnetisch gelagerten Rundtisches*, Otto-von-Guericke-Universität Magdeburg, Dissertation, 2006

[Pet08] Petrikevich, Y. I.: Randomized Methods of Stabilization of the Discrete Linear Systems. In: *Automation and Remote Control* 69 (2008), Nr. 11, pp. 1911–1921

[PF07] Purshouse, R. C. ; Fleming, P. J.: On the Evolutionary Optimization of Many Conflicting Objectives. In: *IEEE Transactions on Evolutionary Computation* 11 (2007), Nr. 6, pp. 770–784

[PFX12] Peng, C. ; Fang, J. ; Xu, X.: Robust Attitude Controller for Spacecraft with Magnetically Suspended Flywheels. In: *The Eighth IEEE International Symposium on Instrumentation and Control Technology (ISICT 2012)*, 2012, pp. 224–228

[PJC13] Ponsich, A. ; Jaimes, A. L. ; Coello, C. A. C.: A Survey on Multiobjective Evolutionary Algorithms for the Solution of the Portfolio Optimization Problem and Other Finance and Economics Applications. In: *IEEE Transactions on Evolutionary Computation* 17 (2013), Nr. 3, pp. 321–344

[Pol08] Poli, R.: Analysis of the Publications on the Applications of Particle Swarm Optimisation. In: *Journal of Artificial Evolution and Applications* 2008 (2008), pp. 4:1–4:10

[PRv+06] Polajžer, B. ; Ritonja, J. ; Štumberger, G. ; Dolinar, D. ; Lecointe, J.-P.: Decentralized PI/PD Position Control for Active Magnetic Bearings. In: *Electrical Engineering* 89 (2006), Nr. 1, pp. 53–59

[PSL10] Pindoriya, N. M. ; Singh, S. N. ; Lee, K. Y.: A Comprehensive Survey on Multi-Objective Evolutionary Optimization in Power System Applications. In: *IEEE Power and Energy Society General Meeting*. Minneapolis, Minnesota, USA, 2010, pp. 1–8

[PY06] Pedersen, G. K. M. ; Yang, Z.: Multi-Objective PID-Controller Tuning for a Magnetic Levitation System Using NSGA-II. In: *Proceedings of*

the Eighth Annual Conference on Genetic and Evolutionary Computation. Seattle, Washington, USA : ACM, 2006 (GECCO '06), pp. 1737–1744

[RDD96] Rundell, A. E. ; Drakunov, S. V. ; DeCarlo, R. A.: A Sliding Model Observer and Controller for Stabilization of Rotational Motion of a Vertical Shaft Magnetic Bearing. In: *IEEE Transactions on Control Systems Technology* 4 (1996), Nr. 5, pp. 598–608

[Rec71] Rechenberg, I.: *Evolutionsstrategie: Optimierung technischer Systeme nach Prinzipien der biologischen Evolution*, Technische Universität Berlin, Dissertation, 1971

[RSJ07] Rahmat-Sami, Y. ; Jin, N.: Particle Swarm Optimization (PSO) in Engineering Electromagnetics: A Nature-Inspired Evolutionary Algorithm. In: *International Conference on Electromagnetics in Advanced Applications (ICEAA)*. Torino, Italy, 2007, pp. 177–182

[Sal87] Salm, J. R.: *Eine aktive magnetische Lagerung eines elastischen Rotors als Beispiel ordnungsreduzierter Regelung großer elastischer Systeme*, Eidgenössische Technische Hochschule Zürich, Dissertation, 1987

[SB08] Sabirin, C. R. ; Binder, A.: Rotor Levitation by Active Magnetic Bearing Using Digital State Controller. In: *The Thirteenth International Power Electronics and Motion Control Conference (EPE-PEMC 2008)*, 2008, pp. 1625–1632

[SCFG97] Schroder, P. ; Chipperfield, A. J. ; Fleming, P. J. ; Grum, N.: Multi-Objective Optimisation of Distributed Active Magnetic Bearing Controllers. In: *Proceedings of the Second International Conference on Genetic Algorithms in Engineering Systems: Inovations and Applications*, IET, 1997, pp. 326–333

[Sch75] Schwefel, H.-P.: *Evolutionsstrategie und numerische Optimierung*, Technische Universität Berlin, Dissertation, 1975

[Sch85] Schaffer, J. D.: Multiple Objective Optimization with Vector Evaluated Genetic Algorithms. In: *Proceedings of the First International Conference on Genetic Algorithms*. Hillsdale, NJ, USA : L. Erlbaum Associates Inc., 1985, pp. 93–100

[Sch03] Schönhoff, U.: *Practical Robust Control of Mechatronic Systems with Structural Flexibilities*, Technische Universität Darmstadt, Dissertation, 2003

[SD94] Srinivas, N. ; Deb, K.: Multiobjective Optimization Using Nondominated Sorting in Genetic Algorithms. In: *Evolutionary Computation* 2 (1994), Nr. 3, pp. 221–248

[SGGF01] Schroder, P. ; Green, B. ; Grum, N. ; Fleming, P. J.: On-Line Evolution of Robust Control Systems: An Industrial Active Magnetic Bearing Application. In: *Control Engineering Practice* 9 (2001), Nr. 1, pp. 37–49

[Shi99] Shi, Y.: Combinations of Evolutionary Algorithms and Fuzzy Systems: A Survey. In: *Proceedings of the 18th International Conference of the North American Fuzzy Information Processing Society (NAFIPS)*, 1999, pp. 610–614

[SI96] Sannomiya, N. ; Iima, H.: Application of Genetic Algorithm to Scheduling Problems in Manufacturing Processes. In: *Proceedings of IEEE International Conference on Evolutionary Computation*, 1996, pp. 523–528

[Sie89] Siegwart, R.: *Aktive magnetische Lagerung einer Hochleistungsfrässpindel mit digitaler Regelung*, Eidgenössische Technische Hochschule Zürich, Dissertation, 1989

[Skr04] Skricka, N.: *Entwicklung eines sensorlosen aktiven Magnetlagers*, Technische Universität Darmstadt, Dissertation, 2004

[Soc08] Socha, K.: *Ant Colony Optimization for Continuous and Mixed-Variable Domains*, Université Libre de Bruxelles, Dissertation, 2008

[SS03] Sim, K. M. ; Sun, W. H.: Ant Colony Optimization for Routing and Load-Balancing: Survey and New Directions. In: *IEEE Transactions on Systems, Man, and Cybernetics* 33 (2003), Nr. 5, pp. 560–572

[SS12] Suri, B. ; Singhal, S.: Literature Survey of Ant Colony Optimization in Software Testing. In: *CSI Sixth International Conference on Software Engineering (CONSEG)*, 2012, pp. 1–7

[TKK96] Tamaki, H. ; Kita, H. ; Kobayashi, S.: Multi-Objective Optimization by Generic Algorithms: A Review. In: *Proceedings of IEEE International Conference on Evolutionary Computation*, 1996, pp. 517–522

[TNA99] Tamaki, H. ; Nishino, E. ; Abe, S.: A Genetic Algorithm Approach to Multi-Objective Scheduling Problems with Earliness and Tardiness Penalties.

In: *Proceedings of the 1999 Congress on Evolutionary Computation (CEC 99)* Bd. 1. Washington, DC, USA, 1999, pp. 46–52

[TS02] Thibeault, N. M. ; Smith, R. S.: Magnetic Bearing Measurement Configurations and Associated Robustness and Performance Limitations. In: *ASME Journal of Dynamic Systems, Measurement, and Control* 124 (2002), pp. 589–598

[TTEL03] Turgut, D. ; Turgut, B. ; Elmasri, R. ; Le, T. V.: Optimizing Clustering Algorithm in Mobile Ad Hoc Networks Using Simulated Annealing. In: *IEEE Wireless Communications and Networking Conference (WCNC)* Bd. 3, 2003, pp. 1492–1497

[Ulb79] Ulbrich, H.: *Entwurf und Realisierung einer berührungsfreien Magnetlagerung für ein Rotorsystem*, Technische Universität München, Dissertation, 1979

[VB93] Vischer, D. ; Bleuler, H.: Self-Sensing Active Magentic Levitation. In: *IEEE Transactions on Magnetics* 29 (1993), Nr. 2, pp. 1276–1281

[Wei09] Weise, T.: *Evolving Distributed Algorithms with Genetic Programming*, University of Kassel, Dissertation, 2009

[WGS13] Wei, C. ; Gausmann, R. ; Söffker, D.: Controller Design and Optimization Strategy for Active Magnetic Bearing Systems. In: *Proceedings of the Tenth International Conference on Vibrations in Rotating Machines (SIRM 2013)*, 2013

[WKA90] Williams, R. D. ; Keith, F. J. ; Allaire, P. E.: Digital Control of Active Magentic Bearings. In: *IEEE Transactions on Industrial Electronics* 37 (1990), Nr. 1, pp. 19–27

[WM09] Will, J. ; Most, T.: Metamodel of Optimized Prognosis (MOP) - An Automatic Approach for User Friendly Parameter Optimization. In: *Weimarer Optimierungs- und Stochastiktage 6.0*, 2009

[WS97] Wagner, N. G. ; Steff, K.: Bestimmung der dynamischen Labyrinthkoeffizienten unter realistischen Betriebsbedingungen mit Hilfe aktiver Magnetlager. In: *Proceedings of Schwingungen in rotierenden Maschinen (SIRM 1997)*, 1997, pp. 267–280

[WS10] Wei, C. ; Söffker, D.: MIMO-Control of a Flexible Rotor with Active Magnetic Bearing. In: *Proceedings of the Twelfth International Symposium on Magnetic Bearings (ISMB 12)*. Wuhan, China, 2010

[WS11] Wei, C. ; Söffker, D.: Optimal Control of a Flexible Rotor by Using Magnetic Bearing. In: Markert, R. (Hrsg.): *Proceedings of Ninth International Conference on Vibrations in Rotating Machines (SIRM 2011)*, Technische Universität Darmstadt, 2011

[WS12a] Wei, C. ; Söffker, D.: Improving PID-Control of AMB-Rotor System Design I: Optimization Strategy. In: *Proceedings of the Thirteenth International Symposium on Magnetic Bearings (ISMB 13)*, 2012

[WS12b] Wei, C. ; Söffker, D.: Improving PID-Control of AMB-Rotor System Design II: Experimental Results. In: *Proceedings of the Thirteenth International Symposium on Magnetic Bearings (ISMB 13)*, 2012

[WS15] Wei, C. ; Söffker, D.: Optimization Strategy for PID-Controller Design of AMB Rotor Systems. In: *IEEE Transactions on Control Systems Technology* (2015). – in press, online available

[Xie09] Xie, L.: *Numerical and Experimental Investitation of AMBs Supported Rotor System with Auxiliary Bearings*, Technische Universität Darmstadt, Dissertation, 2009

[YCZ07] Yang, B. ; Chen, Y. ; Zhao, Z.: Survey on Applications of Particle Swarm Optimization in Electric Power Systems. In: *IEEE International Conference on Control and Automation*. Guangzhou, China, 2007, pp. 481–486

[Zit99] Zitzler, E.: *Evolutionary Algorithms for Multiobjective Optimization: Methods and Applications*, Swiss Federal Institute of Technology Zurich, Dissertation, 1999

[ZL07] Zhang, Q. ; Li, H.: MOEA/D: A Multiobjective Evolutionary Algorithm Based on Decomposition. In: *IEEE Transactions on Evolutionary Computation* 11 (2007), Nr. 6, pp. 712–731

[ZT98] Zitzler, E. ; Thiele, L.: An Evolutionary Algorithm for Multiobjective Optimization: The Strength Pareto Approach / Computer Engineering and Communication Networks Lab (TIK), Swiss Federal Institute of Technology Zurich. 1998 (TIK-Report 43). – Techreport

The thesis is based on the results and development steps presented in the following previous publications :

[WS10] Wei, C. ; Söffker, D.: MIMO-Control of a Flexible Rotor with Active Magnetic Bearing. In: *Proceedings of the Twelfth International Symposium on Magnetic Bearings (ISMB 12)*, Wuhan, China, 2010

[WS11] Wei, C. ; Söffker, D.: Optimal Control of a Flexible Rotor by Using Magnetic Bearing. In: Markert, Richard (Hrsg.): *Proceedings of the Ninth International Conference on Vibrations in Rotating Machines (SIRM 2011)*, Technische Universität Darmstadt, 2011

[MWS11] Marx, M. ; Wei, C. ; Söffker, D.: Optimization of Complex Dynamic Systems with Respect to their Behavior in Time and Frequency Domain. In: *Proceedings of ASME 2011 International Design Engineering Technical Conferences & Computers and Information in Engineering Conference (IDETC/CIE)*, Washington D.C., USA, 2011

[SSW12] Söffker, D. ; Saadawia, M.-S. ; Wei, C.: Modell- und Eigenschaftsbasierte Diagnose Rotierender Maschinen. In: *9. Aachener Kolloquium für Instandhaltung, Diagnose und Anlagenüberwachung (AKIDA)*, Aachen, 2012

[WS12a] Wei, C. ; Söffker, D.: Improving PID-Control of AMB-Rotor System Design I: Optimization Strategy. In: *Proceedings of the Thirteenth International Symposium on Magnetic Bearings (ISMB 13)*, 2012

[WS12b] Wei, C. ; Söffker, D.: Improving PID-Control of AMB-Rotor System Design II: Experimental Results. In: *Proceedings of the Thirteenth International Symposium on Magnetic Bearings (ISMB 13)*, 2012

[SWS13] Saadawia, M.-S. ; Wei, C. ; Söffker, D.: Model- and Feature-Based Diagnostics in Rotating Machinery. In: *Proceedings of DINAME 2013 - XV International Symposium on Dynamic Problems of Mechanics*, Buzios, RJ, Brazil, 2013

[WGS13] Wei, C. ; Gausmann, R. ; Söffker, D.: Controller Design and Optimization Strategy for Active Magnetic Bearing Systems. In: *Proceedings of the Tenth International Conference on Vibrations in Rotating Machines (SIRM 2013)*, 2013

[WS15] Wei, C. ; Söffker, D.: Optimization Strategy for PID-Controller Design of AMB Rotor Systems. In: *IEEE Transactions on Control Systems Technology* (2015). – in press, online available

[SWWS15] Söffker, D. ; Wei, C. ; Wolff S. ; Saadawia, M.-S.: Detection of Rotor Cracks: Comparison of an Old Model- with a New Signal-Based Approach. In: *Nonlinear Dynamics* (2015), pp. 1-18

Im Rahmen von Forschungs- und Projektarbeiten im Lehrstuhl SRS wurden von Chunsheng Wei und Univ.-Prof. Dr.-Ing. Dirk Söffker die nachstehenden Bachelor- und Diplomarbeiten inhaltlich betreut, wobei Bestandteile und Ergebnisse aus den Forschungs- und Projektarbeiten sowie den studentischen Qualifikationsarbeiten wechselseitig in die jeweiligen Arbeiten und somit auch in diese Promotionsarbeit eingeflossen sind.

[Mao11] Mao, J.: *PID-Controller Design for Active Magnetic Bearing System*, University of Duisburg-Essen, Bachelor Thesis, 2011

[Win12] Winkler, J.: *Optimierung technischer Systeme mit evolutionären Algorithmen in Python*, Universität Duisburg-Essen, Diplomarbeit, 2012